NAVAL POSTGRADUATE SCHOOL
Monterey, California

THESIS

FORECASTING MESOSCALE WINDS ON COMPLEX TERRAIN USING A SIMPLE DIAGNOSTIC MODEL

by

Renwick M. Mohammed

September 2000

Thesis Advisor: Douglas K. Miller
Second Reader: R. Terry Williams

Approved for public release; distribution is unlimited

REPORT DOCUMENTATION PAGE			Form Approved OMB No. 0704-0188
Public reporting burden for this collection of information is estimated to average 1 hour per response, including the time for reviewing instruction, searching existing data sources, gathering and maintaining the data needed, and completing and reviewing the collection of information. Send comments regarding this burden estimate or any other aspect of this collection of information, including suggestions for reducing this burden, to Washington headquarters Services, Directorate for Information Operations and Reports, 1215 Jefferson Davis Highway, Suite 1204, Arlington, VA 22202-4302, and to the Office of Management and Budget, Paperwork Reduction Project (0704-0188) Washington DC 20503.			
1. AGENCY USE ONLY *(Leave blank)*	2. REPORT DATE September 2000	3. REPORT TYPE AND DATES COVERED Master's Thesis	
4. TITLE AND SUBTITLE: Title (Mix case letters) Forecasting Mesoscale Winds On Complex Terrain Using a Simple Diagnostic Model			5. FUNDING NUMBERS
6. AUTHOR(S) Renwick M. Mohammed			
7. PERFORMING ORGANIZATION NAME(S) AND ADDRESS(ES) Naval Postgraduate School Monterey, CA 93943-5000			8. PERFORMING ORGANIZATION REPORT NUMBER
9. SPONSORING / MONITORING AGENCY NAME(S) AND ADDRESS(ES) N/A			10. SPONSORING / MONITORING AGENCY REPORT NUMBER
11. SUPPLEMENTARY NOTES *The views expressed in this thesis are those of the author and do not reflect the official policy or position of the Department of Defense or the U.S. Government.*			
12a. DISTRIBUTION / AVAILABILITY STATEMENT Approved for public release; distribution is unlimited			12b. DISTRIBUTION CODE

13. ABSTRACT

The use of mesoscale models to provide an accurate representation of what the atmosphere is likely to do in the near future is one of the tools forecasters utilize to predict atmospheric variables. Because of the large amount of time and computer resources necessary to provide detailed forecasts on the mesoscale, this study looked at forecasting winds utilizing a simple diagnostic model and compared its results to a full physics model. Winds from the Fifth Generation Mesoscale Model (MM5), were run at fairly coarse grid spacings of 81, 27, and 9 kilometers and at a finer grid spacing of three kilometers. The MM5 9 kilometer results were input into the Winds On Critical Streamline Surfaces (WOCSS) model, which is a scaled down physics model designed to adjust winds to fine scale topography. A comparison of how the WOCSS model winds compared against each of the MM5 grid spacings was evaluated for an event during the period 4-7 August 1997 in the SOCAL bight region to determine if the results of the scaled down physics model were comparable to the full physics model. This experiment showed encouraging results for forecasting fine scale winds on complex topography using the simple diagnostic model.

14. SUBJECT TERMS Mesoscale Modeling, Wind Forecasting, Wind Simulation			15. NUMBER OF PAGES 144
			16. PRICE CODE
17. SECURITY CLASSIFICATION OF REPORT Unclassified	18. SECURITY CLASSIFICATION OF THIS PAGE Unclassified	19. SECURITY CLASSIFICATION OF ABSTRACT Unclassified	20. LIMITATION OF ABSTRACT UL

Approved for public release; distribution is unlimited

FORECASTING MESOSCALE WINDS ON COMPLEX TERRAIN USING A SIMPLE DIAGNOSTIC MODEL

Renwick M. Mohammed
Lieutenant, United States Navy
B.S., United States Naval Academy, 1993

Submitted in partial fulfillment of the
requirements for the degree of

MASTER OF SCIENCE IN METEOROLOGY AND PHYSICAL OCEANOGRAPHY

from the

NAVAL POSTGRADUATE SCHOOL
September 2000

ABSTRACT

The use of mesoscale models to provide an accurate representation of what the atmosphere is likely to do in the near future is one of the tools forecasters utilize to predict atmospheric variables. Because of the large amount of time and computer resources necessary to provide detailed forecasts on the mesoscale, this study looked at forecasting winds utilizing a simple diagnostic model and compared its results to a full physics model. Winds from the Fifth Generation Mesoscale Model (MM5), were run at fairly coarse grid spacings of 81, 27, and 9 kilometers and at a finer grid spacing of three kilometers. The MM5 9 kilometer results were input into the Winds On Critical Streamline Surfaces (WOCSS) model, which is a scaled down physics model designed to adjust winds to fine scale topography. A comparison of how the WOCSS model winds compared against each of the MM5 grid spacings was evaluated for an event during the period 4-7 August 1997 in the SOCAL bight region to determine if the results of the scaled down physics model were comparable to the full physics model. This experiment showed encouraging results for forecasting fine scale winds on complex topography using the simple diagnostic model.

TABLE OF CONTENTS

ACKNOWLEDGEMENTS

First I would like to thank Dr. Doug Miller, without your enthusiasm, guidance, patience and motivation this would have never been possible. You kept me on track the entire time and always made yourself available. I've learned a lot throughout this process and you have made it a great experience. Thank you.

My many thanks to my partner in this whole endeavor Lieutenant Chris Sterbis. Without you I may still be looking for many answers and trying to understand things that seem to come naturally to you. You have kept me alive through this process more than you can ever realize.

Thanks to Dr. R. T. Williams for your great inputs and for making my thesis the best it could be. The quick turn around was greatly appreciated.

Thanks to mom for the guidance and for teaching me to "take things one day at a time". Thanks to dad for always believing in me. Thanks to Dale for all the advice, believe it or not, I always listen. Thanks to Renee for all the laughs and for "keeping it real".

Finally, thanks to my girls. I could have never done it without the love and support that I received from you all.

I. INTRODUCTION

Mesoscale forecasting is becoming more and more popular and necessary because of the increased need to forecast mesoscale phenomena not easily captured with synoptic scale models. With the increasing need for finer resolutions in military weapons systems, fighting forest fires, tracking mesoscale weather phenomena and a myriad of other uses, the importance of mesoscale models cannot be underestimated. The United States Navy's operational need for precision and accuracy in guided munitions, combating chemical, biological and radiation hazards, flight deck operations, small boat operations and multiple other duties make mesoscale modeling and forecasting a crucial part of the Navy's safety and success. With increased computer processing power, data can be digested and output in a timely fashion in order to be used by operational forecasters or ingested into tactical decision aids. The accuracy of the mesoscale forecast relies heavily upon the larger scale model, which will provide some of the initial input into the mesoscale model.

As with any model, a degree of forecasting skill and general knowledge of the model's strengths and weaknesses must be taken into account. Before a forecaster utilizes any model, a conceptual model of the current synoptic situation is critical to providing an accurate forecast. Additionally, area climatology and local weather phenomena must be taken into account when forecasting on the mesoscale. Finally, it is imperative to keep in mind that the model is only as good as its input. This is where relying on the conceptual model

is crucial, if the model forecast does not seem correct conceptually, then further scrutiny of the model output or another source of information (if the forecast is very poor) is required for an accurate forecast. Also, the mesoscale model may provide new conceptual models which better explain local weather phenomena.

This study will examine one area of the mesoscale forecast problem, namely, evaluating wind speed and direction diagnosed by the Winds On Critical Streamline Surfaces (WOCSS) model and compare their accuracy with that of winds produced from the Fifth Generation Mesoscale Model Version 5 (MM5) and to the observed winds. The purpose of the evaluation is to determine how a simple diagnostic model such as the WOCSS model compares against a full physics model like the MM5. Many of the mesoscale model parameterization schemes included in MM5 were designed to be applied at relatively coarse grid spacings and generating fine-scale mesoscale model forecasts may have error associated with violating assumptions of these schemes which are valid at large model grid spacings. The WOCSS model, due to its simplified physics, presents an attractive alternative to other models in forecasting mesoscale wind speeds and directions because of the small amount of computer processing power and time required to produce a forecast. It is important to note, however, that the WOCSS model in this study takes information from an MM5 forecast on a coarse domain (nine kilometer) and generates a wind field on a fine-scale (three kilomter) domain. Therefore, any phase error problems in the MM5 forecast will automatically be translated into the WOCSS model's diagnosis.

A. THE IMPORTANCE OF MESOSCALE FORECASTING

The use of mesoscale models at local centers such as the Naval Pacific Meteorology and Oceanography Center, San Diego, provides several benefits as compared to running them at a national center such as the Fleet Numerical Meteorology and Oceanography Center (FNMOC) or the National Climate and Environmental Prediction Center (NCEP). By using a mesoscale model, the local forecast center can focus on a particular area of interest with higher resolutions than that provided by national centers (Miller 1999). The mesoscale model can be initialized with "unique" observations unavailable to the operational forecast centers. Additionally, one can experiment with unique analysis and/or model physics schemes unavailable to the operational forecast centers.

The MM5 Tutorial Class Notes and Users Guide (January 2000) suggest some benefits of using mesoscale models are: high horizontal resolution that resolves local details in the wind field especially in areas of complex orography. Mesoscale models also do a fairly good job in resolving convective systems such as squall lines provided the mechanisms which form them are well observed and have been included in the model initialization. They give good precipitation forecasts, can resolve topographic enhanced precipitation and can resolve frontal boundaries. The ability to resolve and forecast local circulations, land-sea breeze regimes, mountain-valley circulations and gap flows make mesoscale models an essential tool. Also its ability to provide detailed cloud forecasts such as stratus and sea fog make it an essential tool for this study.

B. PREDICTABILITY THEORY

Predicting or depicting mesoscale weather features depends on several factors such as model physics, model set-up (domain size, grid resolution, boundary conditions), and model initialization (how the model handles the meteorological analysis). A forecaster must ask whether or not the model can be used deterministically at finer grid resolutions (Miller 1999). Lorenz (1982, 1993) states that the predictability time limit represents the time frame between the best approximation of the state of the atmosphere based on initial observations and an estimate of its future state. The predictability time limit represents the point at which the forecast becomes unusable due to inherent numerical model forecast errors. Predictability theory states that the ability to predict atmospheric variables varies with time, seasonal variations, geography and synoptic patterns (Anthes 1986). The error related to predictability will increase over time, hence predictability decreases with model forecast larger forecast lead times (Kuypers 2000). A feature is predictable only as long as the measure of forecast accuracy is better than climatology. Smaller-scale weather systems have shorter life cycles and may not be very predictable because of their small spatial and temporal scales. Atmospheric errors or initial uncertainties in small scales of motion propagate toward larger scales and are seen at the mesoscale sooner than at the synoptic scale. As a result, the mesoscale is less predictable (Anthes 1986). Variability will also increase under weak synoptic forcing, which is applicable to summertime conditions as discussed in the synoptic and mesoscale

situation chapter of this thesis. Improving a forecast normally results from reducing model error for atmospheric variables being forecasted over the entire domain. The best tool for improving predictability results from studies that show model tendencies, weaknesses and errors, thus providing end users a way of utilizing and compensating for known and recurrent model errors. Figure 1 depicts theoretical numerical model forecast error (NMFE) growth curves over time and depicts the impact that the initial error has on predictability. At the initial time, the NMFE is small but grows quickly due to the lack of dynamic consistency between the initial model state analyzed by observations and the dynamic allowances set forth in the model physics (Kuypers 2000). As the model is allowed to generate mesoscale structures, this initial state develops into a state consistent with the physical equations of the model at which time a minimum in numerical forecast error occurs. The model forecast error continues to grow to a point at which the model depicts no skill in relation to climatology.

C. VERIFYING MODEL ACCURACY

Verification of a model is usually done by comparing the model's forecast with observations or a model generated analysis. The lack of mesoscale observations is one of the difficulties in verifying a mesoscale forecast (Perkey 1986). For this study, data collected from the South Coast Ozone Study (SCOS) was used to verify the accuracy of the different MM5 model resolutions used in this study as well as the WOCSS model run at 3 kilometer grid spacing . Use of observations hypothetically present the most accurate synopsis of the current

atmosphere, but observations also lend a difficulty of their own when trying to forecast on the mesoscale. Localized effects that are sometimes seen in observations are not always representative of the atmosphere on the larger scale. Forecasters must rely on the conceptual model, other numerical models (for comparison), surrounding observations and experience in an effort to filter out localized effects to verify model performance and produce an accurate mesoscale forecast. Additionally, model verification will naturally be biased towards areas where observations are available (Monterrosa 1999). Similarly, verifying a model forecast with a model analysis presents problems of its own. A model analysis will only be as good as the model itself and the data ingested into it.

D. HYPOTHESIS

This thesis focuses on running the MM5 mesoscale model at several relatively coarse grid spacings of 81, 27 and 9 kilometers and at a finer grid spacing of 3 kilometers. The MM5 9 kilometer results were subsequently input into a simple diagnostic model, the WOCSS model, designed to adjust the winds to fine scale topography. The hypothesis is that simulating the winds on the WOCSS model will provide just as accurate, meaning within a predetermined level of tolerance, if not more accurate surface wind forecasts as running the mesoscale model at very fine resolutions thereby saving the costs of computer time and resources. A description of the models used in this study will be given in Chapter II, a summary of the synoptic situation and mesoscale weather during

the period of study will be described in Chapter III, the data used for the simulations are discussed in Chapter IV and the methodology of this experiment will be described in Chapter V. Chapter VI will provide details on the results of this experiment and Chapter VII will provide an overall summary of this experiment and conclusions.

THIS PAGE INTENTIONALLY LEFT BLANK.

II. MODEL DECRIPTIONS

A. FIFTH GENERATION MESOSCALE MODEL (MM5)

The MM5 is a primitive equation, terrain-following sigma coordinate model that is designed to simulate or forecast mesoscale and regional scale atmospheric motion. It was developed at Penn State University and the National Center for Atmospheric Research (NCAR) with contributions from numerous universities and government institutions. The MM5 has been in use since the early 1990's. The current version (3.3) was released on January 26, 2000. It has multi-nesting capabilities and non-hydrostatic dynamics that allow it to be used at fairly fine resolutions on the scale of a few kilometers. The MM5 model is supported by several auxiliary programs, which are referred to collectively as the MM5 modeling system (Dudhia et al. 2000).

1. Why Use the MM5?

The primary reason for utilizing the MM5 for this experiment is the model's ability to be easily run with different Planetary Boundary Layer (PBL) schemes. The PBL schemes run for this experiment are the Gayno-Seaman (Gayno et al. 1994) and Blackadar (Blackadar 1979) schemes.

Due to the widely varying terrain in the area of study, the MM5 land use categories also give strength for its use as our mesoscale model of choice. The MM5 can assign each gridpoint with a terrain type such as vegetation, water,

urban, desert, etc. In addition, it will assign surface albedos, roughness lengths, longwave emissivity, heat capacity and moisture availability (NCAR 1995).

For summertime weather simulations the MM5 has a tendency to over-amplify the near surface winds associated with the coastal jet and the amplitude of the diurnal cycle should be scrutinized after the 24-hour forecast. Additionally, the PBL scheme does a poor job in capturing details of the coastal marine layer which is present during the time of this study (Miller 1999).

2. MM5 Vertical And Horizontal Grids

The MM5 uses terrain-following vertical coordinates, implying that the lower grid level coordinates follow the terrain and get progressively flatter until the chosen model-top pressure field is reached (Figure 2). All domains for this study utilize 30 vertical levels which are more densely distributed in the lower levels, with the lowest level being at 22 meters above ground. There are a total of 12 levels located between the 850 millibar (mb) level and the surface.

3. Nesting

One of the many strengths of the MM5 is its capability for multiple grid nesting. Its grids can be configured to run at the global scale down to very fine scales. In this study, the MM5 ingested 1° latitude by 1° longitude gridded data from the Navy Operational Global Atmospheric Prediction System (NOGAPS) model which was scaled down to 81, 27, 9 and 3 kilometers in the MM5 with the NOGAPS model used for the boundary conditions. The domain defined for

verification of this study is a box bounded by 33.46° north latitude and 119.38 ° west longitude in the lower left corner then diagonally across to 34.94° north latitude and 117.59° west longitude in the upper right corner and is depicted along with the MM5 3 kilometer terrain elevations in Figure 3. Table I gives details of the four domains used for this study along with terrain, landuse data and the number of gridpoints in the X and Y directions.

The MM5 can run in both two-way and one-way nesting modes. In the two-way mode the input from the coarser mesh is derived from its boundaries. Feedback to the coarser mesh comes from the interior nests that it hosts (NCAR 1995). This study, utilized the one-way mode in which the coarse domains of the mesoscale model drove the finer grids. The one-way nest provides no feedback to the coarser domain and can be initialized with enhanced resolution data and terrain. The nesting configuration can be seen in Figure 4.

4. Initialization of the MM5

Two-dimensional multiquadric interpolation was used to convert first guess NOGAPS grid fields and observations to MM5 grid fields. The multiquadric interpolation technique is very accurate for interpolating scattered data (Nuss and Titley 1994). Two-dimensional multiquadric interpolation is univariate, meaning that it solves for each physical parameter (temperature, winds, moisture, etc.) independently of each other. This method also solves each level independently. Furthermore, the multiquadric analysis resolves features on the smallest scales that are represented by the observations in the domain of this study. The

method is computationally efficient and well behaved in data-void regions and, as a result, applicable to this study (Nuss and Titley 1994).

B. WINDS ON CRITICAL STREAMLINE SURFACES (WOCSS)

The WOCSS model uses objective analysis, the concepts of mass conservation and the critical dividing streamline in order to provide a diagnostic means of forecasting mesoscale winds in complex terrain.

1. WOCSS Basics

The WOCSS model is loosely based upon the wind-energy planning model of Bhumralkar et al. (1980) that used a simple variational calculus numerical scheme applied to sigma coordinates (Ludwig et al. 1991). Many users have modified it over the years with a large amount work being done by F. L. Ludwig and staff of Stanford University from whom the model may be obtained.

Using conservation of mass, the WOCSS starts its wind interpolation by use of a first guess which can be input from another model (in this case the MM5) or by surface and rawinsonde data. WOCSS then adjusts the winds to remove the divergence and assumes that the flow does not penetrate the surfaces. The flow surfaces are derived from the critical dividing streamline concept as described below. For additional information concerning WOCSS details, the reader is referred to Ludwig et al. (1991).

2. The Critical Dividing Streamline Concept

Ludwig et al. (1991) describe that the critical dividing streamline concept applies when the atmosphere is statically stable and the local flow is adiabatic or nearly so. They further explain the basic principle of the concept being that there is some height at which the work done against the buoyant restoring force is equal to that of the original kinetic energy of the wind. The maximum height above ground level, Z_{max}, to which a parcel at height z can be lifted given the potential temperature gradient, $d\theta/dz$, and wind speed V_0 at the lowest layers on the flow surface can be expressed as:

$$Z_{max} - z_0 = V_0 \left(\frac{d\theta}{dz}\frac{g}{\overline{T}}\right)^{-1/2}, \quad (1)$$

Where g is gravitational acceleration and $\overline{T}$ is the average temperature in the layer between z_0 and Z_{max}. Equation (1) provides an objective method for defining the coordinate surface that will approximate the shape of the flow and will intersect the terrain in areas at which the flow cannot pass over it. The WOCSS model utilizes curvilinear coordinates and, with the critical steamline concept, the winds are set to zero at points that are below the terrain. Adjustments toward nondivergence will cause the flow to move around an obstacle as opposed to over it or through it (Ludwig et al. 1991).

3. Application To The Los Angeles Basin

As a part of the SCOS study, the Los Angeles basin contains a very complete meteorological data set for the periods of August 4 through August 7, 1997. Figure 3 shows the area of concern for this study with the MM5 3 kilometer terrain elevations contoured. The stations used from the SCOS data are listed in Table II along with their coordinates and elevations. Due to the wide variety of terrain elevation, which includes valleys, mountains and smooth surfaces, the area provides a rigorous testing ground for the WOCSS model. In the Los Angeles basin, topographic channeling, orography and interaction of the marine layer make for a very challenging forecast with any model. Ludwig et al. (1991) showed the WOCSS as being computationally stable in the Los Angeles Basin and has given indications to some weaknesses of the WOCSS. Referring to these weaknesses, adjustments to the model, especially in its ability to handle flow during neutral and unstable conditions and some atmospheric circulations such as sea-breeze fronts would give a forecaster a warning of under what conditions to exercise caution when using the WOCSS model.

III. SYNOPTIC AND MESOSCALE SITUATION

A. SUMMERTIME CLIMATOLOGY OF THE LOS ANGELES BASIN

Climatology as a rule is one of the first error checks that one can use to determine whether or not your model of choice has a good grasp on the current meteorological situation. Unless there is a pronounced reason for the current pattern to deter from climatology, then all parameters should be within an acceptable tolerance level of climatology. When the model shows significant deviations from climatology, then further inspection of the model is necessary. One needs not commit to memory the minuscule details of daily climatology but should instead be familiar with the general weather pattern for the area and time of year for which the forecast is being evaluated. The following presents a brief synopsis of climatology of the Los Angeles basin relevant to this study obtained from NOAA Technical Memorandum NWS WR-261 (Climate of Los Angeles, California, January 2000).

In the summertime, the northern East Pacific high pressure system, hereafter EASTPAC high, dominates the weather of Southern California (SOCAL) as shown in Figure 5. The EASTPAC high brings warm dry air which descends and caps the cooler ocean air below producing a strong inversion aloft and a marine layer. The marine layer is a very prominent feature in the Los Angeles Basin and is heightened during the warmer months from late spring

through early fall. Daily variations of the EASTPAC high pressure center causes the marine layer to vary in its extent and thickness.

In addition to the fluctuations induced by the high pressure system, sea surface temperatures also affect the strength of the marine layer. During the summer months when the EASTPAC high is strong, it causes upwelling off the coast of the western United States. The northwest winds of the EASTPAC high moves the warmer surface waters offshore and Ekman transport causes the surface waters to be replaced by colder water from deeper depths. This upwelling produces lower sea surface temperatures during the summer months, as a result creating a strongly stable marine layer. Sea surface temperatures off SOCAL range from approximately 13° C in the late spring to 23° C in early fall. With such a large variation, any model used for forecasting should be robust enough to compensate for the effects of varying sea surface temperature on the marine layer, cloud formation, stratus, winds and temperatures.

The variability of summertime atmospheric temperatures in the Los Angeles Basin are a result of the wide variety of classifications of surface types in relatively close proximity to each other. Within this area, there is ocean, desert and mountainous terrain all of which combine to give the area high temperature variations within a matter of several kilometers. The MM5 land use categories include these features and can resolve them on the finer meshes. The marine air also has pronounced effects on the area, bringing relatively cool and constant temperatures, low clouds, fog and haze to the near coastal regions. During

periods of a very warm summer pattern combined with a shallow marine layer less than 300 meters deep, the Los Angeles area can experience extreme temperature contrasts. During such times, the warmest valleys may see temperatures in excess of 25° C hotter than those at the beaches.

The Los Angeles basin is largely dominated by the winds from the strong EASTPAC high producing northwesterly flow over the area. As the wind flow approaches the coast it is subject to regional and local influences that further modify it. The mountains of the basin have a significant influence in modifying the wind stream in addition to the coastal geography of the California bight, which produces an eddy like effect on the winds. The transverse mountain ranges divide the Los Angeles basin into a semi desert and coastal region. The ranges strengthen the predominant sea breeze across the coastal areas of the basin.

The Los Angeles basin usually experiences a light and variable land breeze during the night and early morning (Figure 6a) with a reverse in direction during the late morning and early afternoon producing a relatively stronger sea breeze (Figure 6b). The direction of the sea breeze varies from west-southwest at the Los Angeles Airport (LAX) to south-southeast in the Long Beach area. The lightest winds for the area usually occur in August and September.

The Catalina Eddy is a feature that sometimes occurs from May through October. This eddy causes a change in the wind pattern over the basin to a more southerly direction along the coast. The lower level winds are the reflection of a mesoscale vortex which establishes itself near Catalina Island. A fairly

strong cyclonic circulation establishes itself in the lower atmosphere of the basin. The eddy results in considerable mixing up to nearly 1500 meters above ground level. The southeasterly flow produces increased winds in some areas and brings cooler, purer air to the basin. The Catalina Eddy is caused by the geostrophic wind interacting with the basin's topography. Eddies normally last for three to five days and end with a decrease in northwesterly winds thus suppressing the forced cyclonic flow, a disruption from a strong synoptic-scale weather system, or as a result of the marine layer deepening to 2000 meters.

The other major mesoscale wind producer in the Los Angeles basin are the Santa Ana Winds. The Santa Anas are katabatic offshore winds, usually warm, which flow from the mountains downwards to the coast. Winds of 40 to 50 mph are typical and local gusts of 100 mph can occur. They occur chiefly in the fall and winter and bring light coastal winds, purer air and lowers the humidity in the basin. The Santa Anas last from periods of a day to longer than a week.

B. WEATHER PATTERN DURING THIS STUDY

1. Synoptic Discussion

At 040000Z August, there is a strong upper level ridge located in southern Alaska, with a trough moving in from the west. A low height center in the Gulf of Alaska, located west of Vancouver Island (Figure 7). The 500 mb heights over SOCAL show weak absolute vorticity maxima throughout the period. At the 925 mb level (Figure 14), warm temperatures are seen in SOCAL originating from

Mexico. At 040000Z August there is a 27° C isotherm over SOCAL with ridging from the EASTPAC high off the coast. A reflection of the 500 mb low can be seen at 925 mb. On the surface (Figure 21), the low pressure center west of Canada is reflected from the upper levels and has a central pressure of approximately 1010 mb and can be seen troughing into the EASTPAC high. The EASTPAC high with a central pressure of 1027 mb ridges north into Alaska and to its west, dominates the weather off the SOCAL coast in the bight region. A thermal trough extends from Mexico into the SOCAL area and interacts with the EASTPAC high to produce a weak gradient off the California coast.

By 041200Z August, the 500 mb low height center in the Gulf of Alaska has moved to the northwest and interacts with the gradient of the trough moving in from the western Pacific causing an amplification of the ridge located over Alaska (Figure 8). At the 925 mb level (Figure 15) the SOCAL area cools by about 3° C likely a result of nighttime cooling. The EASTPAC high height center at this level has weakened and the southeast quadrant has spun off a closed circulation located over the open ocean west of California. On the surface (Figure 22), the central pressure of the EASTPAC high weakens due to the movement of the low pressure system to the east. A reflection of the closed circulation noted at the 925 mb level is seen at the surface but is not completely cut off from the main high. The high is ridging into SOCAL and produces an extremely weak gradient over the area. To the west of the EASTPAC high, the

eastward moving trough interacts with the EASTPAC high forcing it to move eastward and weaken slightly.

At 050000Z August (Figure 9) the low height center in the northeast Pacific has moved into the central Gulf of Alaska and the trough moving in from the western Pacific has deepened and shows a large area of vorticity advection. A ridge has moved over the SOCAL area extending over the ocean and Baja California. At 925 mb (Figure 16), there is a closed circulation over the southern Aleutians and the circulation in the Gulf of Alaska is becoming disorganized but continues to move westward weakening the ridge between it and the circulation over the Aleutians. The thermal gradient increases over SOCAL area by 3° C indicative of the diurnal effects. The northern extent of the surface EASTPAC high (Figure 23) has been diminished by the westward moving low pressure center in the Gulf of Alaska and the EASTPAC high builds east of the low pressure center, ridging into Canada and Alaska. The low that has moved over the Aleutians from the west has become more organized and the center has broadened and shows signs of continued deepening.

At 051200Z August, the eastward moving trough and the low height center in the Gulf of Alaska are in close proximity to each other and give indications of merging (Figure 10). The ridge over the SOCAL area has extended its reach to northern California and western Nevada. At 925 mb (Figure 17), the ridge between the two systems in the northeastern Pacific has disappeared as the two circulations move closer to each other. The SOCAL region is approximately 3° C

warmer than 24 hours earlier, with an area of 30° C located over Point Conception. On the surface (Figure 24), the ridging from the EASTPAC high can be seen moving away from the coast. The trough originating from Mexico, now located over SOCAL, blocks the ridge from moving over the area. The low pressure center over the Aleutians deepens and the low pressure center in the Gulf of Alaska continues to move westward and is slowly being absorbed by the deeper low over the archipelago.

By 060000Z August, the 500 mb trough from the western Pacific has closed off into a low height center over the southern Aleutians and continues to interact with the low height center in the Gulf of Alaska (Figure 11). The ridge over the western United States has formed into a closed high height center over most of California, Oregon, Nevada, Arizona and northern Baja. The 925 mb NOGAPS chart shows the merger of the circulations in the northeast Pacific (Figure 18). The 925 mb temperatures, show significant heating originating from the California, Arizona, Mexico border extending up into northern California and into the waters off the southern California coast. The entire SOCAL area show temperatures ranging from 30°-33° C which is 3°-6° C warmer than the previous day. There is also a moderate geopotential height gradient over SOCAL. The surface plot (Figure 25) also shows combining of the lows in the north Pacific and the EASTPAC high continues to build in behind the system. The thermal low over the United States/Mexican border has a closed 1010 mb isobar with a trough extending into the SOCAL bight.

By 061200Z August, the low height centers in Gulf of Alaska have merged and deepened and has a large area of troughing stretching across the Gulf of Alaska with its center located over the Aleutians (Figure 12). The high height center over the western United States has decreased in area (possibly due to diurnal cooling) and is located north of the SOCAL bight extending to the northern California border and extending eastward to central Nevada. At 925 mb (Figure 19) the EASTPAC high is building and interacting with the gradient produced by the thermal trough off the western United States. The SOCAL area is under the influence of the thermal low with temperatures greater than 30° C over Point Conception and the bight region. On the surface (Figure 26), the EASTPAC high continues to build behind the low pressure centers to the north and a second high pressure circulation is seen west of Vancouver Island. The thermal low over SOCAL has weakened due to nighttime cooling and the entire SOCAL region is under the influence of a weak pressure gradient.

By 070000Z August, the diurnal effect over California has become evident as the closed area of higher 500 mb geopotential heights over California has once again extended to encompass the entire state and much of the area off the coast (Figure 13). Ridging extends further towards the central Pacific as the area of troughing in the Gulf of Alaska retreats poleward. At 925 mb (Figure 20), the EASTPAC high has built significantly and is ridging into western Canada and the cyclonic circulation over the Aleutians is weakening. The temperatures have decreased to 27°-30° C over the SOCAL area and the thermal trough can be

seen shifting eastward into Arizona and Nevada. On the surface (Figure 27), the low pressure center over the Aleutians has weakened and the EASTPAC high is once again dominating conditions in the eastern Pacific. The thermal low over the border has deepened slightly and has moved east and is now centered over the California/Arizona border. The EASTPAC high interacts with the thermal low and creates a weak pressure gradient over the SOCAL area.

2. Mesoscale Discussion

From 040000Z August through 070000Z August, during nighttime hours, all coastal stations (Figure 28 through Figure 34) show light winds from varying directions and temperatures ranging from 16°-19° C. By 061200Z August, nighttime temperatures along the coast have increased to 19°-23° C as a result of the thermal trough noted in the synoptic discussion above. Further inland, the temperatures are higher with winds still light and variable with the effects of the thermal trough evident at the end of the period. Daytime temperatures in the domain vary widely due to the location of the individual stations (see climatology discussion in Chapter III). During the period, all stations hint at some diurnal wind variations. During warm times (0000Z), coastal stations HAWH, CASE and OCEA show onshore flow and stations ACTN and DEVO near the mountains show upslope flow. During cold times (1200Z), ACTN and DEVO show downslope flow, CASE and OCEA show offshore flow. Profiler information in the study verification area showed no significant inland penetration of the sea breeze

front throughout the study period, for details the reader is referred to Sterbis (2000).

GOES9 visible satellite imagery (Figure 35 through Figure 37) shows the absence of a stratus deck in over the SOCAL bight region, this suggests either a very shallow marine layer, or significant mixing is occurring which erodes and eliminates the marine layer. The high pressure, as stated in the surface discussion above, ridges toward the California coast and produces an enhanced gradient off the central California coast forcing marine stratus located off the central California coast to move southward off Point Conception. During the period of this study this stratus does not move onshore.

IV. DATA USED FOR THIS STUDY

A. BACKGROUND ON THE SCOS EXPERIMENT

The California Air Resources Board (CARB) sponsored SCOS '97 in the Los Angeles Basin in the summer of 1997. The primary purpose of the SCOS study was to coordinate and enhance scientific research and assessment of tropospheric ozone behavior in an effort to establish strategies for local and regional ozone control (CARB 2000). The large domain of the SCOS area includes areas of air-sea interaction and complex terrain, which makes it a superb region for this study of WOCSS performance.

B. THE SCOS DATA SET

The SCOS dataset contains a total of 259 surface sites, 25 continuous profiler sites and 12 rawinsonde sites (six hourly). For this study, twenty-three surface stations, nine profiler sites and five rawinsonde sites were utilized from the SCOS data set. For location and surface elevations for the various data stations see Table II. All wind data has gone through a quality check for accuracy performed by Boucouvala et. al (2000).

THIS PAGE INTENTIONALLY LEFT BLANK

V. METHODS

The period of 0000Z August 4, 1997 through 0000Z August 7, 1997 was selected as the test period for the WOCSS model's performance. Since there was a fairly complete set of observations from the SCOS study and thus provided an accurate synopsis of the mesoscale winds. As stated earlier, the WOCSS model was initialized from forecasts of the MM5 mesoscale model 9 kilometer domain.

The MM5 was initialized utilizing four different simulations, which consisted of varying PBL schemes, and static and dynamic initializations. For details refer to Sterbis (2000). A static initialization or "cold start" is done by blending observations into the first guess fields of the NOGAPS 1° model and subsequently running the MM5 (Leidner et al. 1999). Mesoscale features are not present in the cold start initially, so the model has to go through an adjustment period whereby it acquires dynamic balance and spins up mesoscale features. Short-term (three, six nine and twelve hour) forecasts were used for comparison in this study. This simulation provided the best results when running the WOCSS model on the study domain, for details on the other initialization schemes and their results see Sterbis (2000). Detailed information on the results of the cold simulation will be described in Chapter VI.

A. STATISTICS

Routine statistical measures were used to evaluate the performance of the WOCSS model's wind direction and wind speed against that of the MM5 model. The WOCSS model at 3 kilometer grid spacing was compared along with the MM5 model at 81, 27, 9 and 3 grid spacing to the SCOS observations. This comparison was made at 6 different layers (Table III). The specific statistical techniques used were:

1. **Mean** which is the average of all the data for a particular parameter which can be described mathematically as:

$$\bar{x} = \frac{1}{n}\sum_{i=1}^{n} x_i = \frac{x_1 + x_2 + \ldots + x_n}{n},$$

where x_n are the observed parameters and n is the number of observations.

2. **Standard deviation** which is a measure of the scatter or variability about the mean in a series of observations, shown mathematically as:

$$x = \sqrt{\frac{1}{n}\sum_{i=1}^{n}(x_i - \bar{x})^2}$$

3. **Root mean square difference (RMSD)** is used to describe the accuracy that encompasses both random and systematic errors and is described mathematically as:

$RMSD = \sqrt{\frac{1}{n}\sum_{i=1}^{n}(x_{m,i} - x_{o,i})^2}$, where x_m and x_o are equal to the model and observed parameter, respectively.

4. **Bias** is used to describe whether a specific parameter being evaluated is under- or over-forecasted. Taking the simple difference of the forecast minus the verifying analysis or observation is how the bias is derived. This method provides a quick look at the model's performance and is described mathematically as:

$$Bias = \frac{1}{n}\sum_{i=1}^{n}(x_{m,i} - x_{o,i}),$$

where x_m and x_o are as described for RMSD.

B. VERIFICATION

Soundings from the MM5 model solution generated on the 9 kilometer domain were subsequently input into the WOCSS model which was run at 3 kilometer grid spacing. The winds were then compared on the entire verification domain (Figure 3) horizontally and vertically at the six different layers shown in Table III. There are 37 observation sites where data was gathered within the study domain (Table II). The topography listed in Table II will vary somewhat from the model topography as seen in Figure 3 because the model represents gridded terrain elevation values which has a smoothing effect on topographic features. For model verification and comparison, the winds from the model's gridded data points were interpolated horizontally and vertically to the

observation points. For the surface statistics, the lowest vertical level in MM5, 22 meters above ground level, was compared to the actual surface observations from the SCOS data, also note the "surface" in the WOCSS model is at 25 meters above ground level. For the remaining layers, the vertical levels of the model were interpolated to the vertical levels of the profilers and rawinsondes. The MM5 and WOCSS were then evaluated using the statistics described in the previous chapter. Tests were conducted for the four experiments mentioned above by comparing both models at all six layers. Sterbis (2000) gives details on the results of these tests.

VI. RESULTS

In formulating the results of this study, several tests were done to compare the WOCSS model to the MM5. Sterbis (2000) shows that the MM5 model forecasts performed better under the cold start simulations described in Chapter V. Based on this, the WOCSS wind fields produced from the MM5 9 kilometer cold start forecasts will be the focus of this study. The first step in validating the WOCSS model is to determine if there is a clear improvement in the winds of the MM5 forecasts at 3 and 9 kilometers grid spacings over that of the MM5 27 and 81 kilometer grid spacing models. If there is an improvement, the WOCSS model then needs to be evaluated to determine if the 9 kilometer grid spacing input from the MM5, when scaled down by WOCSS to 3 kilometers, is comparable or gives an advantage in forecast accuracy to that of the MM5 3 and 9 kilometer domains. Table IV through Table IX shows the results of the mean, standard deviation, RMSD and Bias for wind speed, wind direction and temperature of all the models at the six layers used in this study.

A. WIND SPEED

When looking at a comparison between different model grid spacings it is important to remember that the 27 and 81 kilometer grid spacings are not going to resolve mesoscale and topographic features as well and the finer grid spacing models. Figures 38 through 61 displays a comparison of the MM5 27, 9 and 3 domain forecasted winds, the WOCSS model diagnosed winds and their

respective terrain elevations for 041200Z August through 070000Z August. The effect of the finer resolved topography and finer grid spacing on the winds is noticeable and when the winds are averaged over the domain, it may seem to present a poorer result as compared with the coarser grid spacing models. Hence, because the 3 and 9 kilometer domains may be experiencing influences of mesoscale features, they may not be as poor as they appear and need to be compared individually against the observations. Table 1 gives the number of points and terrain resolution of each MM5 domain. The number of points contained in the verification domain for each model is as follows: the MM5 81 kilometer grid spacing model; 3 points, the MM5 27 kilometer grid; 36 points, the MM5 9 kilometer grid; 322 points and the MM5 3 kilometer grid; 2,912 points.

The MM5 and WOCSS model fields (Figures 38 through 61) reflect the mesoscale situation as discussed in Chapter III.B.2 above. Along the mountains at 0000Z upslope flow can clearly be seen while at 1200Z downslope flow is depicted by all models. The models also depict the onshore flow along the coast at 0000Z and offshore flow at 1200Z. During the entire period, all models show light winds along the coast of the study domain . In the mountains and through the passes some higher wind speeds of 15-20 knots are seen in the models.

In the following discussion on the time series analysis, it should be emphasized that a three hour forecasts corresponds to times 0300Z and 1500Z, a six hour forecast corresponds to times 0600Z and 1800Z, a nine hour forecast corresponds to times 0900Z and 2100Z and a twelve hour forecast corresponds

to times 1200Z and 0000Z. The time series for mean surface wind speeds (Figure 62) shows a diurnal effect in observed wind speed. During the warm part of the day observations show a maximum in wind speed which occurs between 2100Z and 0000Z each day. Observations show minimum wind speeds occurring between 0700Z and 1300Z daily. All models show some nature of diurnal fluctuation but none capture the observed mean wind speed sinusoidal form properly. All models show a three to six hour wind speed lag during the warm part of the day and depict lower wind speeds during the colder part of the day very briefly before continuing to warm again. Additionally, all models depict relative wind speed maxima during the colder part of the day that is not seen in the observations. The WOCSS model appears to show more skill in forecasting wind speed over all other models as can be seen in Table IV which lists the mean, standard deviation, RMSD and bias for observations and models averaged over the study period in the surface layer. The WOCSS model shows a mean wind speed closer to that of the observed wind speed than the other models.

The surface wind speed standard deviation time series (Figure 63) emphasizes the poorer performance of the models during the cold cycles when compared with the observed standard deviation. The finer domain models all follow the same general trend with none displaying clear superiority as a whole. In Table IV the standard deviation of the wind speed averaged over the time period shows the WOCSS model has a standard deviation closer to the observed

standard deviation than all other models with the exception of the 81 kilometer domain MM5, which as noted above may not see mesoscale effects, suggesting on the average the WOCSS model provided a better surface wind forecast than all other models.

The RMSD time series (Figure 64) show the WOCSS model's mean differences at the surface are smaller during the cold periods and are fairly close to the other models during the warmer times of day. However, during the lag noted above, the WOCSS model does show a lower RMSD as compared to the other models implying that it may in fact handle the diurnal cycle slightly better. Overall, all MM5 domains show a higher RMSD as compared to the WOCSS model when averaged over the period (Table IV). Also, none of the forecast RMSD values are less than the observed standard deviation curve, this implies no forecast skill according to the Kuypers (2000) criterion.

The surface wind speed bias time series (Figure 65) shows all models overestimate wind speeds during cold times and underestimate during warm times. The WOCSS model does show a fairly regular lower bias than the other models (with exception of the 81 kilometer domain MM5 model) which is consistent with Ludwig and Sinton (2000). Averaged over the entire period the WOCSS model shows a lower bias as seen in Table IV.

The mean surface temperatures of all MM5 domains shown in Table IV are all within one degree (C) to the actual observed mean temperatures, their standard deviation however is not as close to the observed mean surface

temperature standard deviation suggesting a possible reason for wind speed errors seen in the surface layer.

At layer two, the MM5 81 and 27 kilometer domains over-amplify wind speeds considerably, the lag and second maxima noted at the surface layer is persistent at this layer as well (Figure 66). The finer domain models all perform better than the coarser domain models, but still show a lag in wind speed and secondary maxima. The wind speed differences between models and observations at 060000Z, correspond to the presence of a moderate geopotential height gradient at 925 mb level (Figures 86 and 87). Table V shows that averaged over the time period, the WOCSS model performed best in forecasting wind speeds. The WOCSS model has a standard deviation closer to the observed standard deviation, signifying it has a better handle on the observed wind speed variability. The RMSD in Table V shows that the likely error of the WOCSS model is lower than the other models and the low bias noted previously is persistent in this layer as well and has become negative. The model mean temperatures at this layer (Table V) show greater error than at the surface layer (Table IV) again hinting at possible reasons for the greater wind speed errors seen at this layer.

Layer three mean wind speeds over the time period (Figure 67) continue to show the lag and secondary maxima as in the previous layers. Table VI shows the WOCSS model's mean wind speed averaged over the time period is closer to the observed wind speed than the other models, still, the standard

deviation does not show the amount of variability as seen in the observations. The speed problems between the models and observations at 060000Z are also seen in this layer. The bias is significantly lower than all other models and has thus far shown an increasing negative bias with height increases. Table VI also shows that the temperatures of the finer domain MM5 models are closer to the observed mean temperature averaged over the time period.

Layer four shows the observed mean wind speed fairly constant until 051800Z August at which time the winds increase speed by approximately four meters per second and then decrease by the same amount 12 hours later to return to approximately three meters per second (Figure 68). Although the observed wind speed is constant (with the exception of the 052100Z-061200Z period), the models continue to force diurnal fluctuations throughout the time period. The WOCSS model performs best in forecasting wind speeds when averaged over the period (Table VII) but once again it does not accurately depict the variability with its standard deviation lower than the other finer domain models. The RMSD of the WOCSS model has the lowest value of all MM5 domains with the exception of the 81 kilometer domain. Once again, the lower WOCSS model bias is seen in this layer but the increasing negative bias trend with height has stopped (Table VII).

In layer five (Figure 69), the same trends as in lower layers (wind speed lags and secondary maxima) are seen throughout the time series. The model forecasts are more closely packed around the observations with the exception of

the very beginning and end of the forecast period. Table VIII shows the MM5 3 and 9 kilometer domain models forecasted better average wind speeds at this layer than the WOCSS model but the WOCSS model shows a lower RMSD. The MM5 3 kilometer domain model continues to show a closer standard deviation as compared with the observed standard deviation. The WOCSS model shows a larger bias than the other models and is once again the only model with a negative bias. With the exception of the WOCSS model, all models also show a lower bias for wind speed than lower layers. At this layer the MM5 3 kilometer domain model showed the best mean wind speed compared to the observations. The WOCSS model underestimated wind speeds but consistent with lower layers it shows less error and less variability. The mean temperature for the MM5 3 and 9 kilometer domains models are less than a half degree (C) from the observed mean temperature.

In layer six, from 041200Z August through 06000Z August all models follow the observations fairly well remaining within about one meter per second (Figure 70). Outside the aforementioned time frame the models do not perform as well. At this layer, like the previous layer, the WOCSS model shows no superiority in forecasting wind speeds. The MM5 27 kilometer domain model does best at forecasting wind speeds as can be seen in Table IX and with the MM5 3 kilometer domain showing the closest approximation to the observed standard deviation. No model shows a clear superiority in the RMSD column

and, with the exception of the 81 km domain, the WOCSS model bias is again the most negative of all models.

B. WIND DIRECTION

Wind direction for the study area's topography is very challenging to forecast due to the close proximity of the domain to the ocean, the mountain ranges and significant temperature differences within short distances. All directions in this thesis will be in true degrees based on the true north direction of a compass. The northwest-southeast orientation of the SOCAL bight region gives light and variable land breezes and sea breezes from a west-southwest direction. In the statistics discussion that follows, the point needs to be made that wind direction error was not computed for model winds or observed winds less than 3 ms^{-1} due to the variable nature of such winds. This may bias the statistics towards layers away from the surface where wind speeds tend to be higher.

Figure 71 shows the surface layer, observed wind directions show the diurnal fluctuation of the study area with the peak sea breeze occurring at approximately 0000Z daily with an average direction of 250° and land breezes occurring at 1200Z daily with an average direction of 120°. The times of the peak maximum wind directions correlate well with the times of wind speed extrema described above. At the surface, all models capture a diurnal land-sea breeze effect but do not do give an accurate reproduction as compared to the observed wind direction. The MM5 81 kilometer domain consistently forecasts maximums

too extreme from observed wind directions and shows a three hour lag in peak wind direction during the warm part of the day (sea breeze), it does however, accurately capture the time of the peak wind direction during the cold part of the day but the direction is more easterly than the observations suggest. The other models do slightly better at simulating wind directions but still do not show any consistency in following a trend. During the initial period from 041900Z August through 050700Z August all models, with the exception of the 81 kilometer domain MM5, are fairly representative of the wind direction as compared to the observations. After 050700Z August, the models depart from the observed wind directions and do not seem to regain an accurate portrayal of them. All finer domain models are muddled together throughout the period with none showing a clear advantage over another. Table IV shows the average wind direction over the time series. The mean wind direction of the MM5 3 and 9 kilometer domains show a mean that is more representative of the actual wind direction mean. The WOCSS model also provides a fairly decent representation of the mean wind direction.

The wind direction standard deviation time series (Figure 72) shows that all finer domain models perform better during sea breeze episodes but also have a notable lag of at least three hours. This time series also prominently displays that the 81 kilometer domain MM5 has significant rapid changes in wind direction when shifting between land and sea breeze regimes.

The RMSD time series (Figure 73) give confirmation the models perform better during sea breeze regimes. The WOCSS model throughout most of the period shows a lower RMSD but after 061500Z August it starts to increase its error showing no clear advantage. Table IV shows the averaged RMSD of all models are reasonably close to each other with the MM5 27 kilometer domain model having a slight advantage in accuracy. The observed standard deviation is packed closely with the RMSD values, indicating that the models show forecast skill according to the Kuypers (2000) criterion.

The wind direction bias time series (Figure 74) shows the tendency for the MM5 81 kilometer domain model and WOCSS model to overestimate wind direction during the warmer times of day, namely 050000Z-050300Z and 060000Z-060300Z. The MM5 3 and 9 kilometer domain models have a bias that indicate very little deviation from the wind direction observations during the day time with the MM5 27 kilometer domain model showing a slight overestimation during this time. During the cold times of day, all models show an underestimation of wind direction with the WOCSS model showing a more negative bias than the other models. Table IV shows that averaged over the period, the 81 kilometer domain MM5 model has the smallest bias followed closely by the 9 kilometer domain MM5 model.

At layer two, diurnal wind shifts are still seen in the observations and models (Figure 75). The MM5 81 kilometer domain model continues to overemphasize and lag the observed wind directions. The other models capture

the peak sea breeze relatively well but do poorly in simulating the land breeze. Table V shows the WOCSS model's mean wind direction over the period is almost identical to the observations. All other statistics for the WOCSS model do not show it to be a clear advantage over the other models.

Figure 76 shows the models at layer three perform extremely poorly during the transitions from land to sea breeze. All models simulate the actual sea breeze peak very well, but onshore flow extremes are very poorly simulated. Overall it is unclear whether any of the models outperforms the other at this layer. Table VI also emphasizes the poor model simulation of layer three with the mean wind directions for all models at least 60° to the east of the observed wind direction mean. Standard deviation for the MM5 3 kilometer domain model is close to that of the observed standard deviation but the other models are not within an accurate level of tolerance. The 81 kilometer domain MM5 model has a lower RMSD but this low error is most likely due to its coarse resolution. Based on the bias, the 3, 9 and 27 kilometer domain MM5 models show a strong tendency to underforecast wind direction at this layer while the WOCSS model shows a slight tendency to overforecast the directions.

Layer four shows a fairly constant observed wind direction from the beginning of the period until 051800Z August (Figure 77). This is consistent with the rather uniform wind speed at this layer. All models still force the diurnal land-sea breeze wind shifts at 0300Z and 1500Z in this layer although observations suggest otherwise. The models plainly do not have a good grasp of this layer.

Table VII shows the best model simulation of the mean wind direction is done by the 81 kilometer domain MM5 model but the observed standard deviation is best simulated by the MM5 3 kilometer domain model with the 27 kilometer domain showing the lowest RMSD.

At layer five, the simulated wind direction fluctuation can once again be seen (Figure 78) although the wind shifts are not as strong as layers three and below prior to 050600Z August. The models continue to do poorer during cold times and better during the warm times. Table VIII shows all model mean wind directions are significantly different from the observed wind directions. The standard deviation also show the variability observed is not well represented by the models. The 9 kilometer domain MM5 model shows a standard deviation closer to the observed standard deviation and has a lower bias than the other models, but none of the models stand out as a better performer.

At layer six (Figure 79), all models (except the 81 kilometer domain MM5 model) depict wind directions accurately at 050600Z August and 051800Z August. The remainder of the time series shows the models do not simulate the wind directions accurately. Table IX shows the mean wind directions averaged over the time period show a more easterly direction being off in direction by at least 150°. All other statistics also show the poor model performance in this layer with the 27 kilometer domain MM5 providing the most accurate simulation as compared with the other models.

C. VERTICAL PROFILE COMPARISONS

The statistics do not give any indication of one model being superior in forecasting wind direction. Figure 80 through Figure 85 depict mean vertical wind speed, wind direction and temperature profiles averaged over the verification area for comparing the three finer grid spacing models to observations at synoptic times. Overall, the models all do equally poorly in the vertical and never seem to get the correct structure as compared with the observations. Note that when referring to the vertical profiles, a height of "0" encompasses the entire surface layer (0-30 meters above ground level), with layer two depicted from "0" to "500" meters above ground level, etc. Table III lists the minimum and maximum heights for layers one through six.

The model vertical profile comparison for 041200Z August (Figure 80) shows the WOCSS model wind speed curve has the same overall positive slope as the mean observation profile but does not do well in simulating the wind speeds. At the surface the WOCSS model shows a wind speed higher than observed and decreases with height until layer two at which point the wind speeds increase. The 3 and 9 kilometer domain MM5 models show an overall negative slope with height and have much higher surface wind speeds than the WOCSS model or observed wind speeds. The wind direction comparison for this time also shows a disparity in the vertical. As noted above, the wind direction at layer four shows a significant difference between modeled and observed winds. The temperature profile shows the models have a significantly higher

temperature than the observed temperature, which is quite possibly one reason for the wind high wind speed discrepancy at the surface. The observed inversion occurs approximately in layers two and three while the models show the inversion only up to layer two. The models do an excellent simulation of the temperature profile in layers four through six.

At 050000Z August the model wind speed curves (Figure 81) all show the same general shape as the observed wind speed. The actual speeds however show significant discrepancies above the surface layer. The models also show the maximum wind speed in layer two which incidentally coincides with the minimum observed temperature. Below layer three the models do not accurately replicate the observed temperature structure although the surface temperature is very close. Within and above layer three, the models follow the temperature slope of the observations but all show cooler temperatures as compared with the observations.

The 051200Z August vertical profile (Figure 82) shows a large difference between observed wind speed and all model wind speeds. All model wind directions also are simulated very poorly but layer four also shows an extreme difference of approximately 200°. The surface temperatures of the models are warmer but cool faster than the observed temperatures above the surface layer.

Wind speed vertical comparison at 060000Z August (Figure 83) shows the models perform poorly in all layers. The WOCSS model does not accurately capture the surface layer well and its vertical structure is more deviant from the

observed wind speeds than the MM5 models. Both MM5 models show a maximum wind speed in layer two which compares with the observations, however, the models' wind speeds are significantly lower than the observed wind speeds. Additionally, the observations show a gradual decrease in wind speeds above layer two but the models show an abrupt decrease. It should be noted that this time period corresponded to the presence of the moderate geopotential height gradient along SOCAL which may have not been accurately depicted in the model forecasts (Figures 18, 86 and 87). The observed wind directions for this time are closely modeled at the surface but diverge above this layer. The models all converge at layer five to a direction of 55° which is almost opposite of the observed wind direction at this height. The observed temperature structure shows an inversion layer between layers two and three that is shown to be fairly isothermal in the models. Above the inversion layer the model shows the same temperature lapse as the observations, but with colder temperatures.

In the 061200Z August vertical profile (Figure 84) the slope of the WOCSS model and the 9 kilometer domain MM5 model follow the general slope of the observed wind speeds. The 3 kilometer domain MM5 model does not follow the observed slope as closely showing a significant difference in layer four. The modeled wind directions on the surface all are within 20° of the observed wind direction. The MM5 models follow the general slope of the observations showing an initial veering with height and the backing above layer two returning to veering and then backing again further up in the atmosphere. The WOCSS model shows

continued backing with height up to layer six. In layer five, the observed wind direction is almost 100° different from either model. The temperature profile shows the MM5 once again displays higher than observed surface temperatures which cool more rapidly than the observed temperatures with height.

At 07000Z August (Figure 85), the WOCSS model's wind speed is significantly lower than the other models and observed wind speeds. In layer two, the MM5 models and the observed wind speeds converge to 3.5 meters per second but the WOCSS model shows a wind speed of 1.5 meters per second. Above layer two, the models all converge and depict essentially the same wind speeds (within 1 meter per second) up to layer five at which point the WOCSS model shows less wind speed (and closer to the observed wind speed) than the MM5 models. All models (above layer three) seem to correctly simulate the slope of the observed wind speeds but are overly high. The wind direction vertical profile shows a significant departure of the model wind direction from the observed wind direction above layer two. In layer five, the difference between actual and observed wind directions are over 200° with the models showing a more northeasterly direction as compared to the west-southwesterly direction of the observations. The vertical temperature profile of the models show a slope very similar to that of the observed temperature profile but the models remain 2°-3° cooler than the observations.

VII. SUMMARY

In evaluating whether simulating winds on complex terrain using a simple diagnostic model provided just as accurate, if not more accurate surface wind forecasts as running a full physics mesoscale model, this study showed that the WOCSS model was just as accurate as the MM5 3 and 9 kilometer model forecasts. The wind speeds of the WOCSS were better forecasted than the finer grid spacing MM5 domains as a whole. The wind directions performed just as well (or poorly) as the MM5. In using the WOCSS model for forecasting winds on complex terrain, this study showed that there is just as much accuracy with the scaled down diagnostic model as with a full physics mesoscale model. For end-users wishing only to receive accurate wind forecasts, the WOCSS model provides a forecast comparable to that of the MM5 with a significant savings in computing resources. Although, this study only encompassed a small time period, the results are encouraging.

It is important when forecasting on the mesoscale that the background (synoptic scale) pattern is accurately represented. The problem noted at 060000Z August in the discussions above show that the synoptic scale errors when reflected on the mesoscale present very inaccurate forecasts. Figure 86 shows the NOGAPS 1° model forecast has a relatively strong 925 mb geopotential height gradient over Point Conception with a 20 knot wind barb over the Channel Islands. The MM5 9 kilometer grid spacing model shows a weak 925 mb geopotential height gradient and weak winds over the same area

(Figure 87). This inconsistency was reflected over the SOCAL bight region and was evident at 060000Z in the time series and vertical profiles as discussed previously.

The summertime Los Angeles basin weather provided a good basis in which to test the WOCSS model. Despite the diurnal effects in temperature, wind direction and wind speed and the complex topography, the WOCSS was able to perform as well if not better than the MM5 model. With input from a different model better able to handle the complex scenario in this study, the WOCSS may have provided better results in wind direction, as it is, it did well in forecasting wind speeds.

Some of the reasons the results of the MM5 and WOCSS models did not simulate the observed winds well have to do with the complex nature of the scenario under which they were tested. The light and variable wind speeds that were observed during the nighttime land breezes are difficult to forecast and this was evident in the model forecasts being poorer during the evening and early morning hours. Another potential factor contributing to the differences between the modeled and observed winds was the finer grid spacing under which the models were run. As noted previously, many of the parameterization schemes used in this experiment were intended for coarser grid spacings and the finer model domains used in this study may go against various physical assumptions associated with applications on a larger domain (which is possibly another advantage of the WOCSS due to its simplified physics). Because of the finer

scales used in the models, the disparity between the modeled "surface" and the surface observations may have added to the differences seen between the model and observations (Monterrosa 1999). The lowest vertical level in MM5 is at 22 meters above ground level and the lowest vertical level in the WOCSS model is at 25 meters above ground level. Ludwig et al. (1991) notes the WOCSS model performs better in a stably stratified atmosphere. The vertical model comparisons (Figure 80 through Figure 85) confirm this. During the cooler hours when the observed temperature profiles show a deep stable layer next to the surface, the WOCSS model performed better in forecasting wind speeds than during the warmer periods at which an elevated inversion was seen. At 070000Z August, the vertical temperature profile shows a very slight (near neutral) negative lapse rate (Figure 85), although this is a warm time of day, the WOCSS model does better at simulating wind speeds than previous warm times that show a stronger lapse rate next to the surface.

Future studies that may be addressed as a result of this study would be to test the WOCSS under more widely varying conditions. Testing in an area that has a relatively low temperature fluctuation may provide interesting results in seeing how much the diurnal change in temperature affected the results. An experiment conducted in an area in which the diurnal wind fluctuation is not as great may also provide interesting results in support of simple diagnostic models. Another test would be to examine a case where the MM5 does better in forecasting wind speeds and directions on the larger spacing domains (nine

kilometers) and investigate if the WOCSS low speed bias makes it perform poorly. Testing the sensitivity of the WOCSS model parameters discussed in Ludwig and Sinton (2000) is another area that may also be addressed future studies. A wintertime scenario may also lend to the strength of the WOCSS's potential and add more information to the understanding of the diverse conditions under which the model may be operated successfully. Conducting an experiment during frontal passage or in a mesoscale circulation such as a low pressure system or other eddy type feature is another possible focus for future studies. Initializing the WOCSS model with a mesoscale model other than MM5, such as the Navy's Coupled Ocean/Atmosphere Mesoscale Prediction System (COAMPS) model, would assist in confirming or refuting these findings. Studies on the apparent lag during warm time periods would prove beneficial to potential users as would trying to correct wind directions at elevation, although this may simply be due to the input model that is driving the WOCSS model.

The WOCSS model is a serious contender for forecasting winds on complex terrain. The original hypothesis, that running a mesoscale model at relatively coarse resolutions and feeding its results into a simple diagnostic model designed to adjust the winds to fine-scale topography will provide just as accurate if not more accurate surface wind forecasts as running a mesoscale model at very fine resolutions, is still valid. The WOCSS model provided more accurate wind speeds than the MM5 model and comparable wind directions. In this study, the WOCSS model may have given reasonable results because its

low speed bias and the high speed bias of MM5 may have partially cancelled one another implying that the WOCSS model gave the right answer for the wrong reason. With continued tests and development, the WOCSS model could prove to be a very reliable forecasting tool.

THIS PAGE INTENTIONALLY LEFT BLANK

APPENDIX A. TABLES

The following pages of tables are grouped together in this appendix for easier reading.

Nested Grid Domain Details

Domain	Horizontal Resolution	Terrain Resolution	Land use Resolution	No. of X Gridpoints	No. of Y Gridpoints
1	81 kilometers	19 kilometers	19 kilometers	41	45
2	27 kilometers	19 kilometers	19 kilometers	43	43
3	9 kilometers	9 kilometers	9 kilometers	73	73
4	3 kilometers	1 kilometer	1 kilometer	97	97

Table I. Nested grid domain details.

Station ID	Latitude	Longitude	Elevation (m)
Surface Stations			
ACTN	34.45 N	118.20 W	793
ANAH	33.82 N	117.91 W	45
BRBK	34.18 N	118.32 W	168
CALB	34.15 N	118.61 W	320
ELDO	33.80 N	118.09 W	5
ELRO	34.26 N	119.13 W	34
EMMA	34.29 N	119.33 W	3
HAWH	33.93 N	118.37 W	21
IRVI	33.69 N	117.72 W	125
LANM	34.07 N	118.24 W	87
MBLD	34.24 N	117.65 W	1219
MILL	34.38 N	118.07 W	1070
NLGB	33.82 N	118.19 W	6
OJAI	34.45 N	119.27 W	231
PICO	34.01 N	118.06 W	75
PIRU	34.38 N	118.79 W	195
ROSE	34.54 N	119.18 W	1016
STAM	34.04 N	118.48 W	104
SVAL	34.28 N	118.68 W	310
SVLM	34.29 N	118.80 W	366
TOMP	34.21 N	118.87 W	232
SCLA	34.39 N	118.53 W	375
TUST	33.70 N	117.82 W	5
Rawinsondes			
EDW	34.90 N	117.92 W	723
PMG	34.11 N	119.20 W	2
POM	34.07 N	117.75 W	274
TUS	33.70 N	117.83 W	17
UCL	34.06 N	118.45 W	149
Profilers			
EMT	34.09 N	118.03 W	95
LAS	33.79 N	118.05 W	7
LAX	33.94 N	118.44 W	47
PDE	34.61 N	118.09 W	777
PHE	34.16 N	119.22 W	2
SMI	34.28 N	118.79 W	279
TTN	33.71 N	117.84 W	16
USC	34.02 N	118.28 W	67
VNS	34.22 N	118.49 W	241

Table II. Station location and elevations.

Layer	Lower Limit (m)	Upper Limit (m)
1	Surface	30
2	30	500
3	500	1000
4	1000	1500
5	1500	2000
6	2000	2500

Table III. Layers used to evaluate model statistics. All heights are meters above ground level.

COLD Case
Cold Start
Gayno-Seaman PBL Scheme

Surface Layer

Wind speed	Mean	StdDev	RMSD	Bias
Obs	2.028	0.991	--	--
81km	3.419	0.576	2.570	1.390
27km	3.584	1.428	2.829	1.557
9km	3.679	1.538	2.663	1.652
3km	3.660	1.793	2.757	1.631
WOCSS	2.409	1.314	2.049	0.381

Wind direction	Mean	StdDev	RMSD	Bias
Obs	194.865	73.535	--	--
81km	206.566	35.580	80.094	2.030
27km	175.714	52.660	78.164	-4.736
9km	192.460	59.982	78.243	-2.357
3km	196.540	67.183	78.930	3.845
WOCSS	197.640	56.768	78.551	3.718

Temp	Mean	StdDev	RMSD	Bias
Obs	27.101	3.499	--	--
81km	26.899	1.201	4.435	-0.201
27km	27.133	1.404	4.328	0.033
9km	27.324	2.061	4.088	0.222
3km	27.598	2.573	4.040	0.499
WOCSS	--	--	--	--

Table IV. Surface layer statistics.

COLD Case
Cold Start
Gayno-Seaman PBL Scheme

Layer 2

Wind speed	Mean	StdDev	RMSD	Bias
Obs	3.205	1.511	--	--
81km	6.035	1.248	4.156	2.830
27km	5.790	2.447	4.200	2.583
9km	5.093	2.486	3.733	1.885
3km	4.947	2.472	3.663	1.740
WOCSS	3.023	1.180	2.371	-0.184

Wind direction	Mean	StdDev	RMSD	Bias
Obs	189.440	64.800	--	--
81km	181.51	32.007	67.044	-0.554
27km	175.714	52.660	78.164	-4.736
9km	192.460	59.982	78.243	-2.357
3km	196.540	67.183	78.930	3.845
WOCSS	188.220	52.673	75.208	-10.09

Temp	Mean	StdDev	RMSD	Bias
Obs	27.263	3.603	--	--
81km	29.607	1.207	3.368	-0.241
27km	28.466	1.795	3.730	-1.380
9km	28.472	2.349	3.128	-1.375
3km	29.015	2.428	3.078	-0.831
WOCSS	--	--	--	--

Table V. Layer 2 statistics.

COLD Case
Cold Start
Gayno-Seaman PBL Scheme

Layer 3

Wind speed	Mean	StdDev	RMSD	Bias
Obs	3.774	1.535	--	--
81km	5.294	.929	3.271	1.519
27km	4.513	1.520	3.960	1.940
9km	5.247	2.102	3.696	1.473
3km	4.513	2.289	3.506	0.738
WOCSS	3.526	.855	2.754	-0.281

Wind direction	Mean	StdDev	RMSD	Bias
Obs	201.41	66.12	--	--
81km	152.423	28.070	65.297	0.148
27km	145.813	44.966	72.124	-4.326
9km	142.223	52.003	78.433	-4.383
3km	158.082	69.960	84.763	-5.077
WOCSS	138.128	32.569	78.37	0.739

Temp	Mean	StdDev	RMSD	Bias
Obs	30.604	1.063	--	--
81km	29.098	0.834	3.517	-3.063
27km	29.188	1.050	3.352	-2.971
9km	29.836	1.033	2.825	-2.324
3km	29.818	1.144	2.869	-2.343
WOCSS	--	--	--	--

Table VI. Layer 3 statistics.

COLD Case
Cold Start
Gayno-Seaman PBL Scheme

Layer 4

Wind speed	Mean	StdDev	RMSD	Bias
Obs	3.580	1.589	--	--
81km	4.146	0.696	2.307	0.567
27km	5.263	1.240	3.271	1.684
9km	5.356	1.682	3.442	1.775
3km	5.041	1.873	3.511	1.463
WOCSS	3.427	0.860	2.462	-0.151

Wind direction	Mean	StdDev	RMSD	Bias
Obs	224.84	66.754	--	--
81km	138.327	24.976	81.413	5.310
27km	136.265	41.707	91.217	10.959
9km	133.114	48.873	93.762	8.059
3km	134.706	61.679	93.758	14.825
WOCSS	125.297	29.774	94.074	7.481

Temp	Mean	StdDev	RMSD	Bias
Obs	28.203	1.446	--	--
81km	26.267	1.075	3.952	-3.845
27km	27.001	1.310	3.305	-3.110
9km	27.969	1.366	2.385	-2.143
3km	28.107	1.401	2.353	-2.007
WOCSS	--	--	--	--

Table VII. Layer 4 statistics.

COLD Case
Cold Start
Gayno-Seaman PBL Scheme

Layer 5

Wind speed	Mean	StdDev	RMSD	Bias
Obs	3.548	1.505	--	--
81km	3.098	0.627	2.054	-0.448
27km	4.007	1.135	2.304	0.460
9km	4.100	1.237	2.199	0.552
3km	3.991	1.348	2.428	0.444
WOCSS	2.882	0.818	2.080	-0.667

Wind direction	Mean	StdDev	RMSD	Bias
Obs	214.39	66.750	--	--
81km	131.478	29.236	91.506	16.699
27km	151.369	40.082	96.075	17.314
9km	129.643	50.567	101.636	5.314
3km	127.446	41.006	99.184	11.261
WOCSS	114.609	43.081	99.684	9.001

Temp	Mean	StdDev	RMSD	Bias
Obs	24.491	1.558	--	--
81km	22.337	1.353	3.325	-3.251
27km	23.610	1.718	2.222	-1.978
9km	24.678	1.623	1.399	-0.908
3km	24.773	1.578	1.350	-0.814
WOCSS	--	--	--	--

Table VIII. Layer 5 statistics.

COLD Case
Cold Start
Gayno-Seaman PBL Scheme

Layer 6

Wind speed	Mean	StdDev	RMSD	Bias
Obs	3.658	1.486	--	--
81km	2.720	0.571	2.104	-0.938
27km	3.474	0.934	2.186	-0.184
9km	3.430	0.952	2.229	-0.229
3km	3.279	0.980	2.266	-0.380
WOCSS	2.855	0.638	2.124	-0.800

Wind direction	Mean	StdDev	RMSD	Bias
Obs	187.51	62.062	--	--
81km	116.032	28.774	90.489	-17.471
27km	135.136	50.758	94.552	-11.944
9km	112.395	43.190	98.218	-15.109
3km	116.565	40.005	97.933	-13.852
WOCSS	116.173	31.815	95.902	-17.895

Temp	Mean	StdDev	RMSD	Bias
Obs	20.537	1.561	--	--
81km	18.303	1.339	3.278	-3.213
27km	19.687	1.768	2.001	-1.831
9km	20.795	1.641	1.143	-0.722
3km	20.909	1.592	1.034	-0.608
WOCSS	--	--	--	--

Table IX. Layer 6 statistics.

APPENDIX B. FIGURES

The following pages of figures are grouped together in this appendix for easier reading.

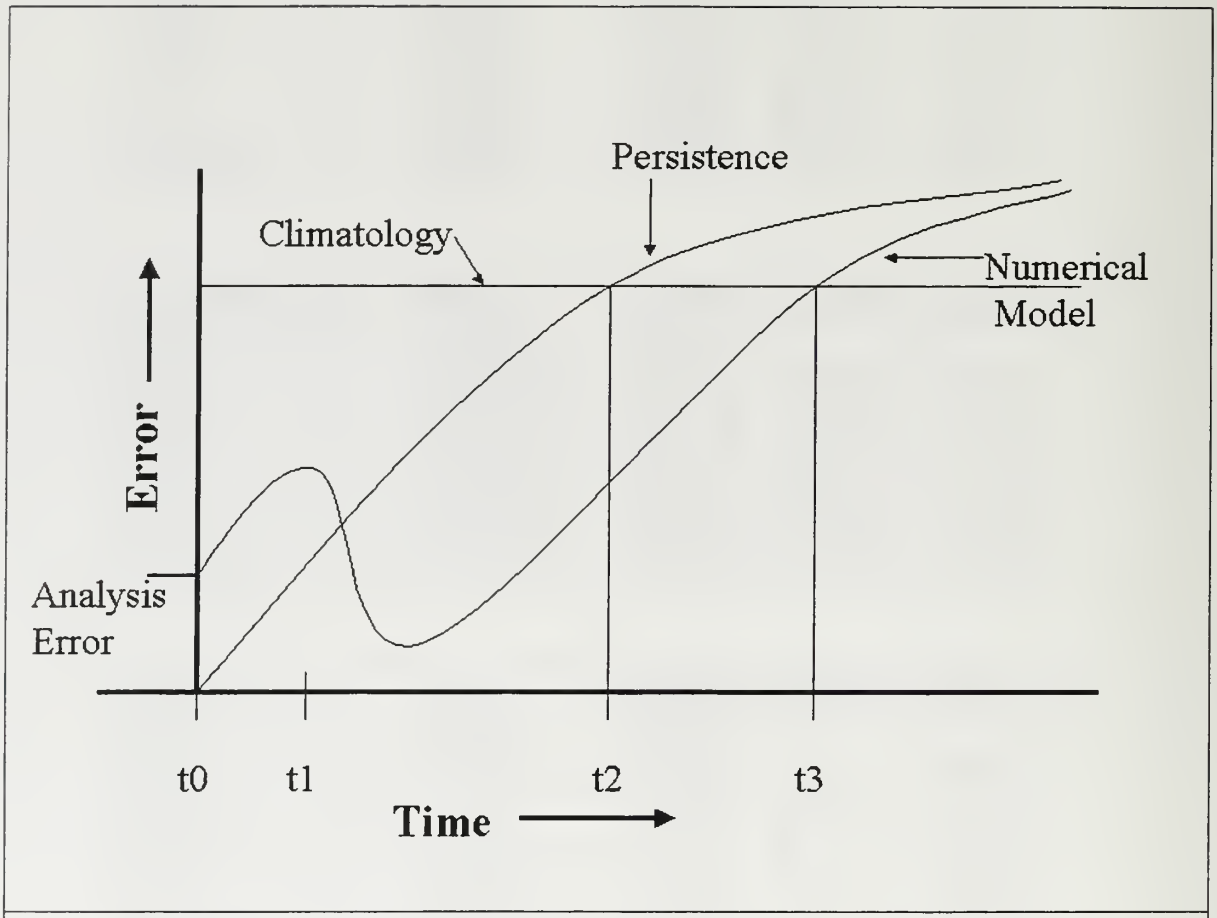

Figure 1. Theoretical Numerical Forecast Error growth curves (from Kuypers 2000).

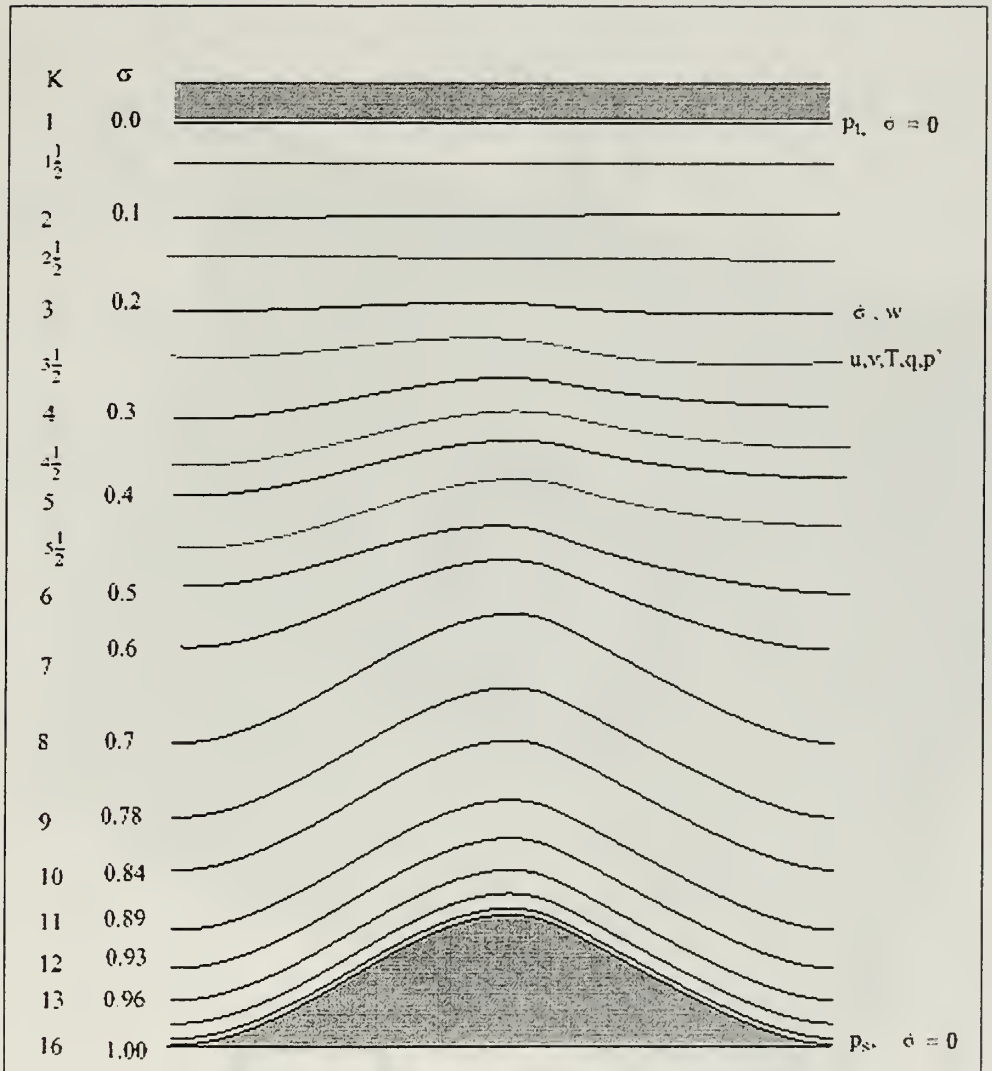

Figure 2. Schematic of the vertical structure of the MM5 model (15 vertical levels depicted) (from Dudhia et al. 2000).

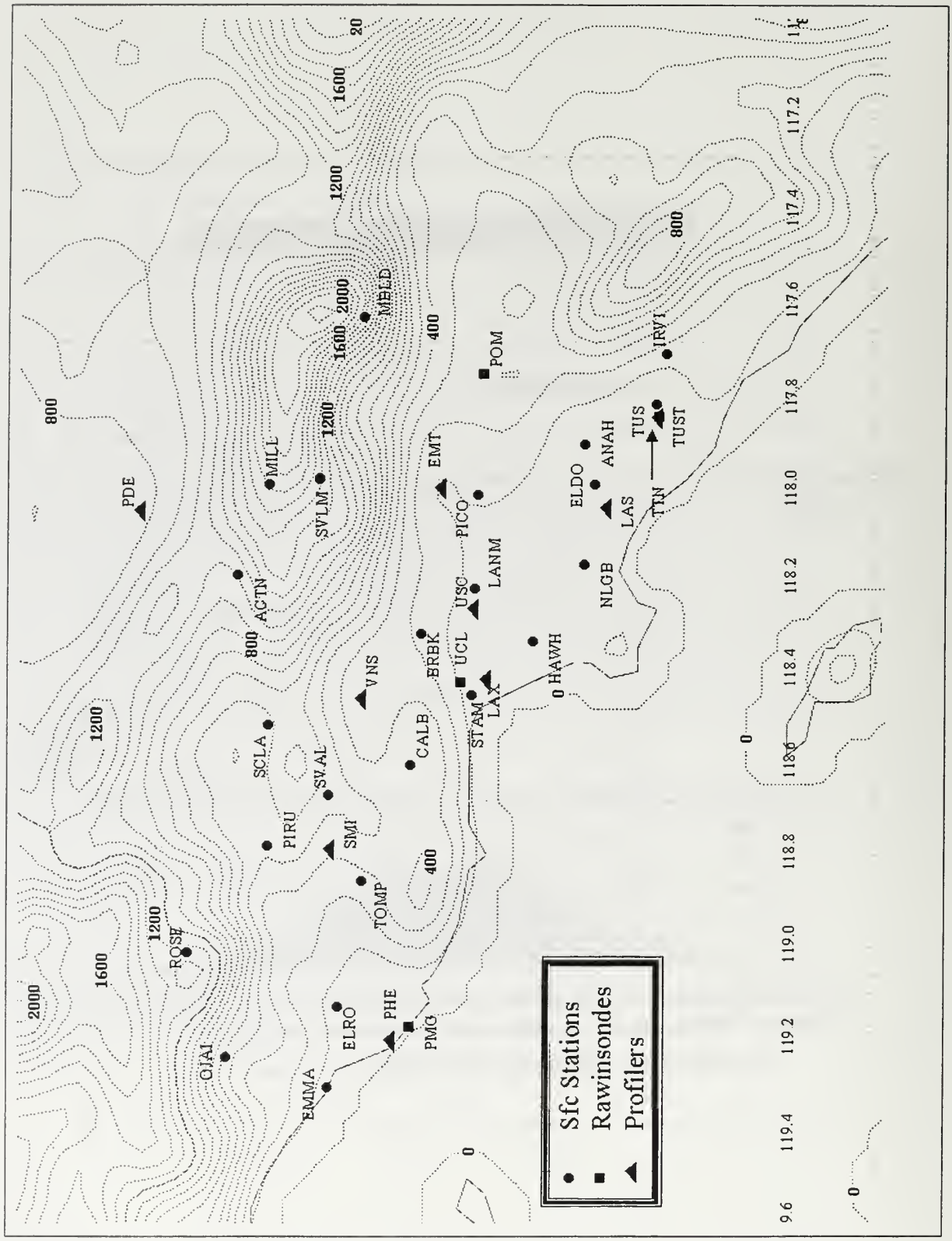

Figure 3. Area of study observation stations and 3 kilometer grid spacing terrain.

Figure 4. Grid nesting configuration.

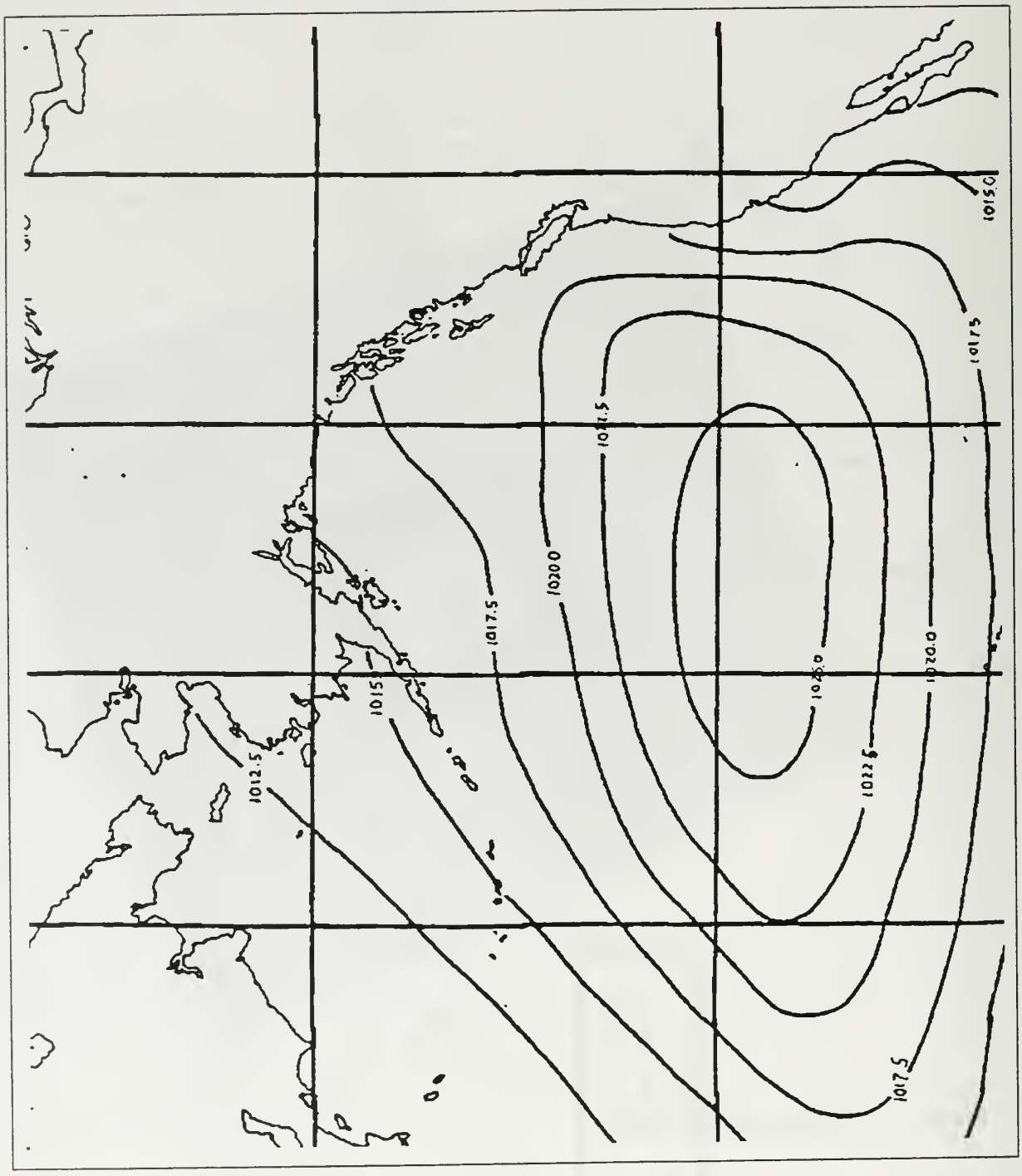

Figure 5. Summertime northern East Pacific high pressure system.

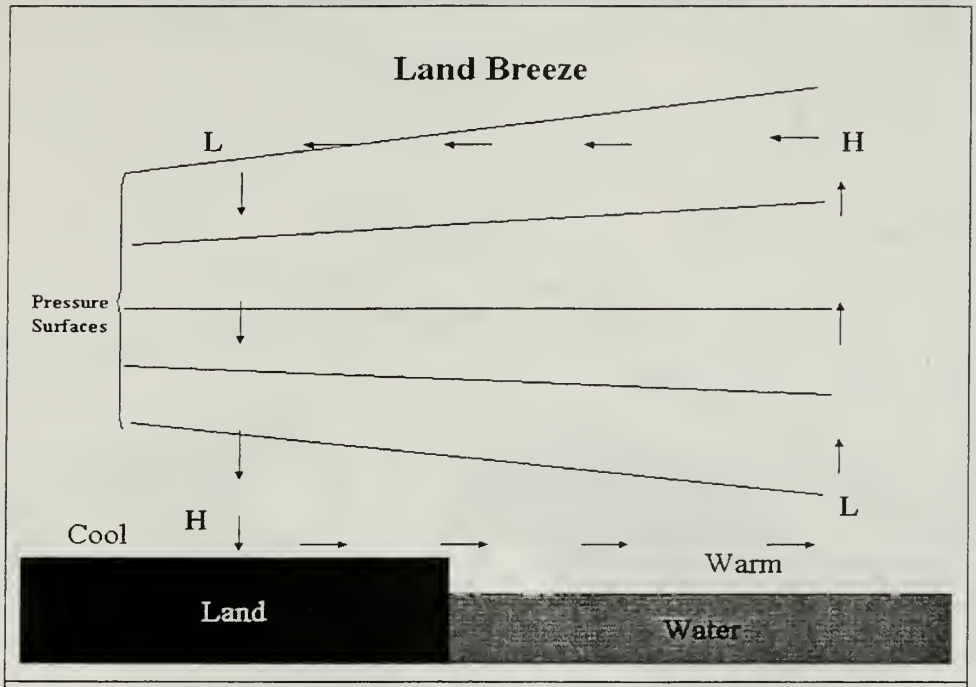

Figure 6a. Schematic of Land Breeze circulation.

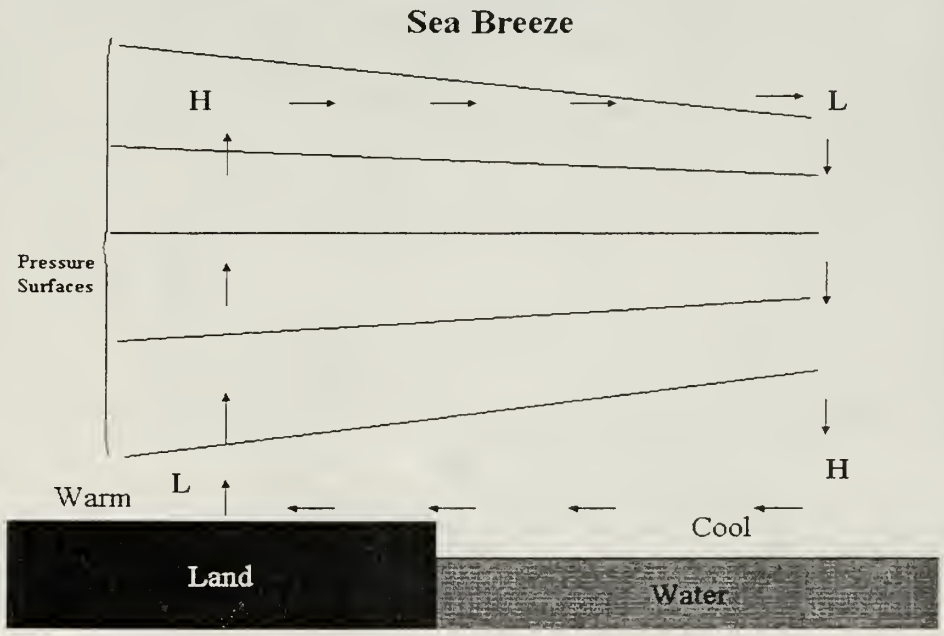

Figure 6b. Schematic of sea breeze circulation.

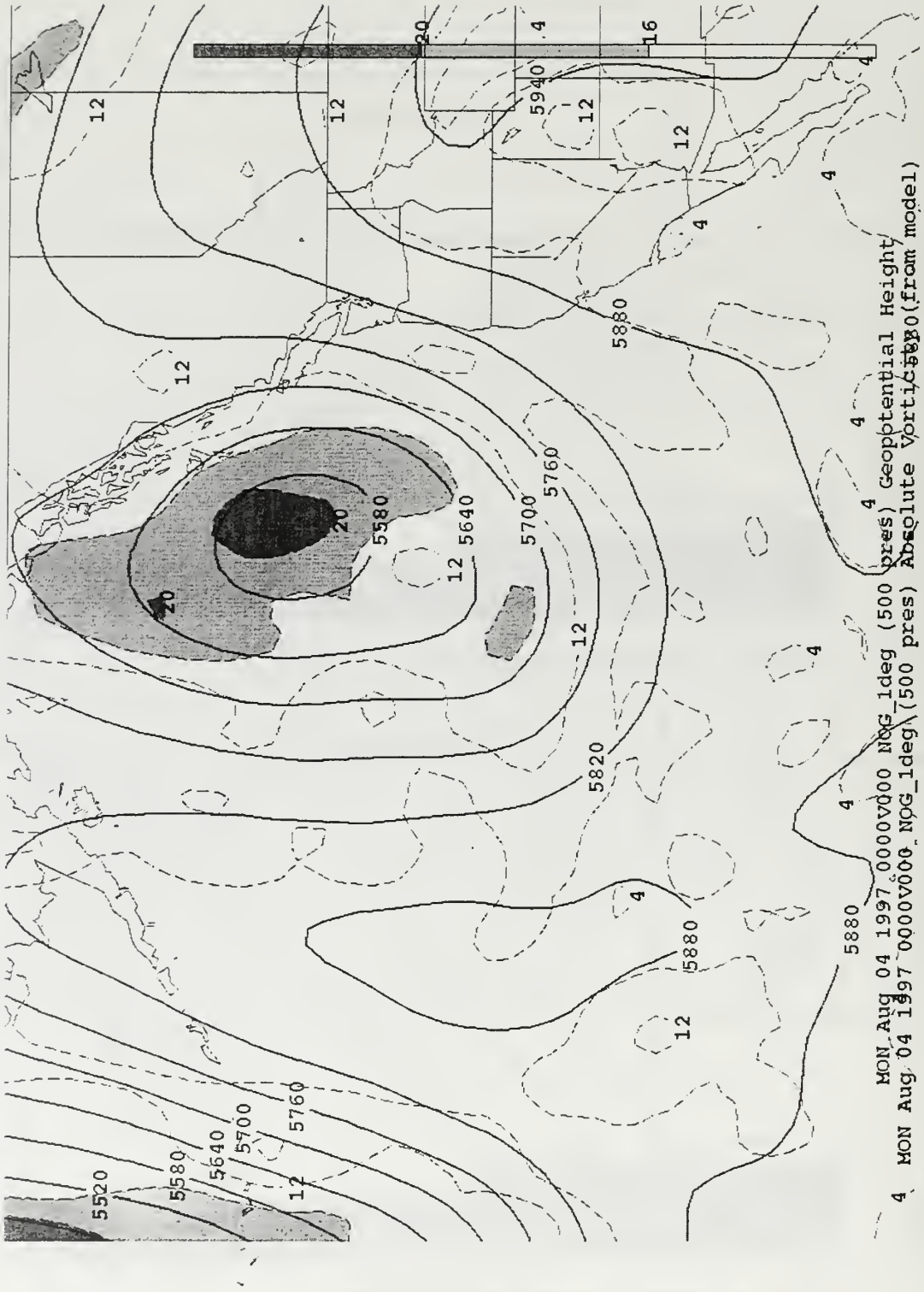

Figure 7. 040000Z Aug 97 500 mb Geopotential Heights and Abs. Vorticity.

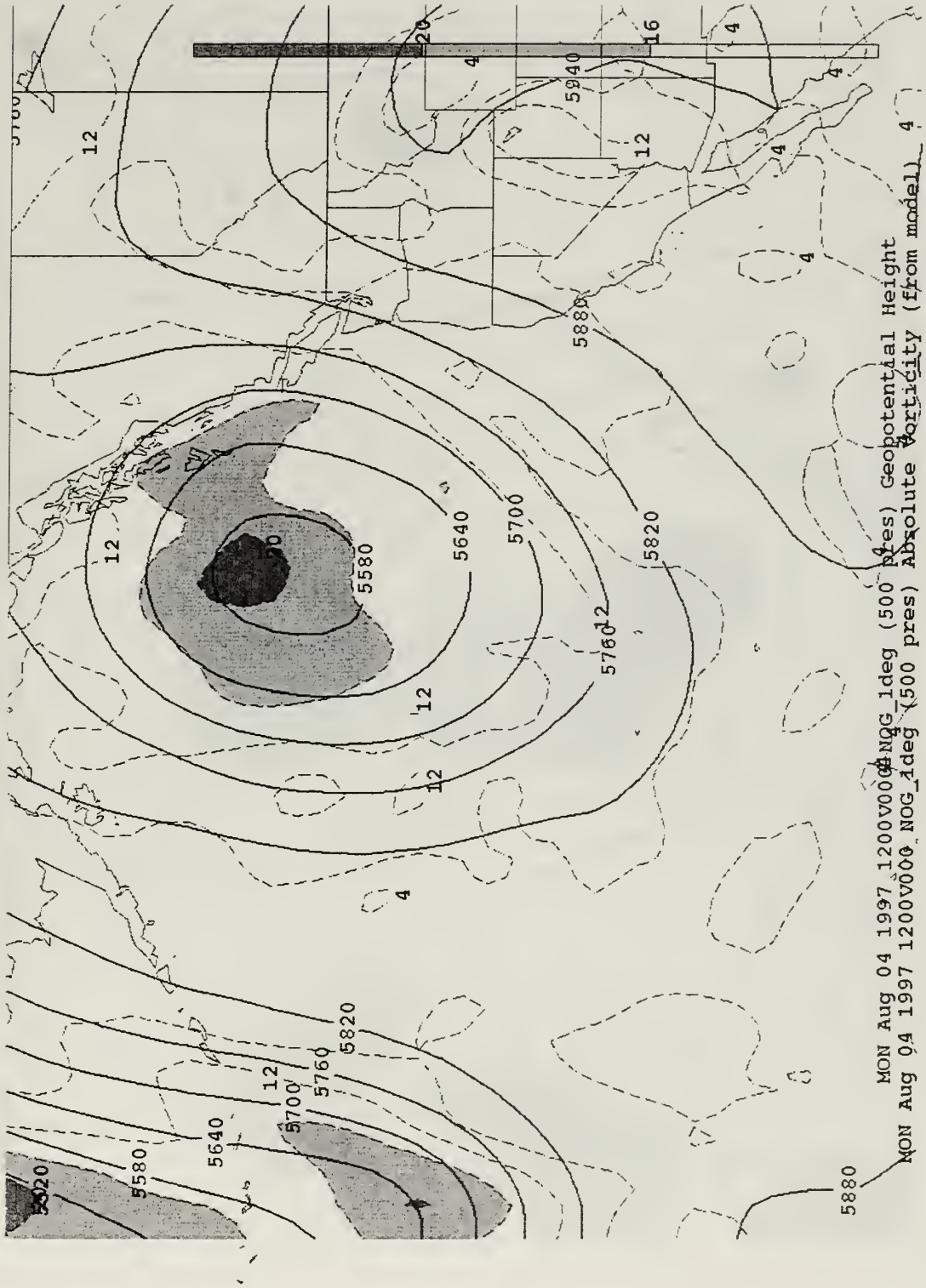

Figure 8. 041200Z Aug 97 500 mb Geopotential Heights and Abs. Vorticity.

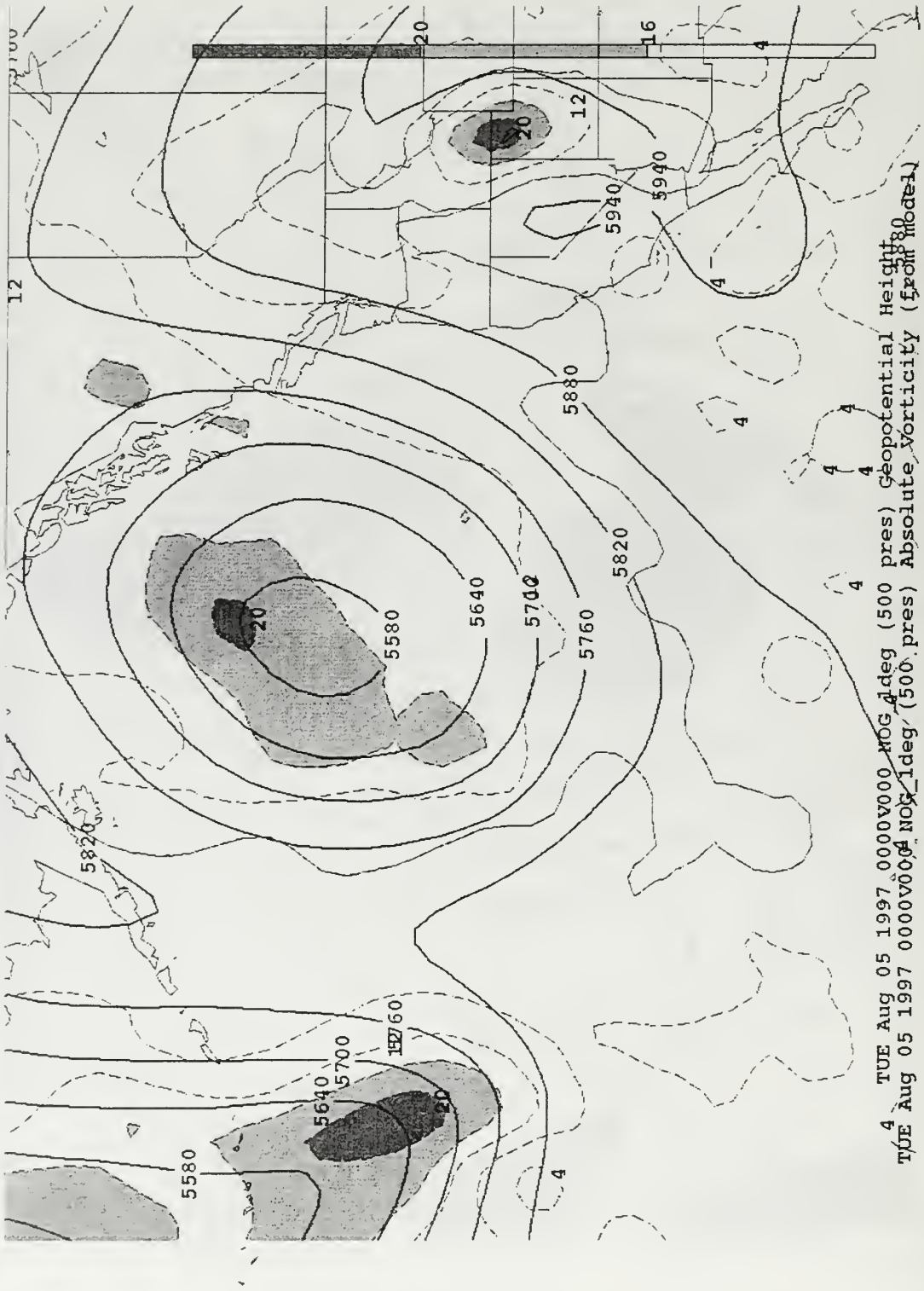

Figure 9. 050000Z Aug 97 500 mb Geopotential Heights and Abs. Vorticity.

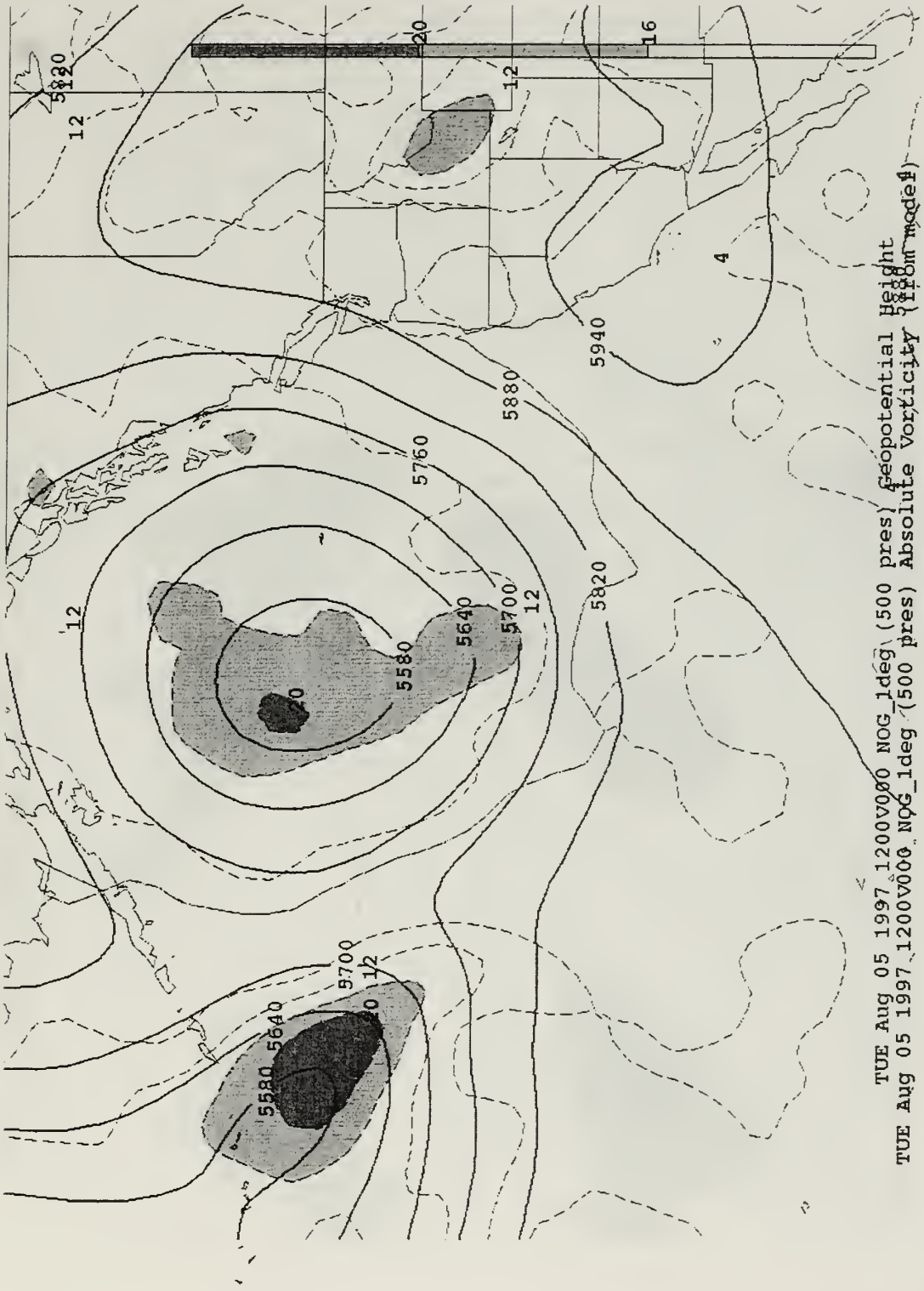

Figure 10. 051200Z Aug 97 500 mb Geopotential Heights and Abs. Vorticity.

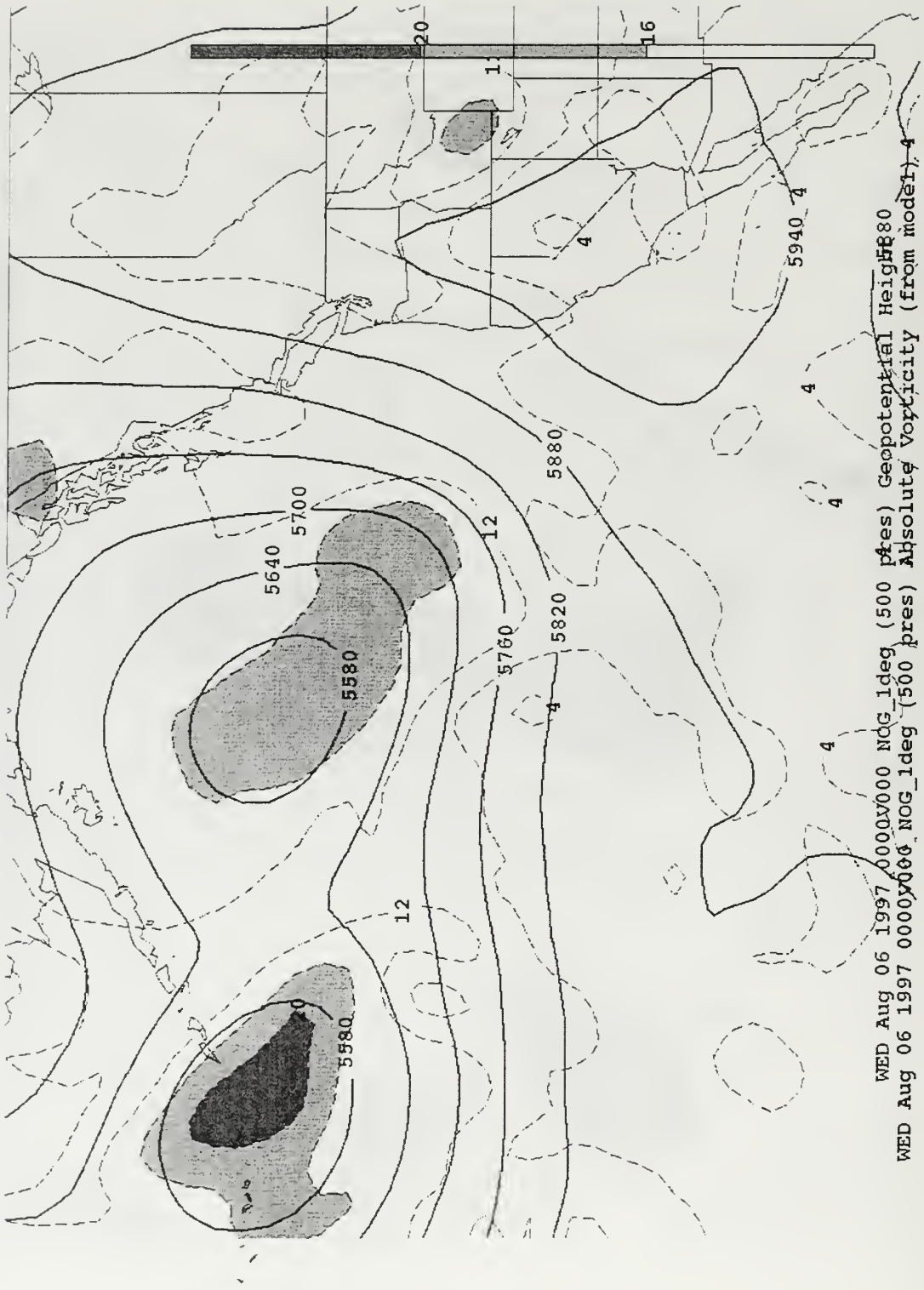

Figure 11. 060000Z Aug 97 500 mb Geopotential Heights and Abs. Vorticity.

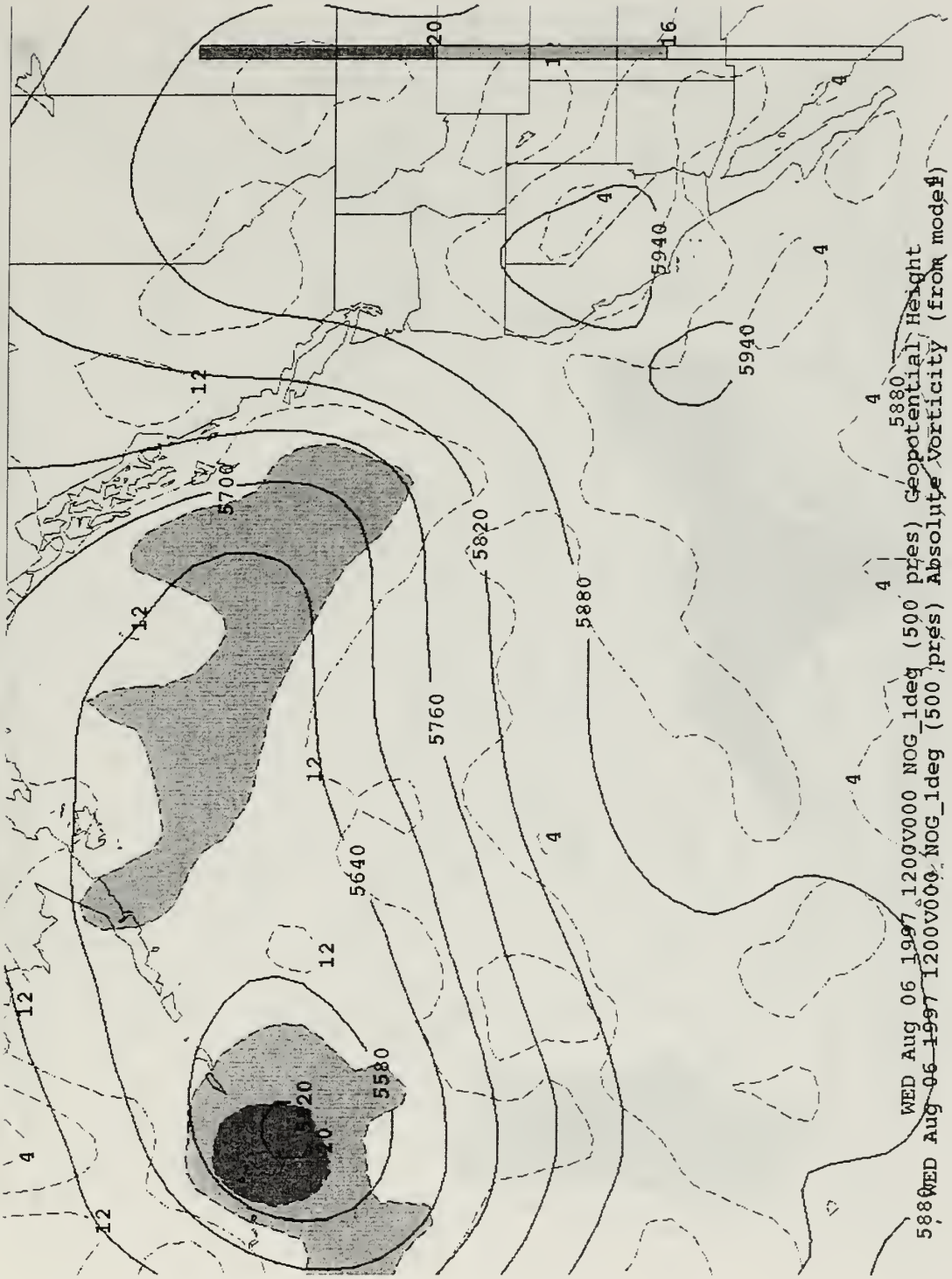

Figure 12. 061200Z Aug 97 500 mb Geopotential Heights and Abs. Vorticity.

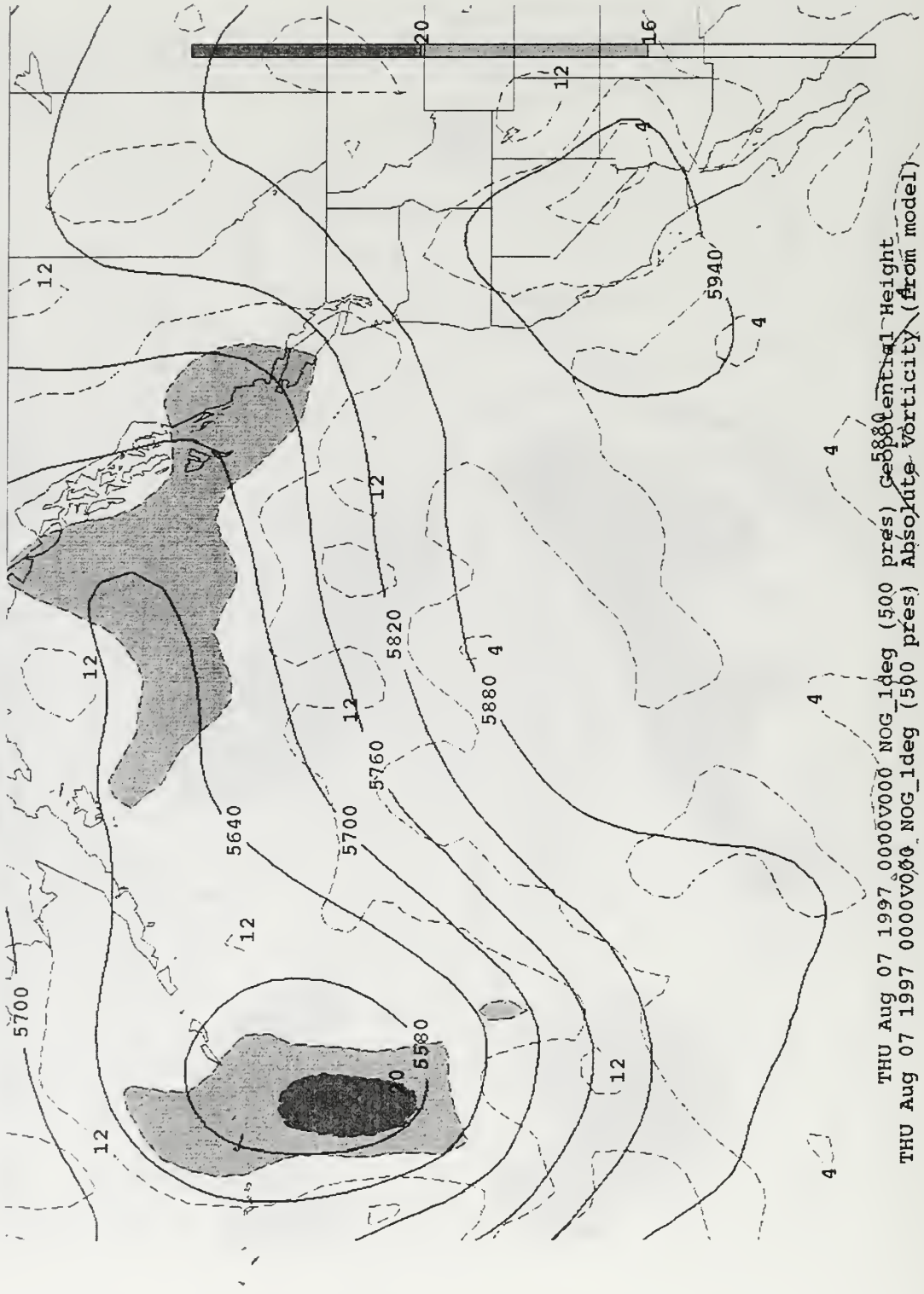

Figure 13. 070000Z Aug 97 500 mb Geopotential Heights and Abs. Vorticity.

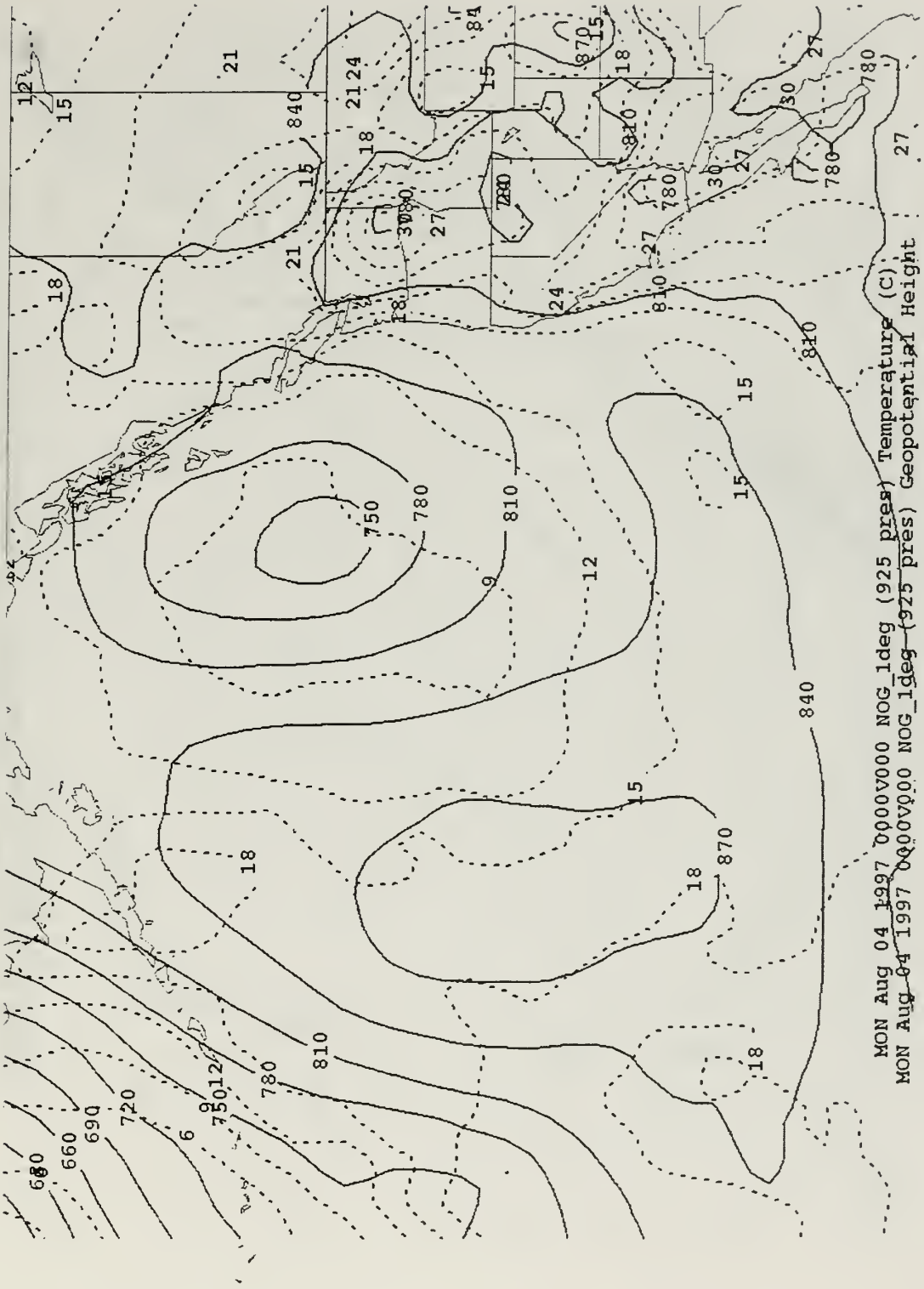

Figure 14. 040000Z Aug 97 925 mb Geopotential Heights and Temp. (C).

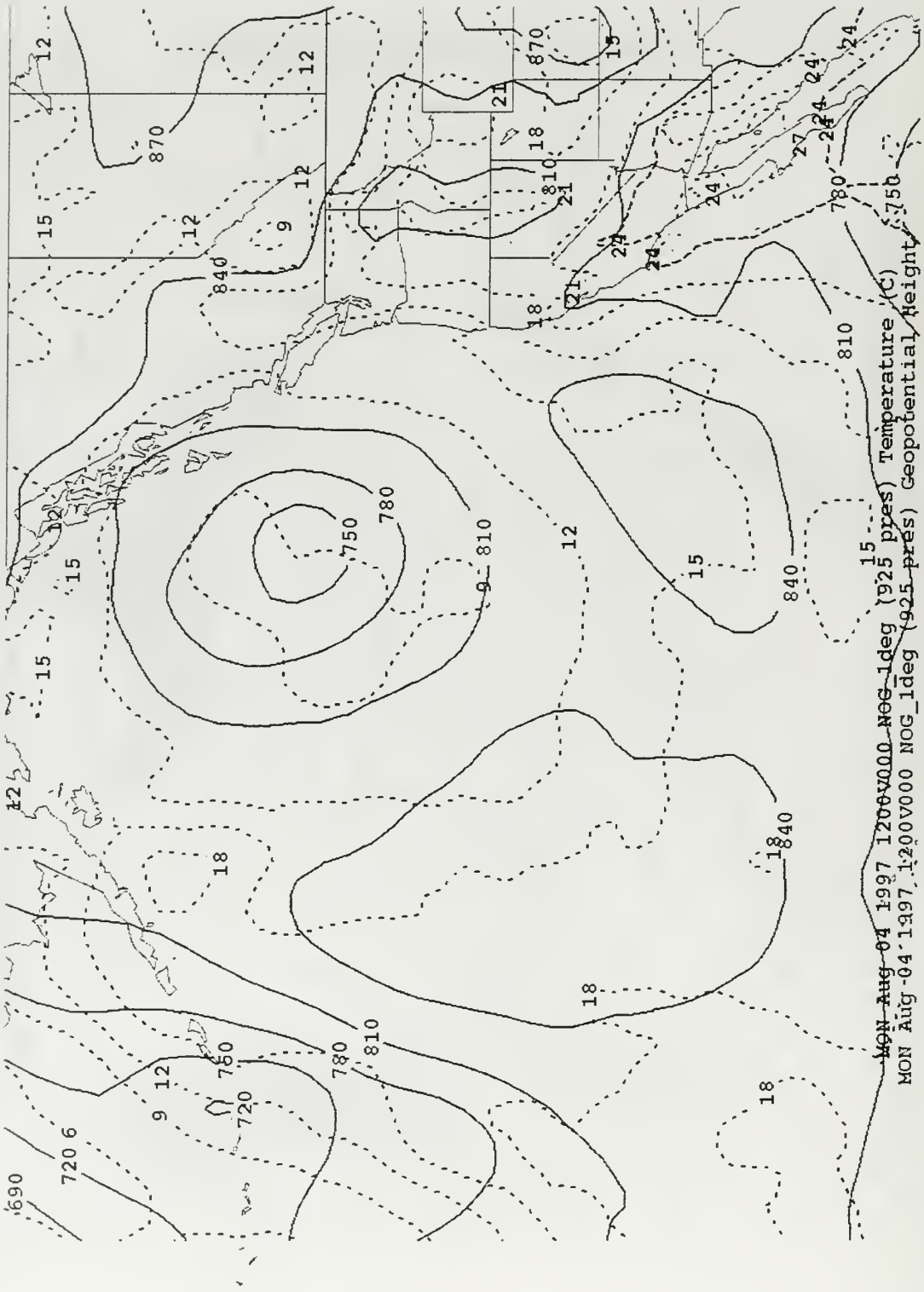

Figure 15. 041200Z Aug 97 925 mb Geopotential Heights and Temp (C).

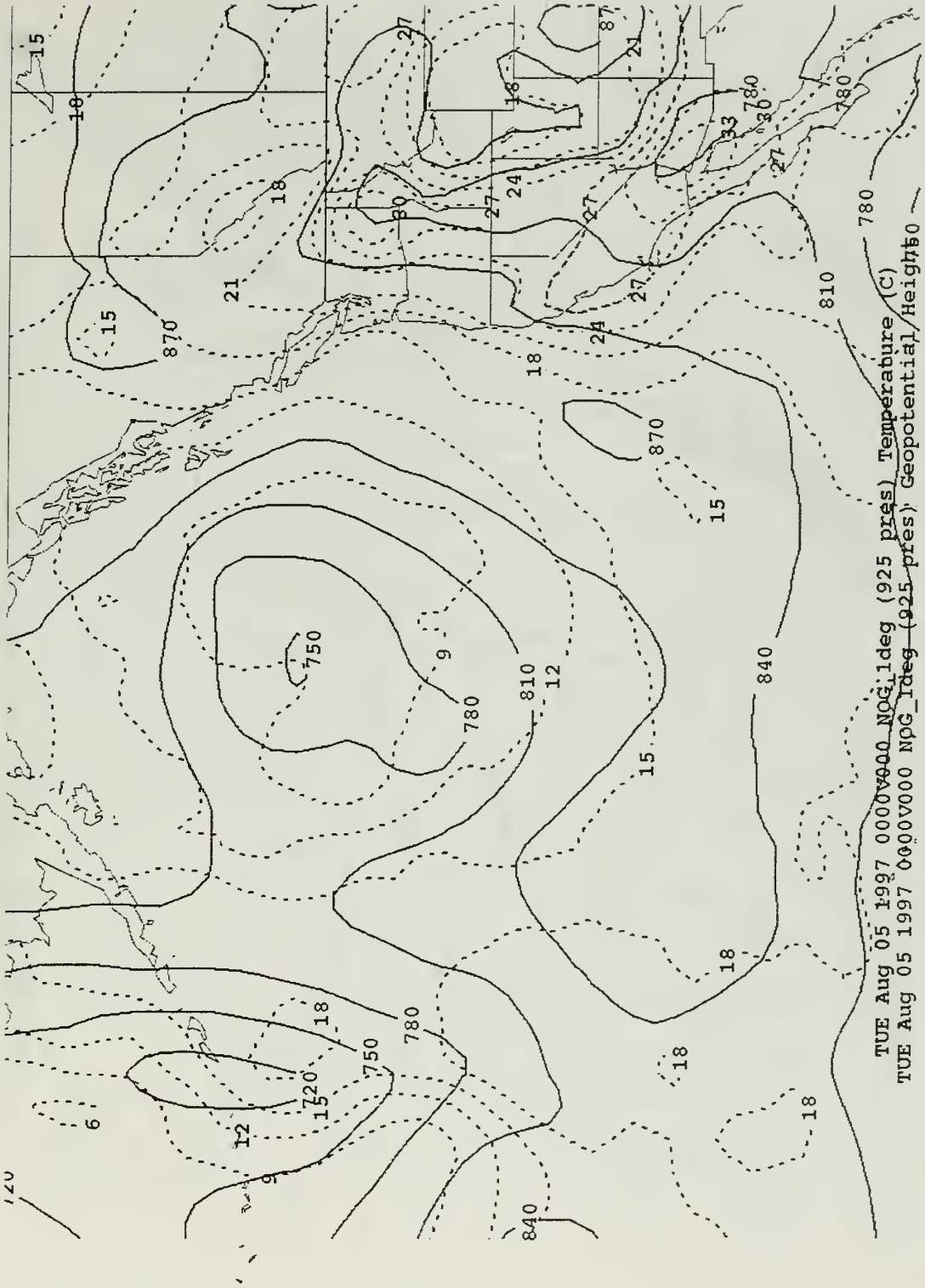

Figure 16. 050000Z Aug 97 925 mb Geopotential Heights and Temp. (C).

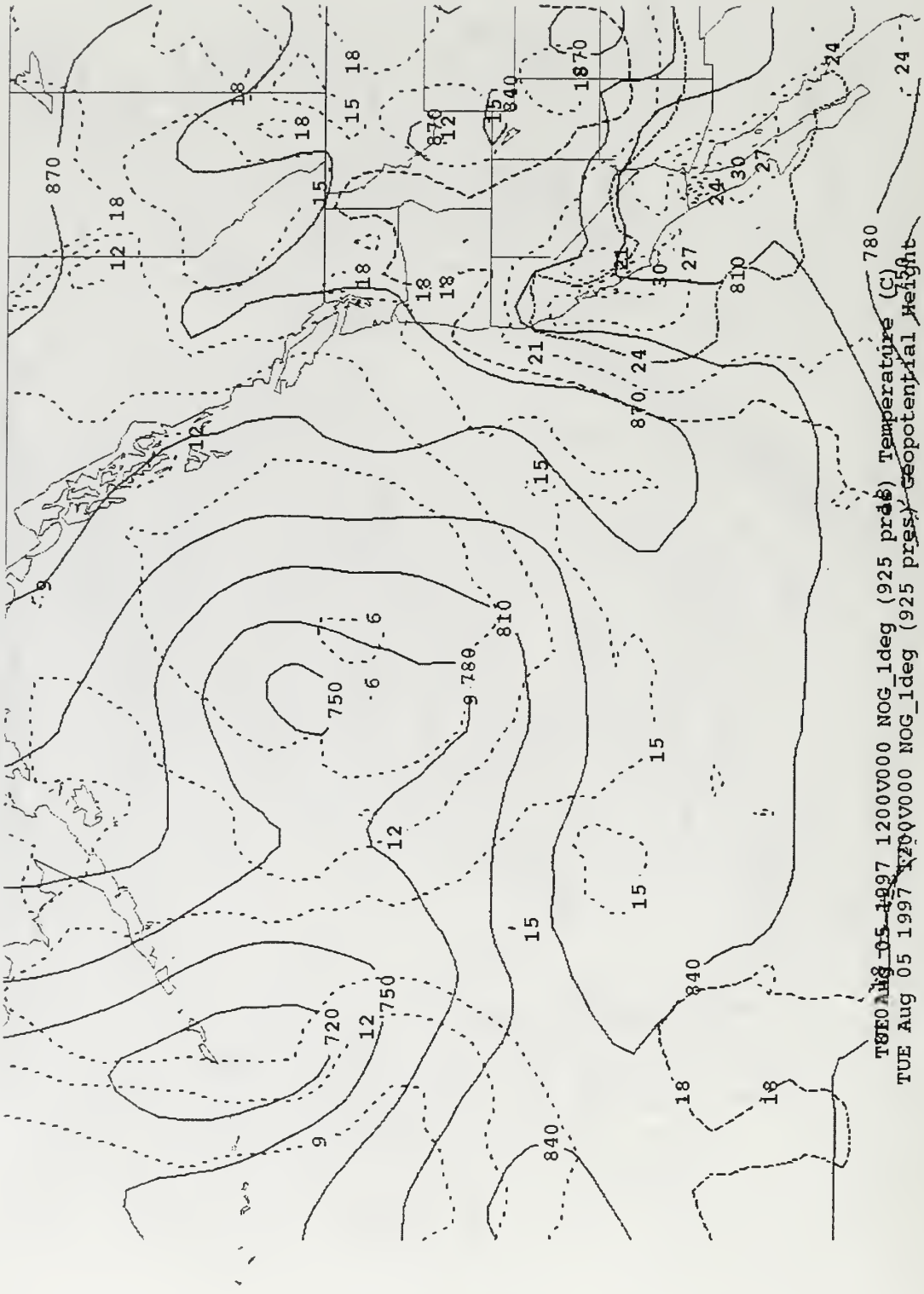

Figure 17. 051200Z Aug 97 925 mb Geopotential Heights and Temp. (C).

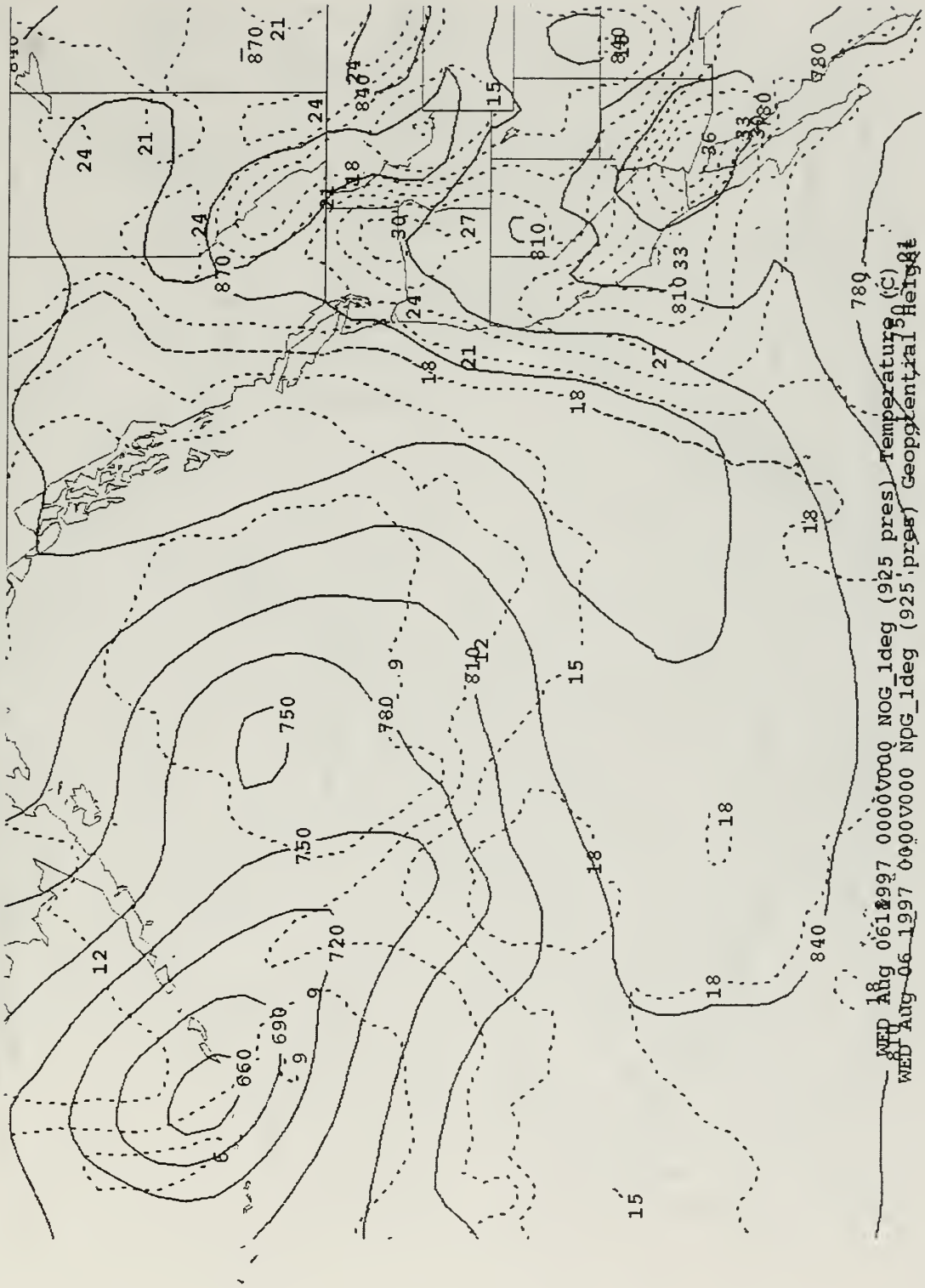

Figure 18. 060000Z Aug 97 925 mb Geopotential Heights and Temp. (C).

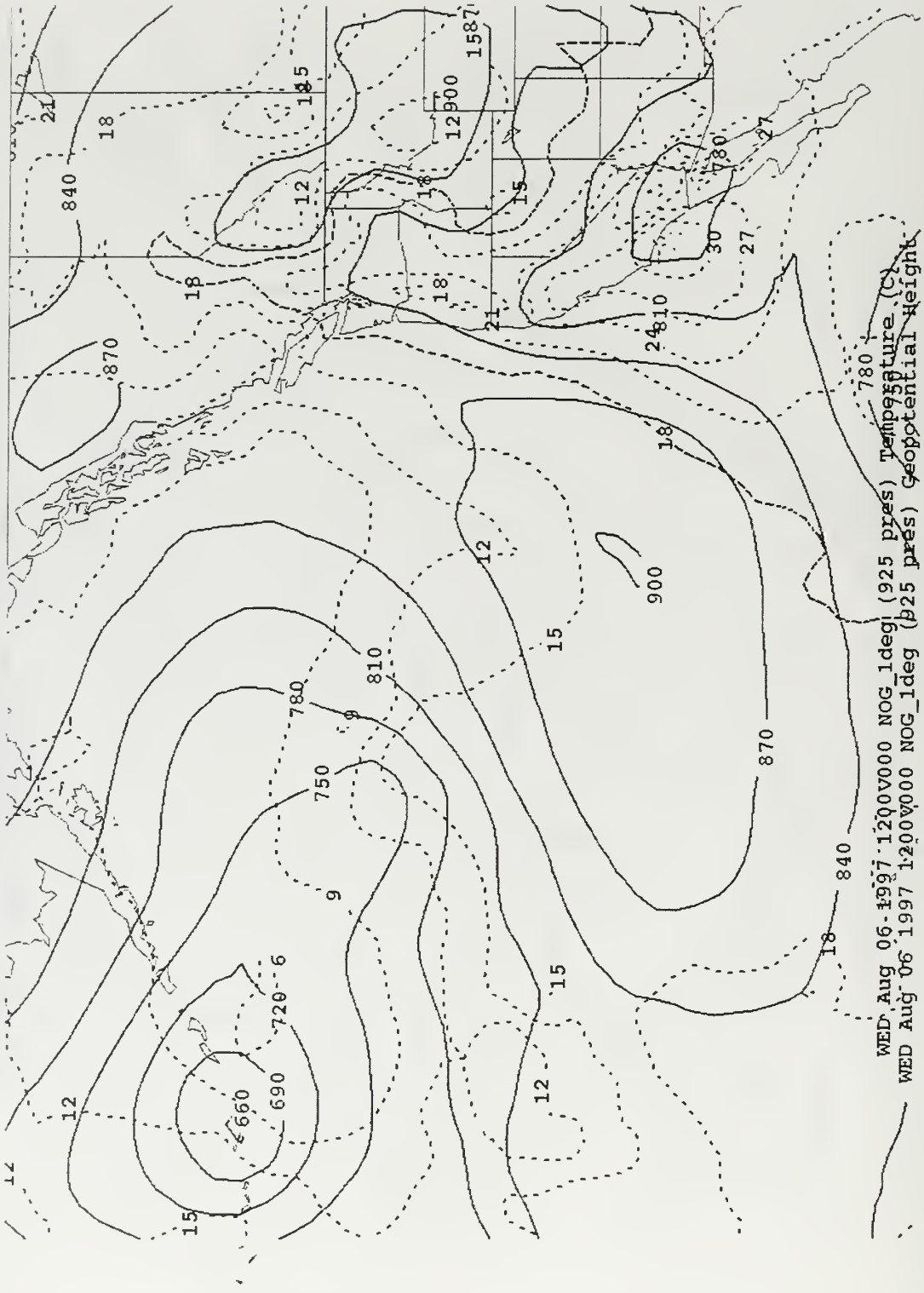

Figure 19. 061200Z Aug 97 925 mb Geopotential Heights and Temp. (C).

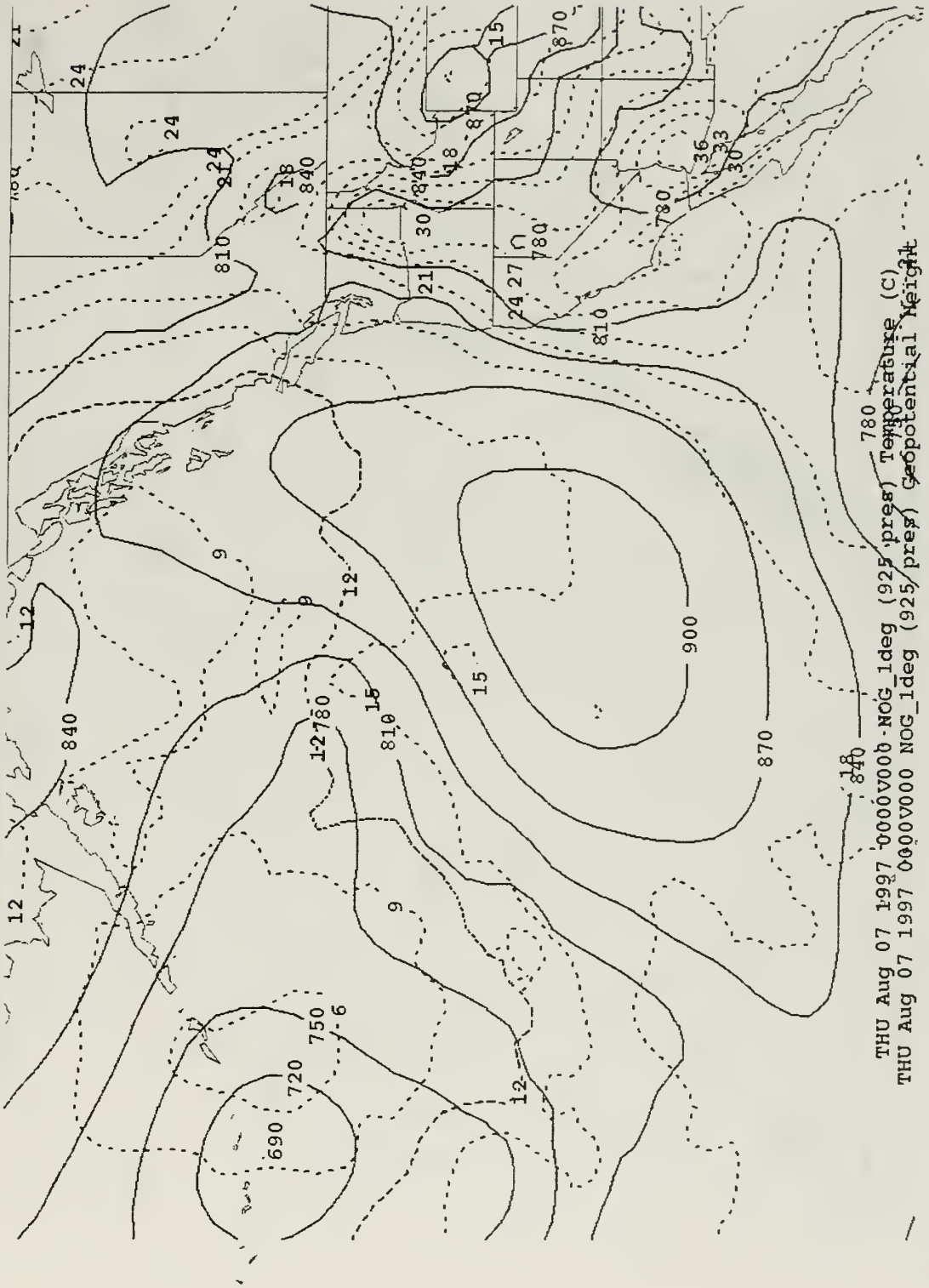

Figure 20. 070000Z Aug 97 925 mb Geopotential Heights and Temp. (C).

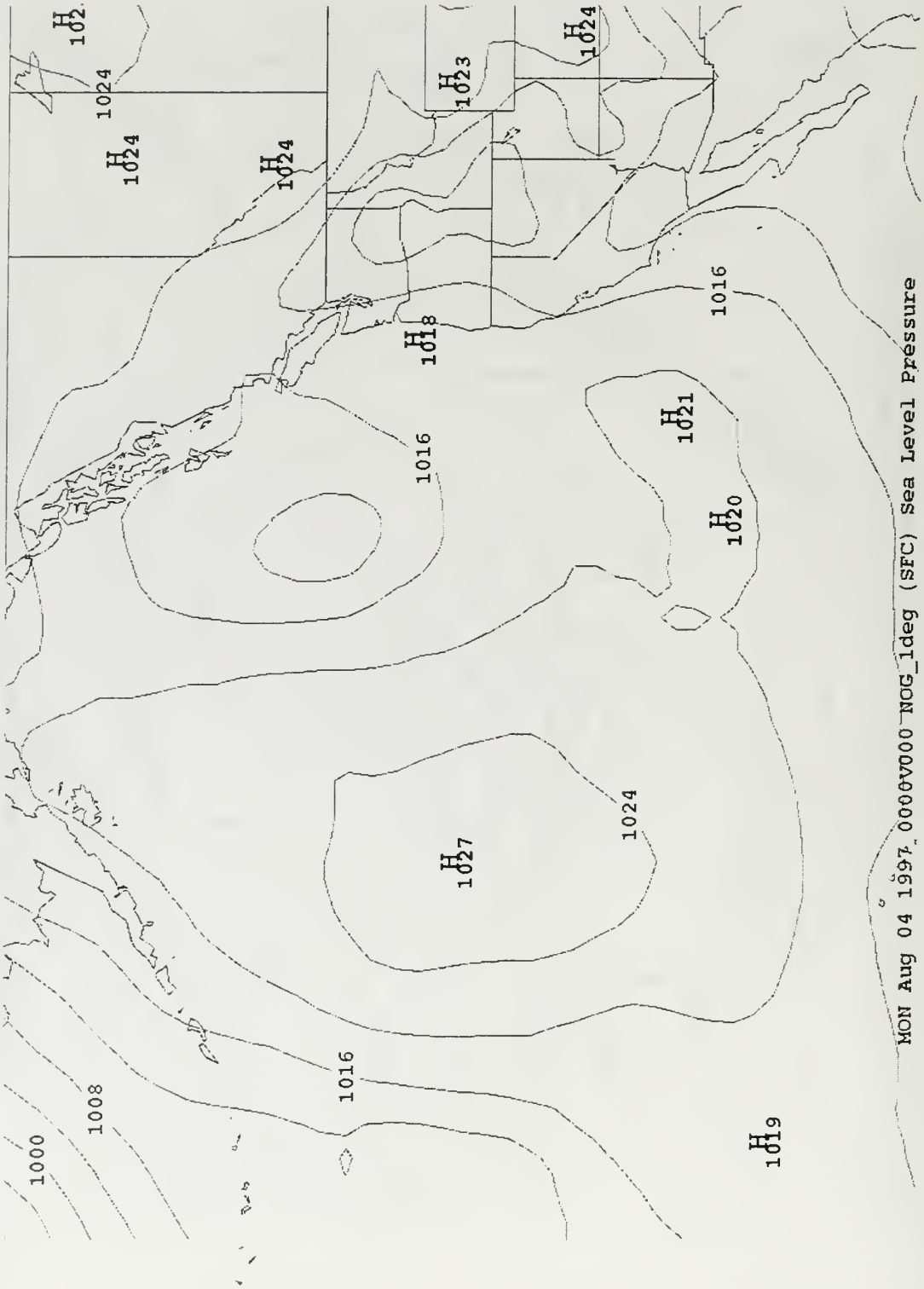

Figure 21. 040000Z Aug 97 Surface Sea Level Pressure.

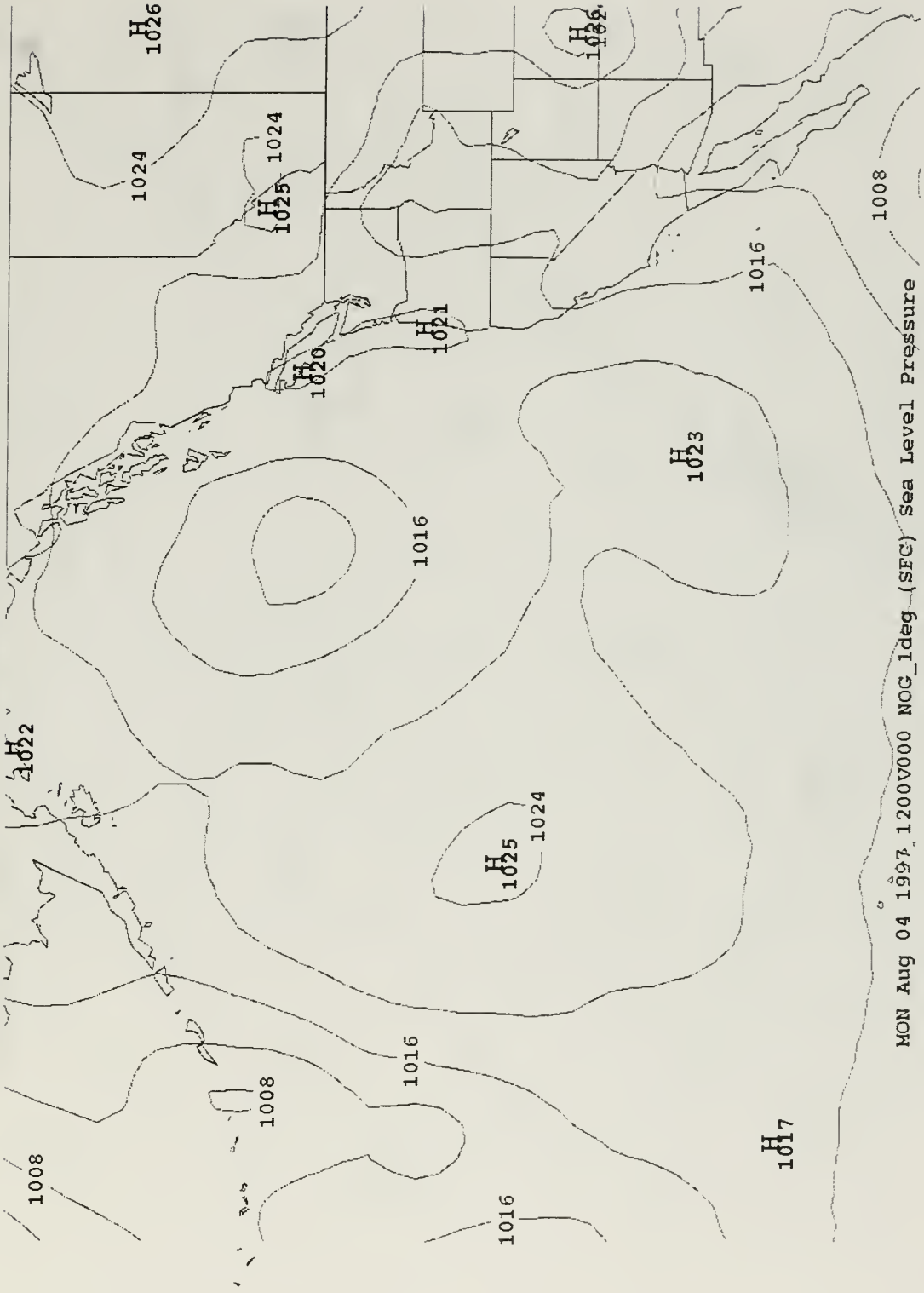

Figure 22. 041200Z Aug 97 Surface Sea Level Pressure.

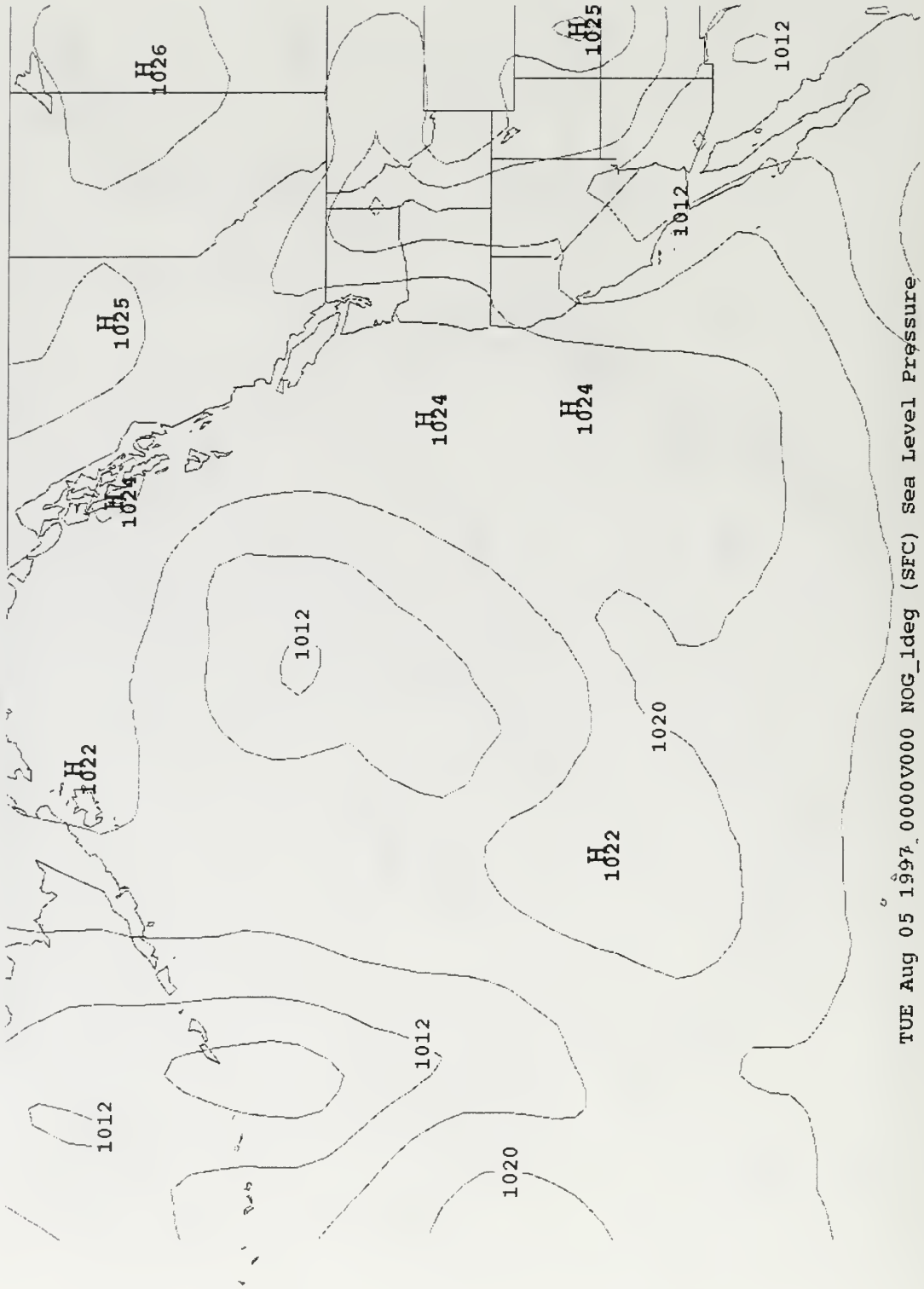

Figure 23. 050000Z Aug 97 Surface Sea Level Pressure.

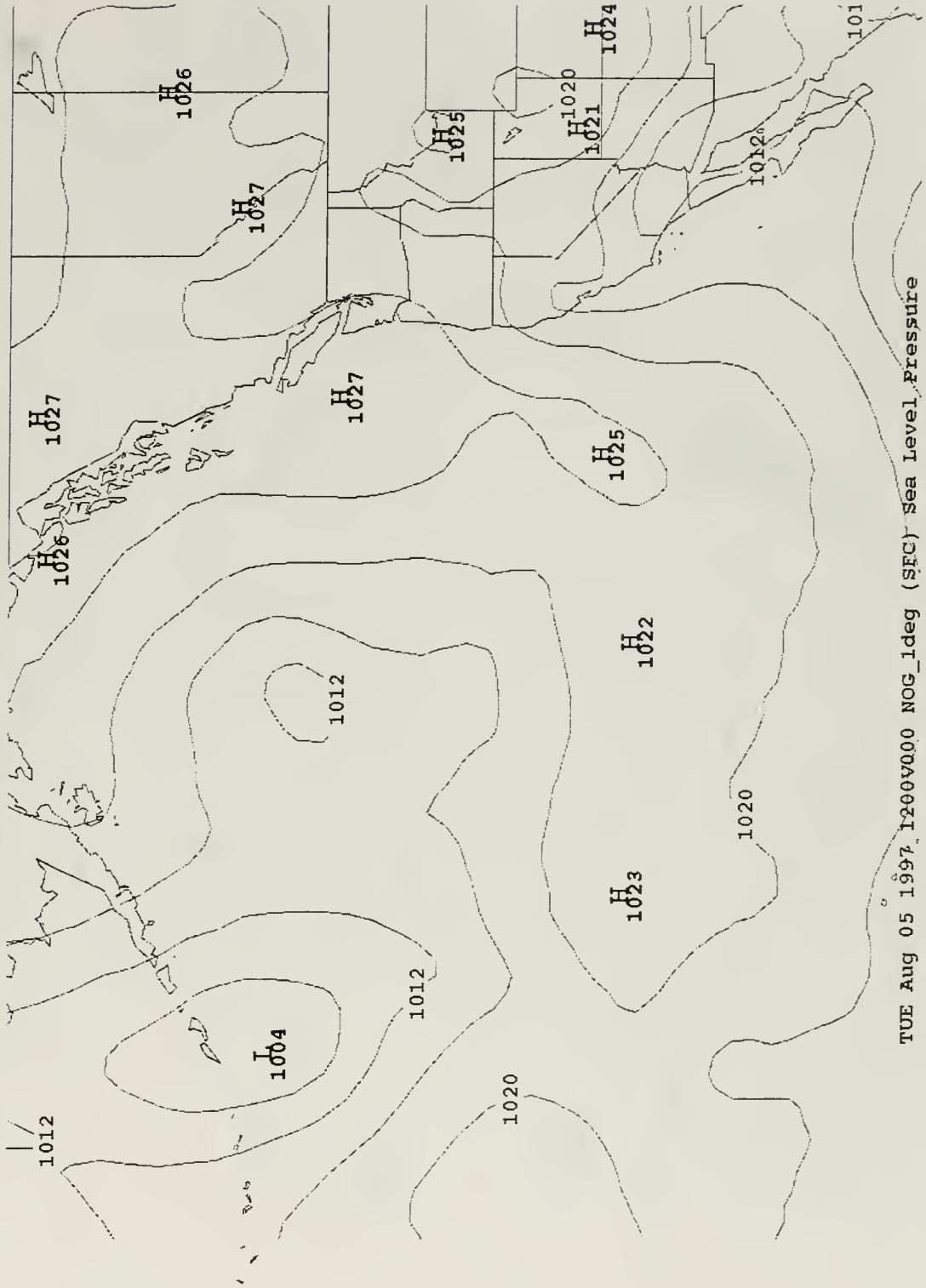

Figure 24. 051200Z Aug 97 Surface Sea Level Pressure.

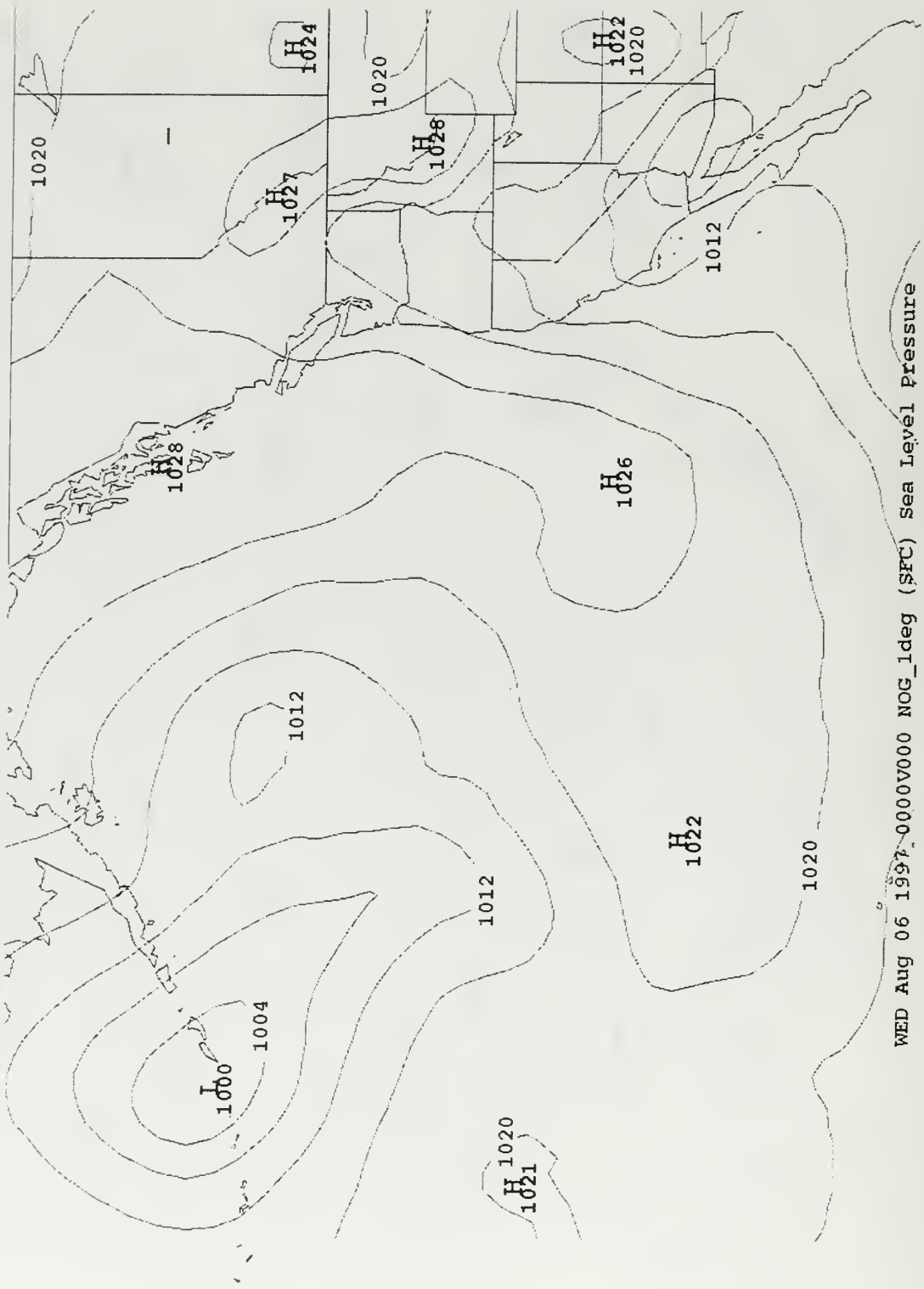

Figure 25. 060000Z Aug 97 Surface Sea Level Pressure.

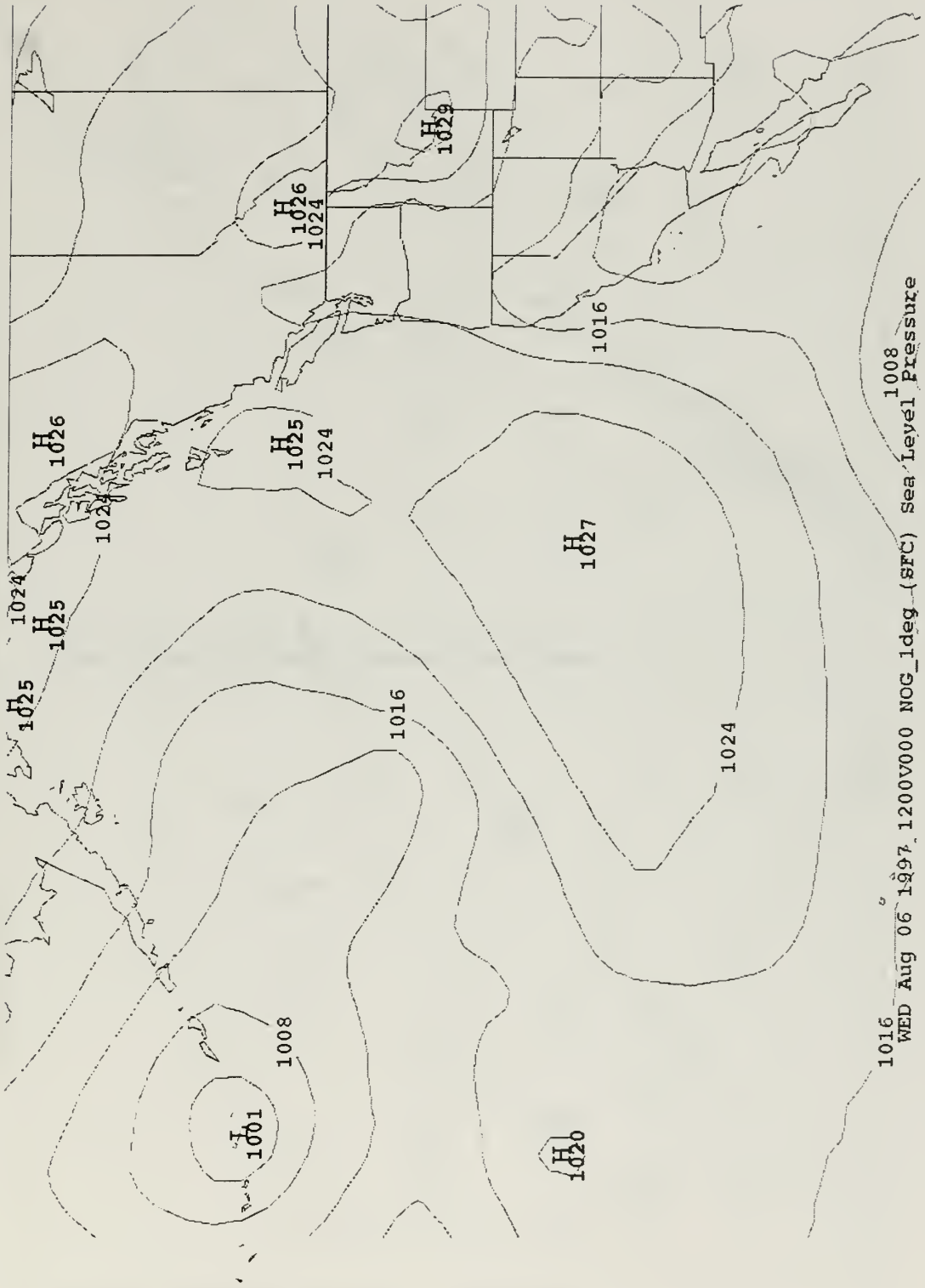

Figure 26. 061200Z Aug 97 Surface Sea Level Pressure.

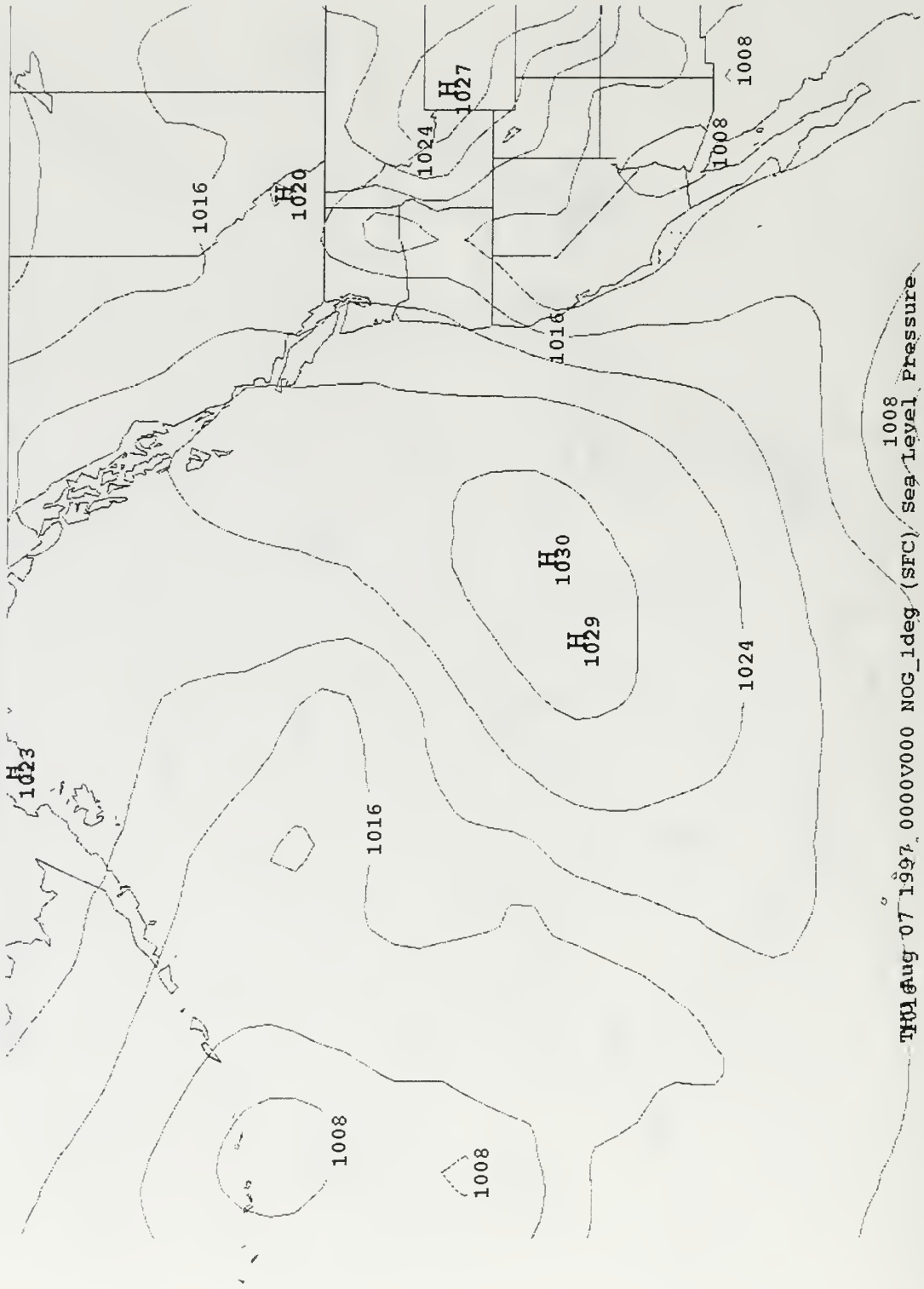

Figure 27. 070000Z Aug 97 Surface Sea Level Pressure.

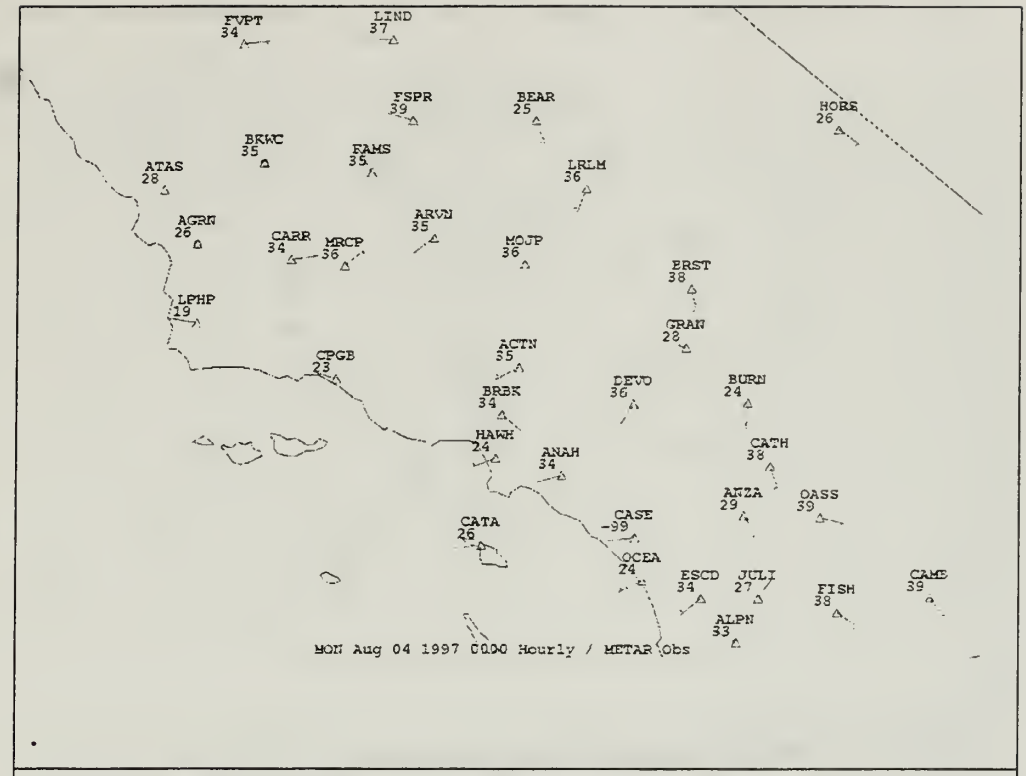

Figure 28. 040000Z August Surface Observations.

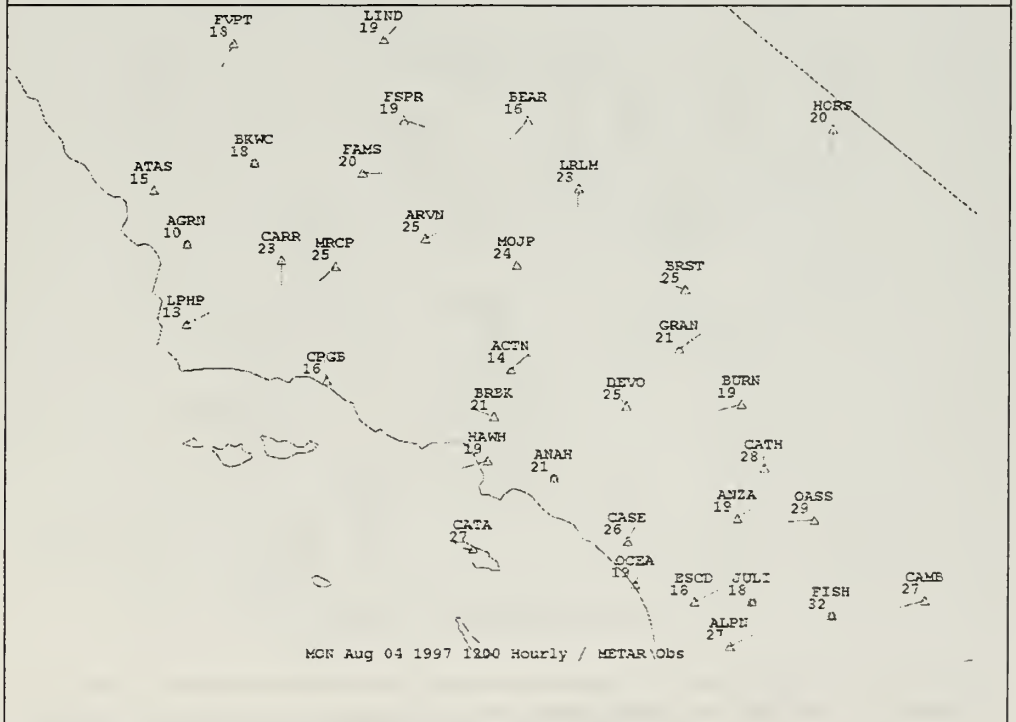

Figure 29. 041200Z August Surface Observations.

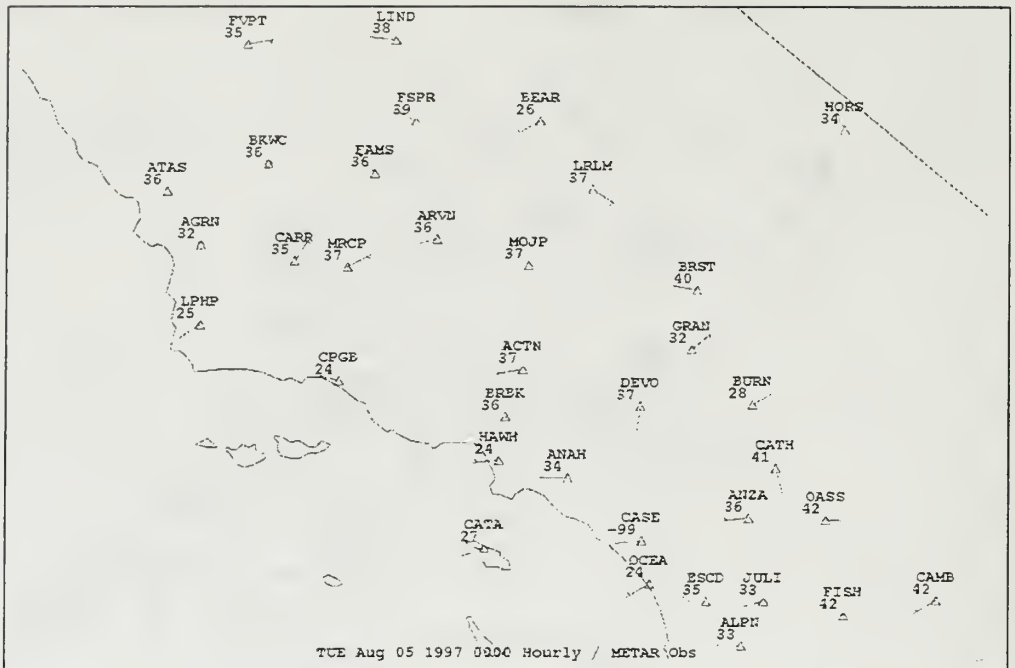

Figure 30. 050000Z August Surface Observations.

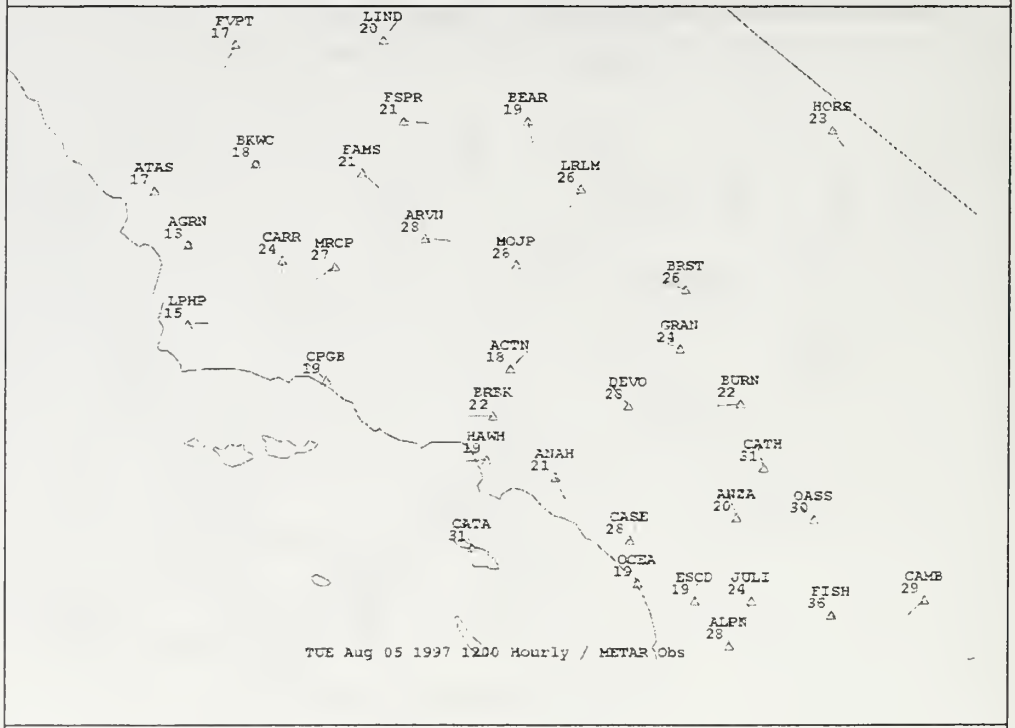

Figure 31. 051200Z August Surface Observations.

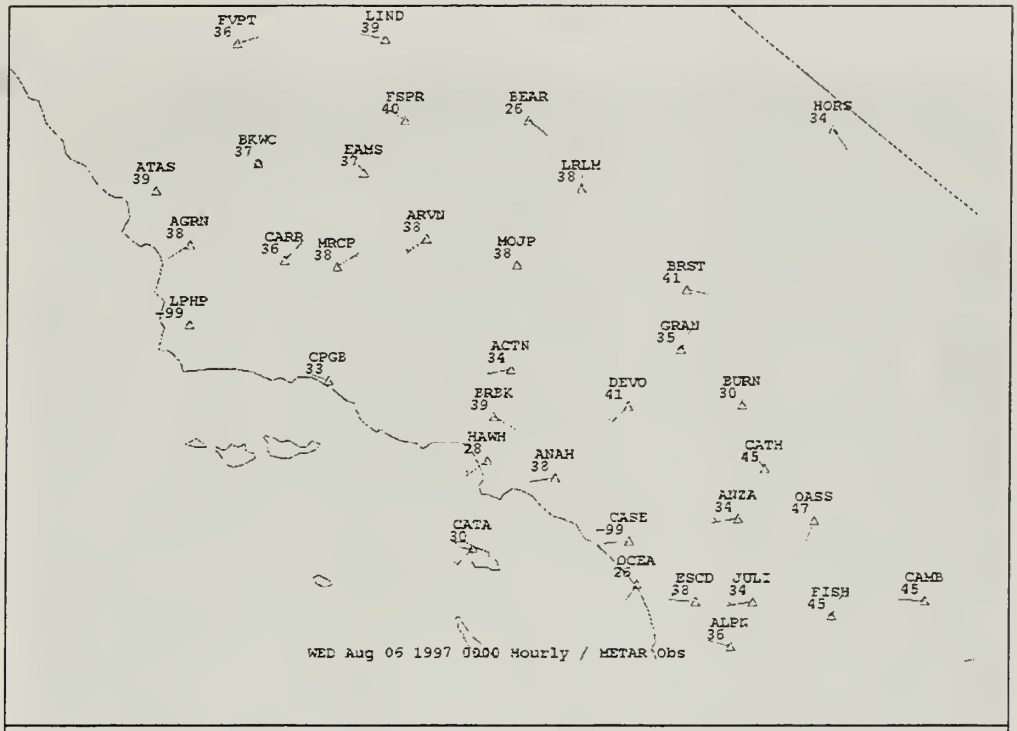

Figure 32. 060000Z August Surface Observations.

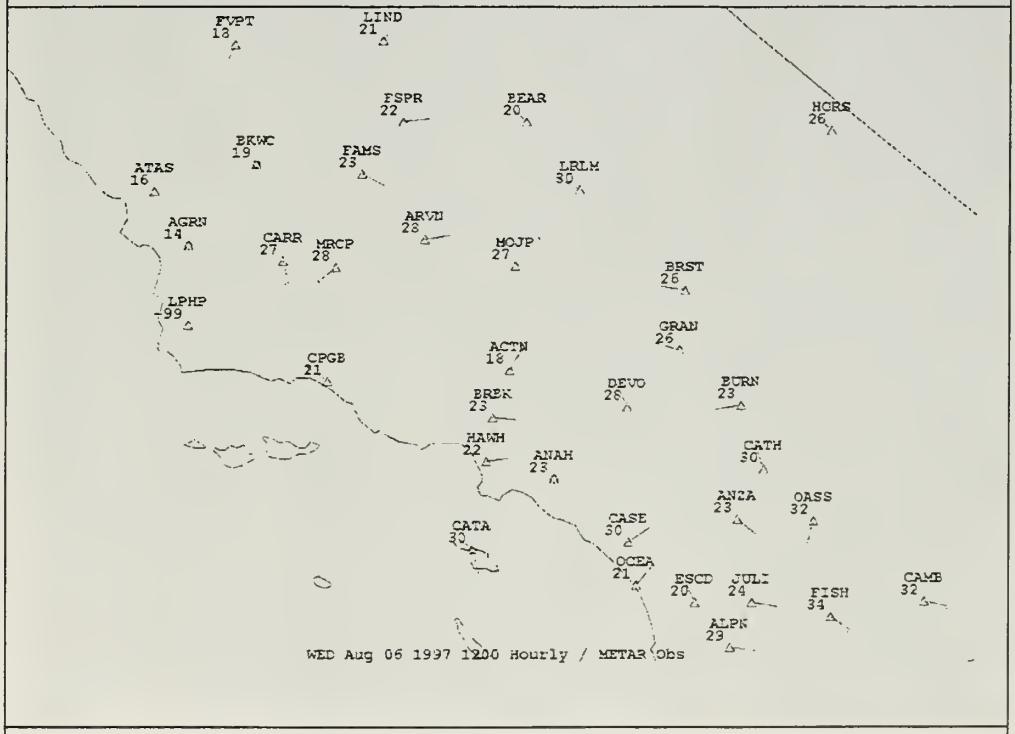

Figure 33. 061200Z August Surface Observations.

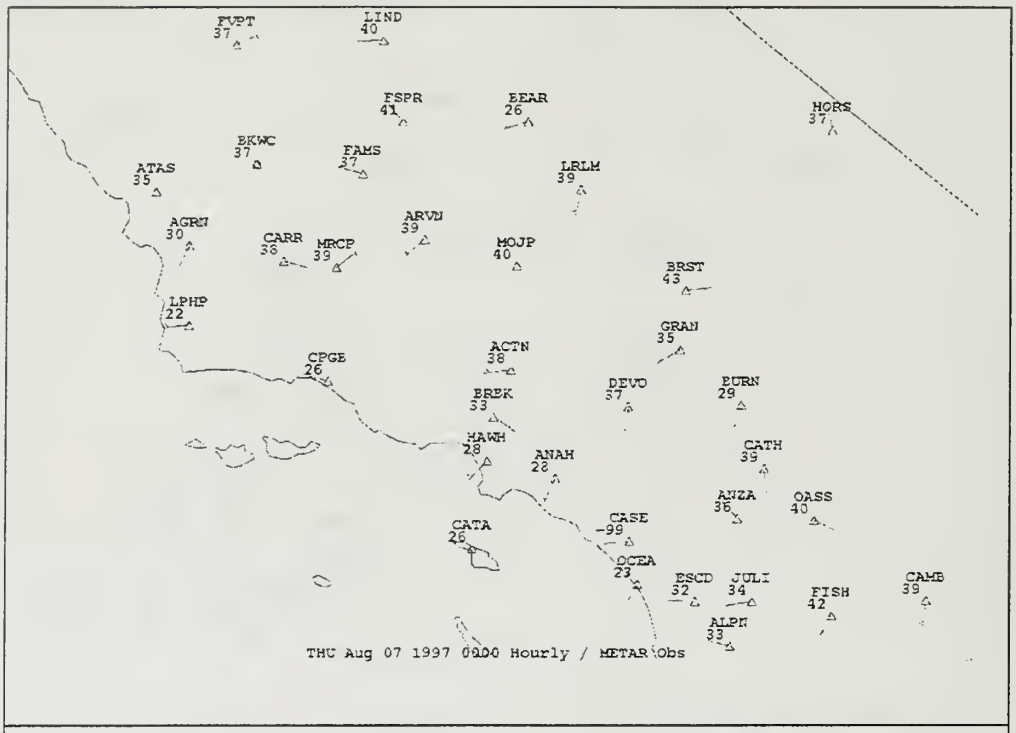

Figure 34. 070000Z August Surface Observations.

Figure 35. 050000Z Aug 97 GOES VIS.

Figure 36. 060000Z Aug 97 GOES VIS.

Figure 37. 070000Z Aug 97 GOES VIS.

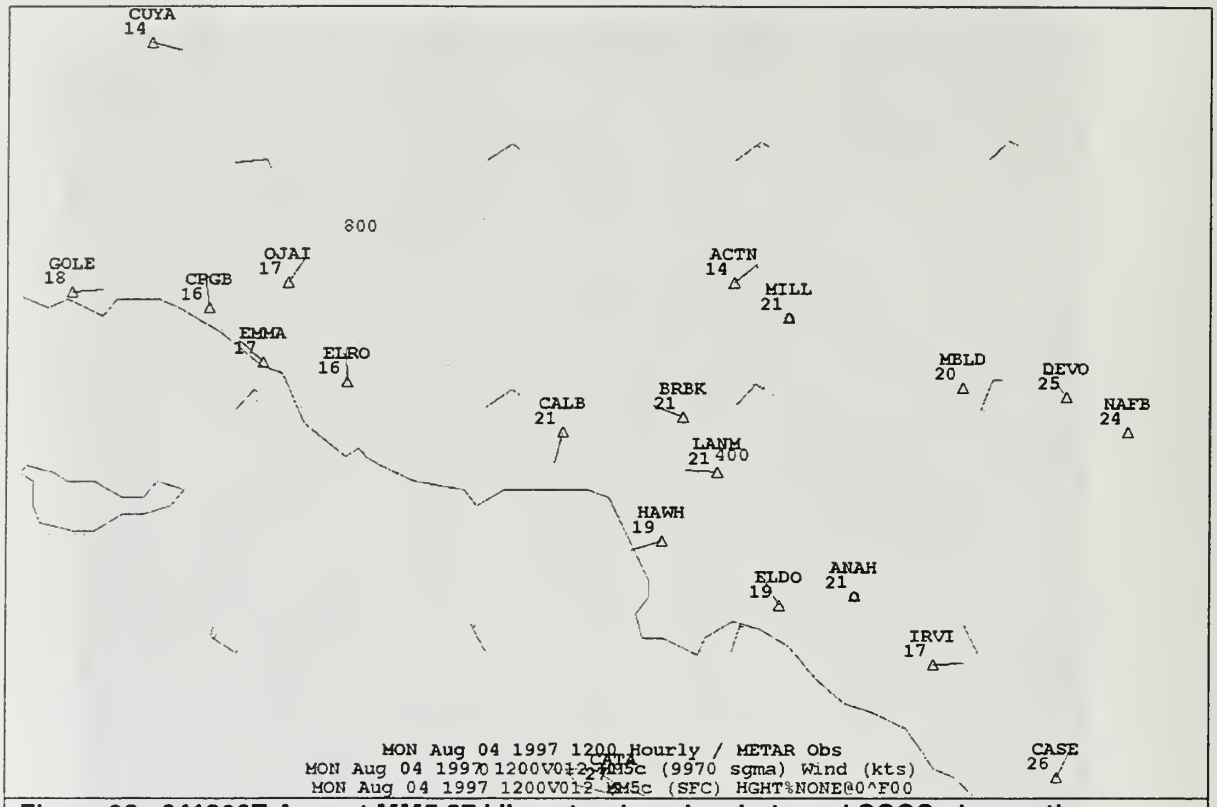

Figure 38. 041200Z August MM5 27 kilometer domain winds and SCOS observations.

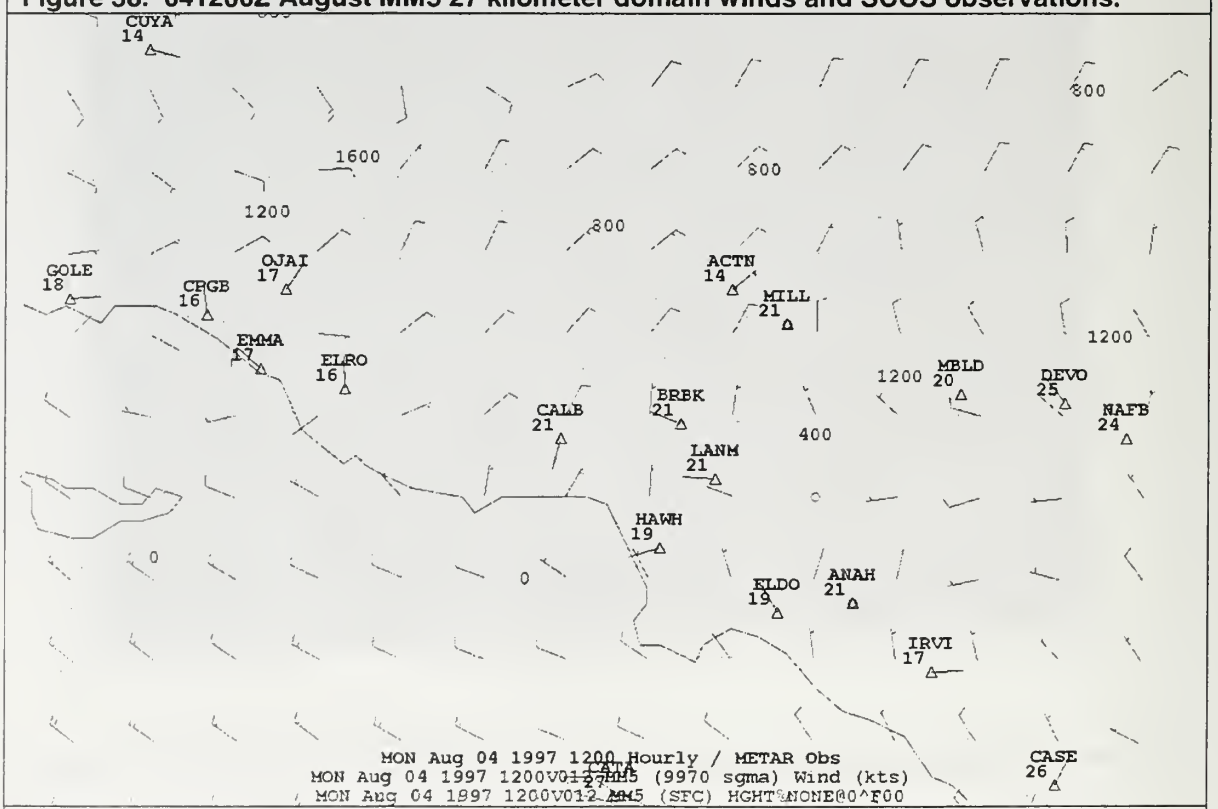

Figure 39. 041200Z August MM5 9 kilometer domain winds and SCOS observations.

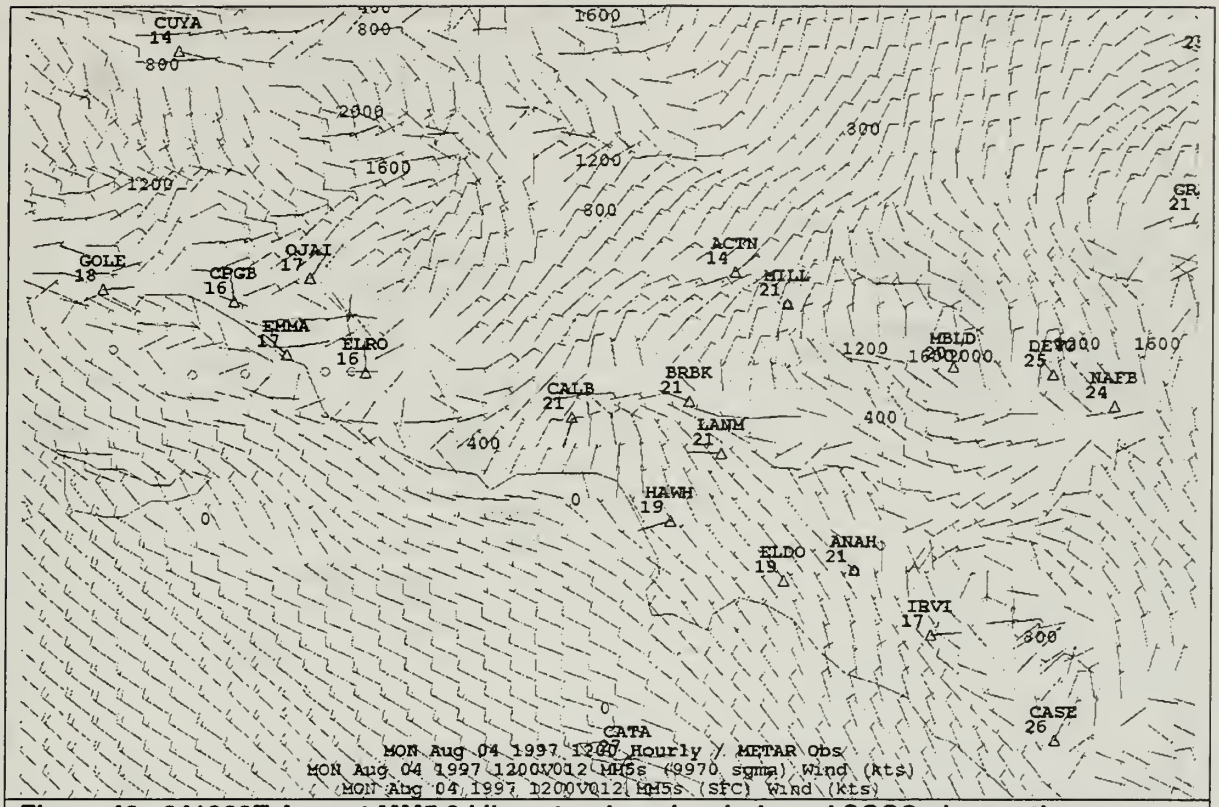

Figure 40. 041200Z August MM5 3 kilometer domain winds and SCOS observations.

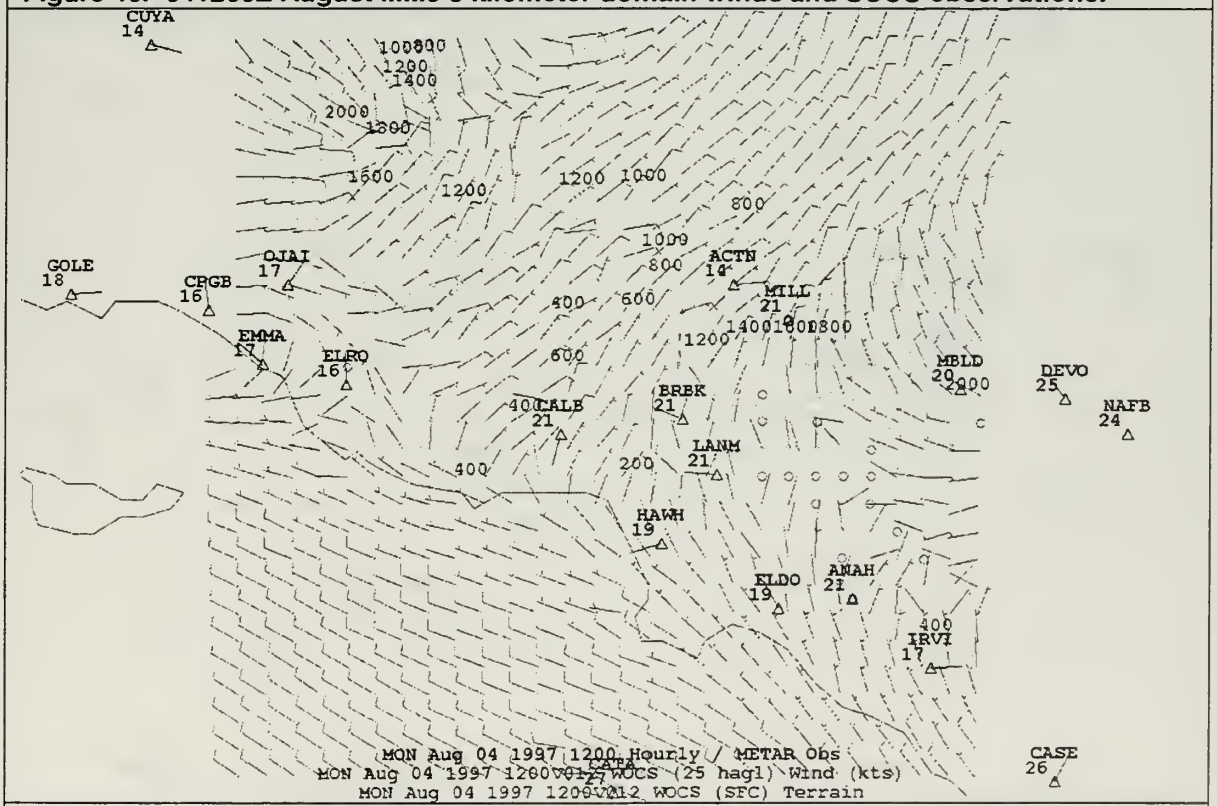

Figure 41. 041200Z August WOCSS winds and SCOS observations.

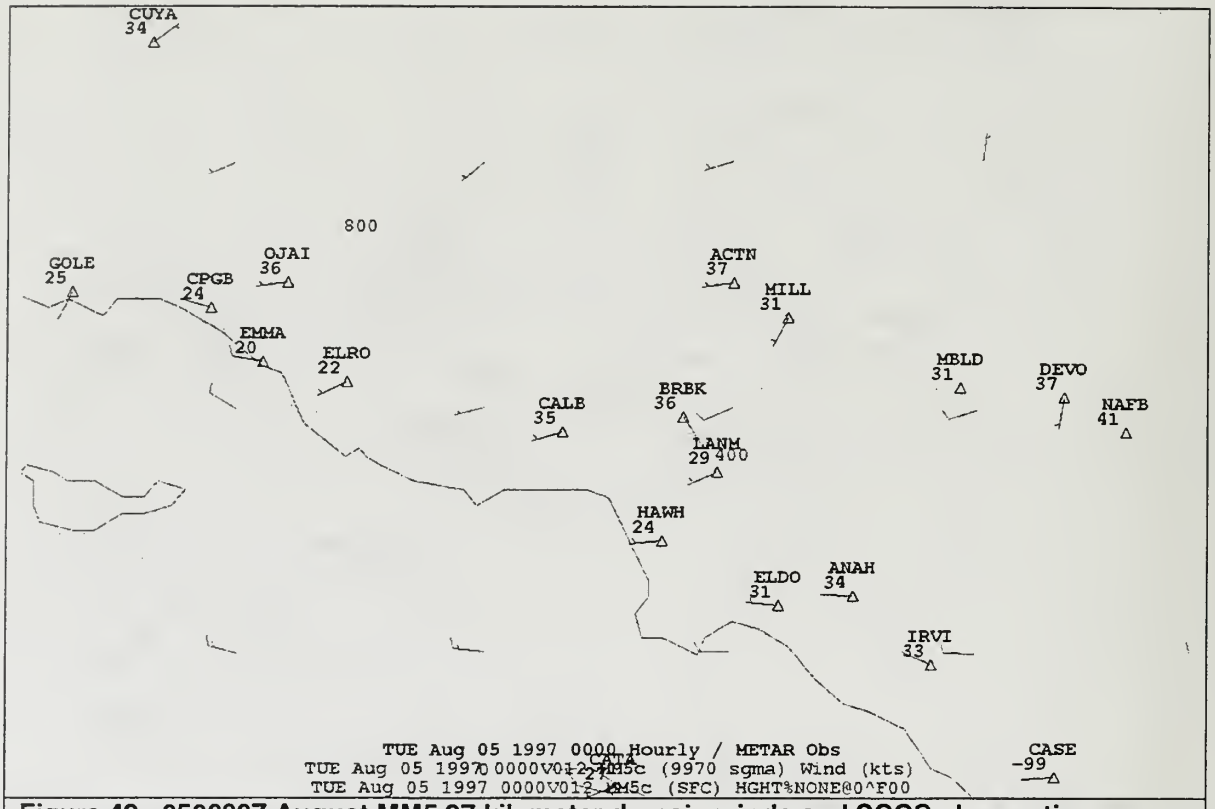

Figure 42. 050000Z August MM5 27 kilometer domain winds and SCOS observations.

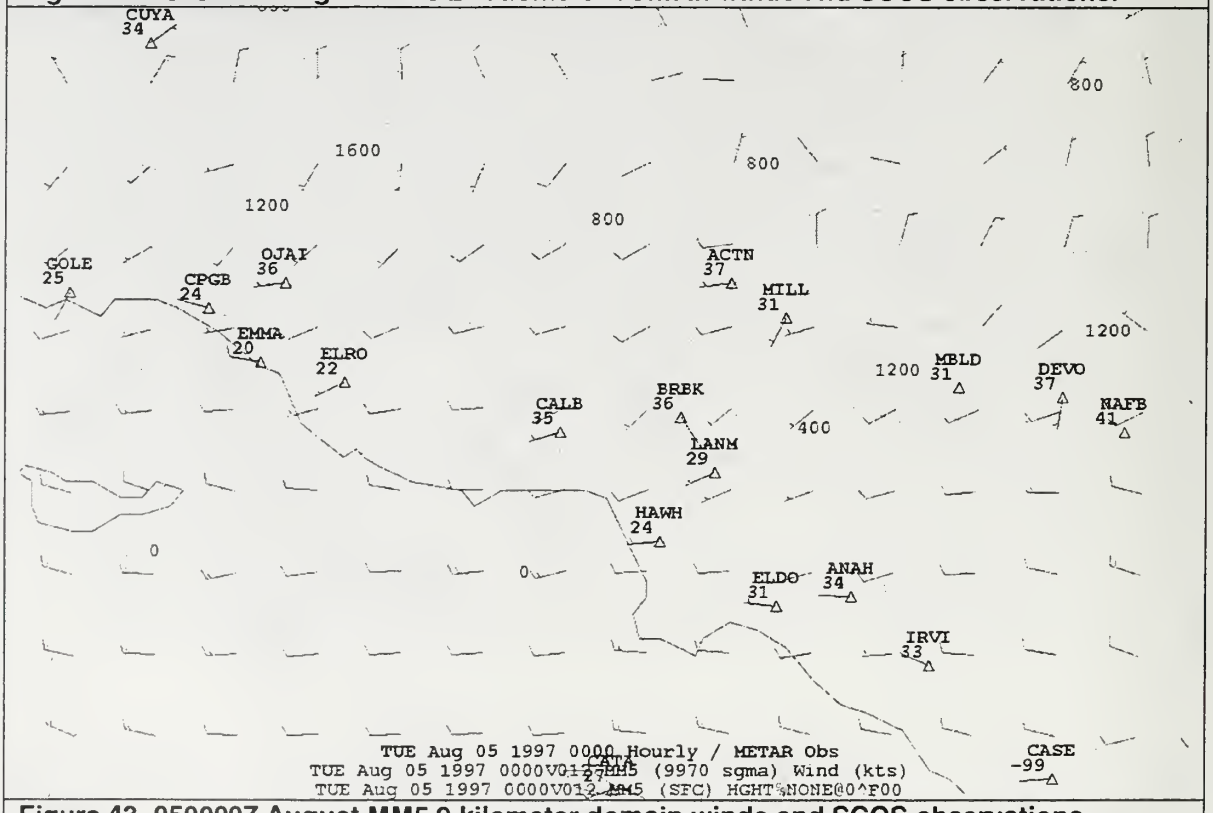

Figure 43 050000Z August MM5 9 kilometer domain winds and SCOS observations.

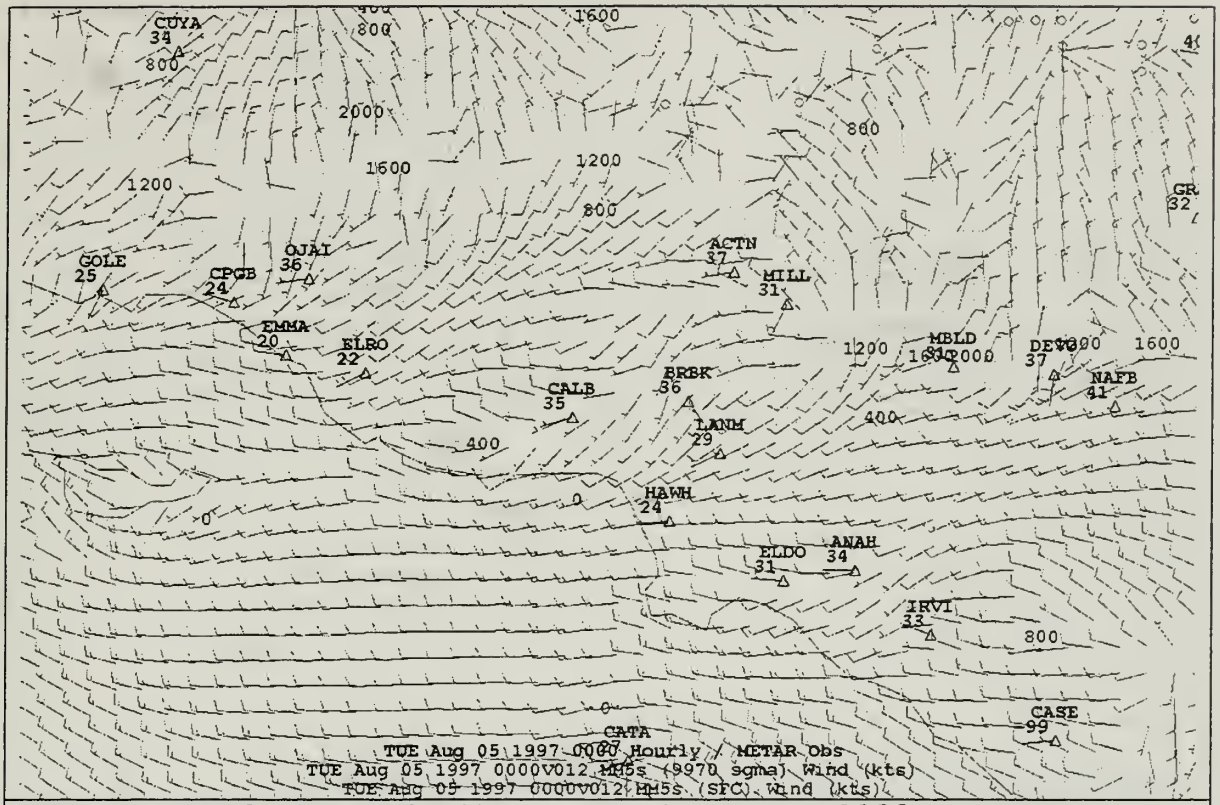

Figure 44 050000Z August MM5 3 kilometer domain winds and SCOS observations.

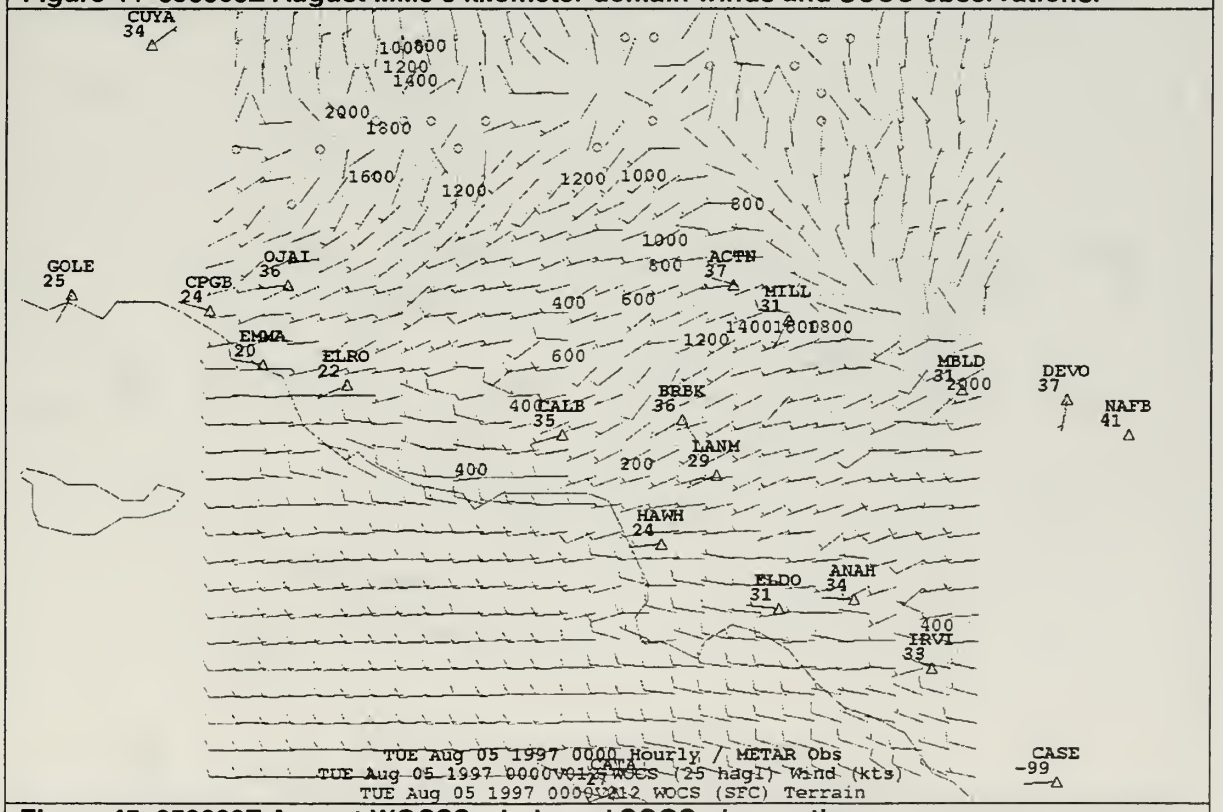

Figure 45 050000Z August WOCSS winds and SCOS observations.

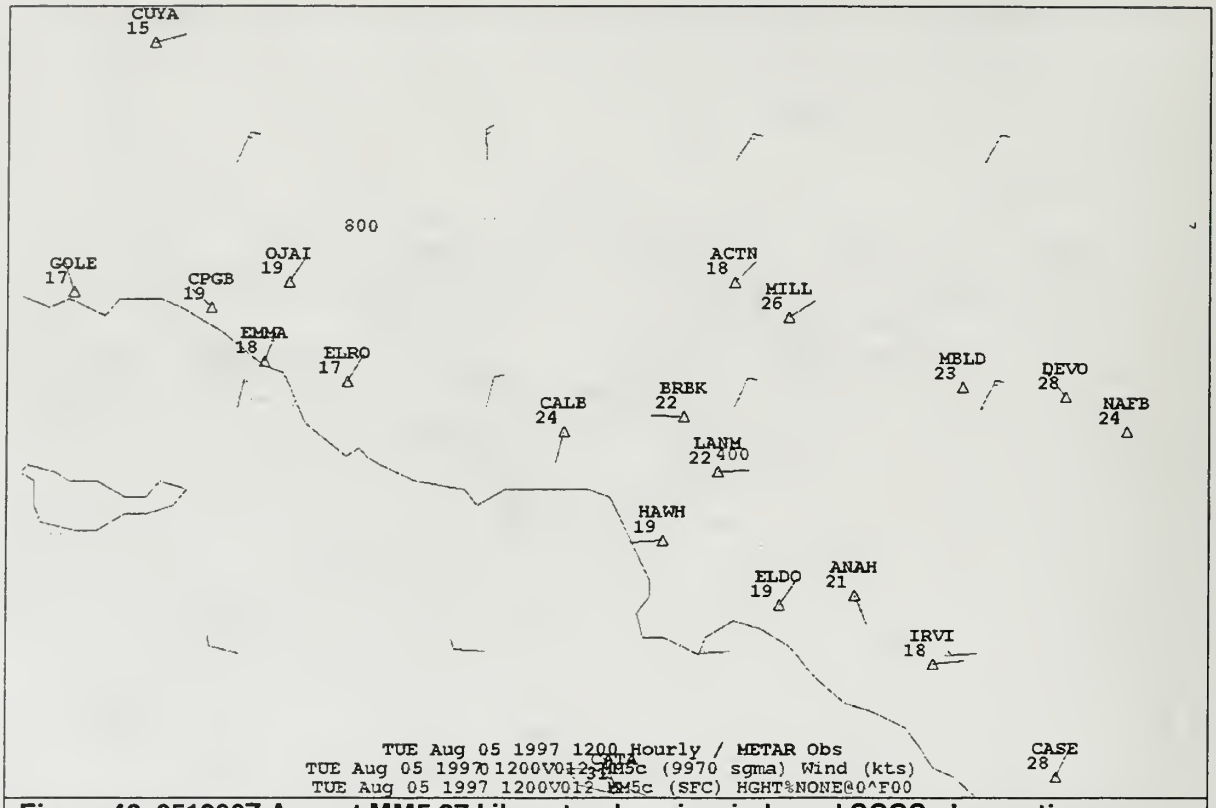

Figure 46 051200Z August MM5 27 kilometer domain winds and SCOS observations.

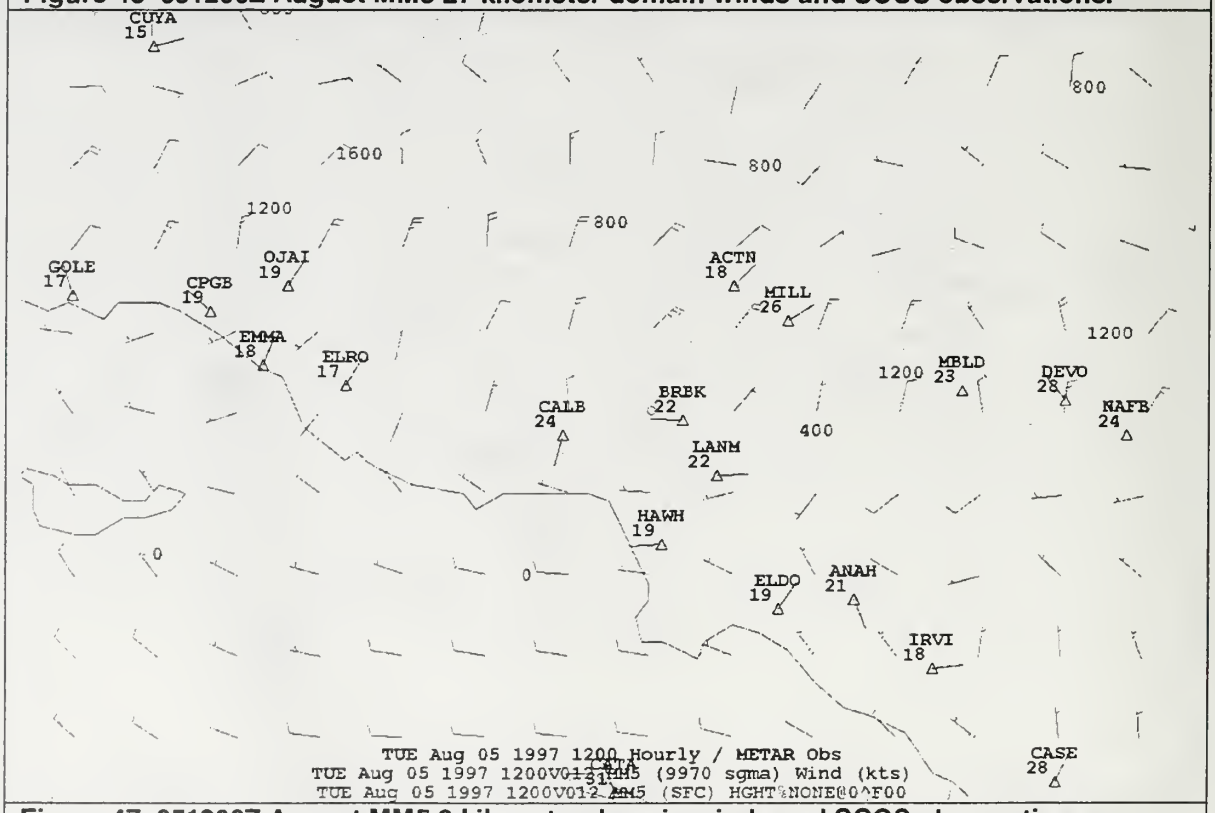

Figure 47 051200Z August MM5 9 kilometer domain winds and SCOS observations.

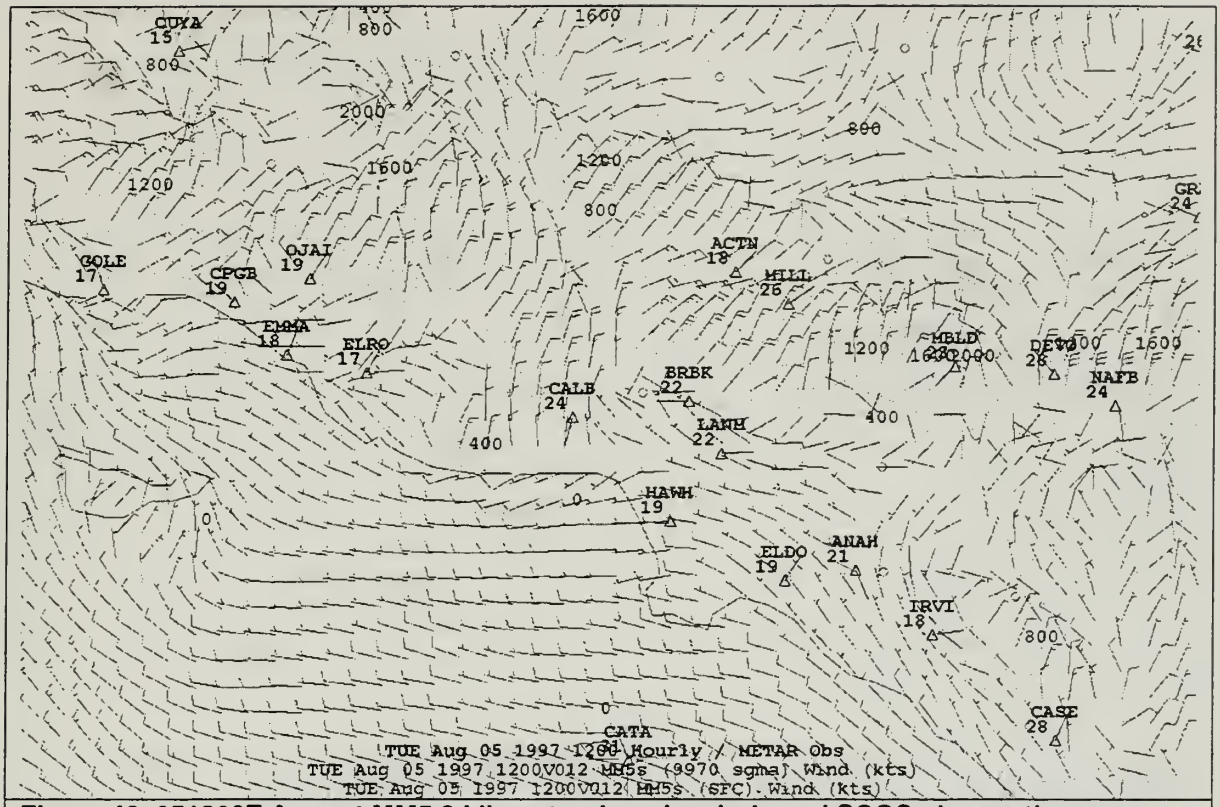

Figure 48 051200Z August MM5 3 kilometer domain winds and SCOS observations.

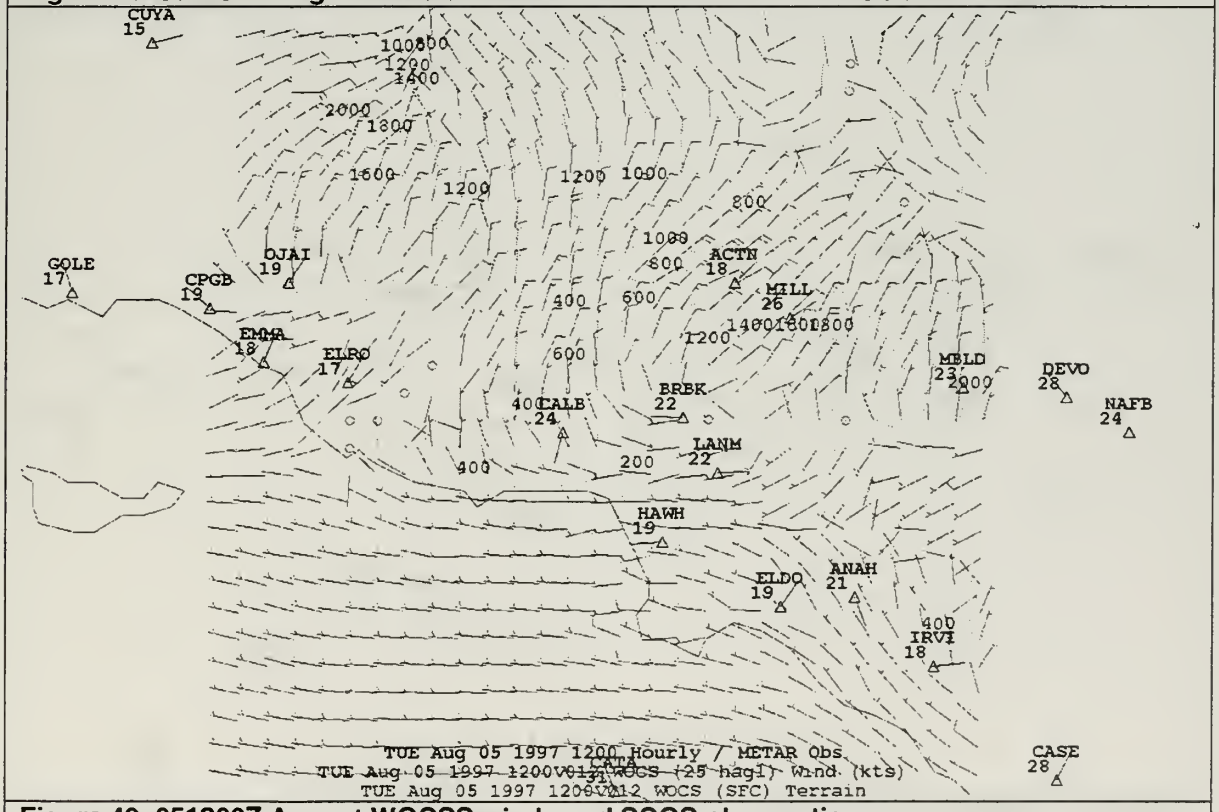

Figure 49 051200Z August WOCSS winds and SCOS observations.

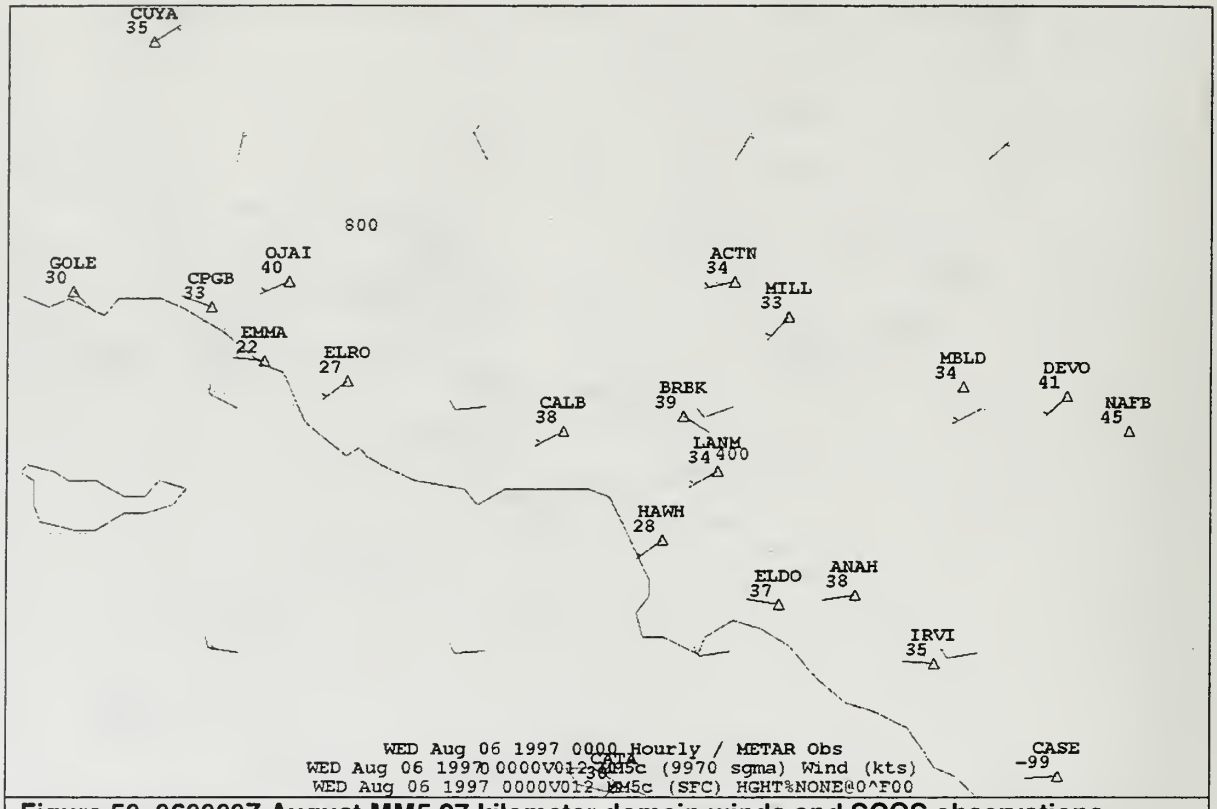

Figure 50 060000Z August MM5 27 kilometer domain winds and SCOS observations.

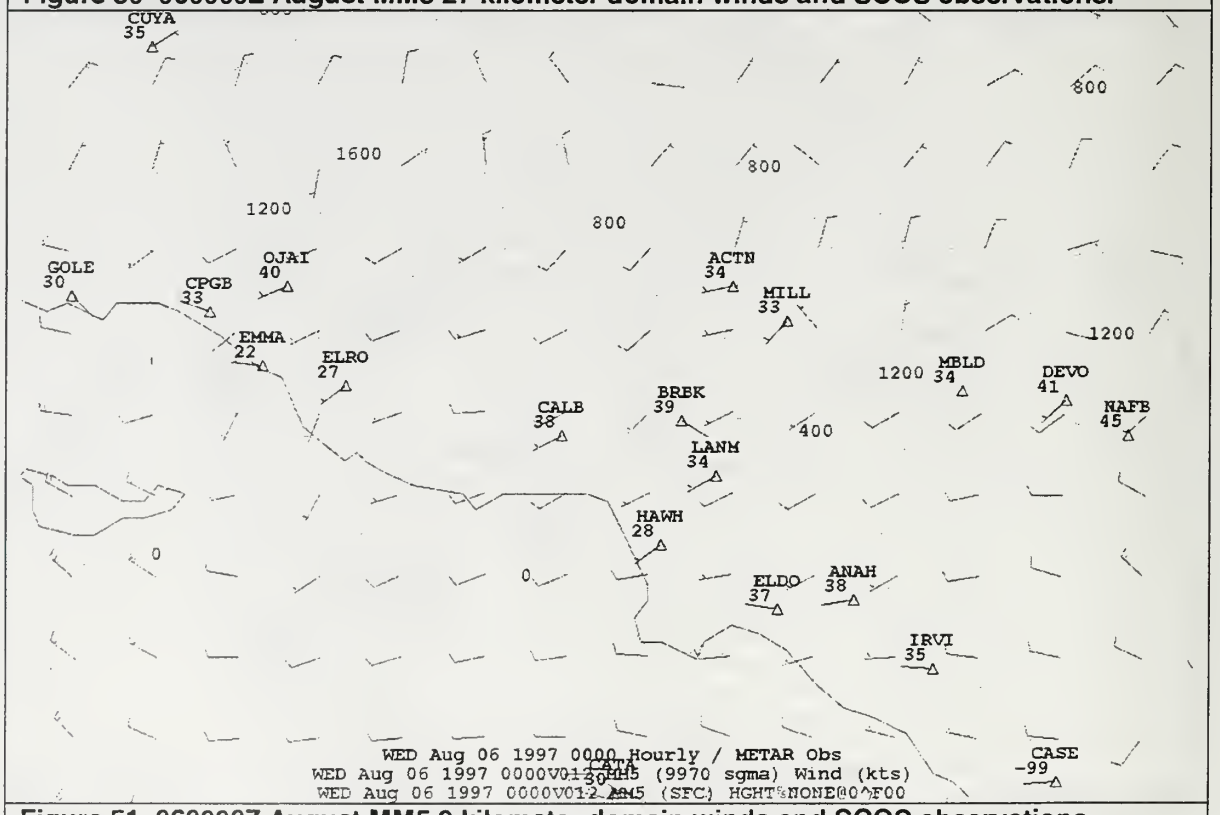

Figure 51 060000Z August MM5 9 kilometer domain winds and SCOS observations.

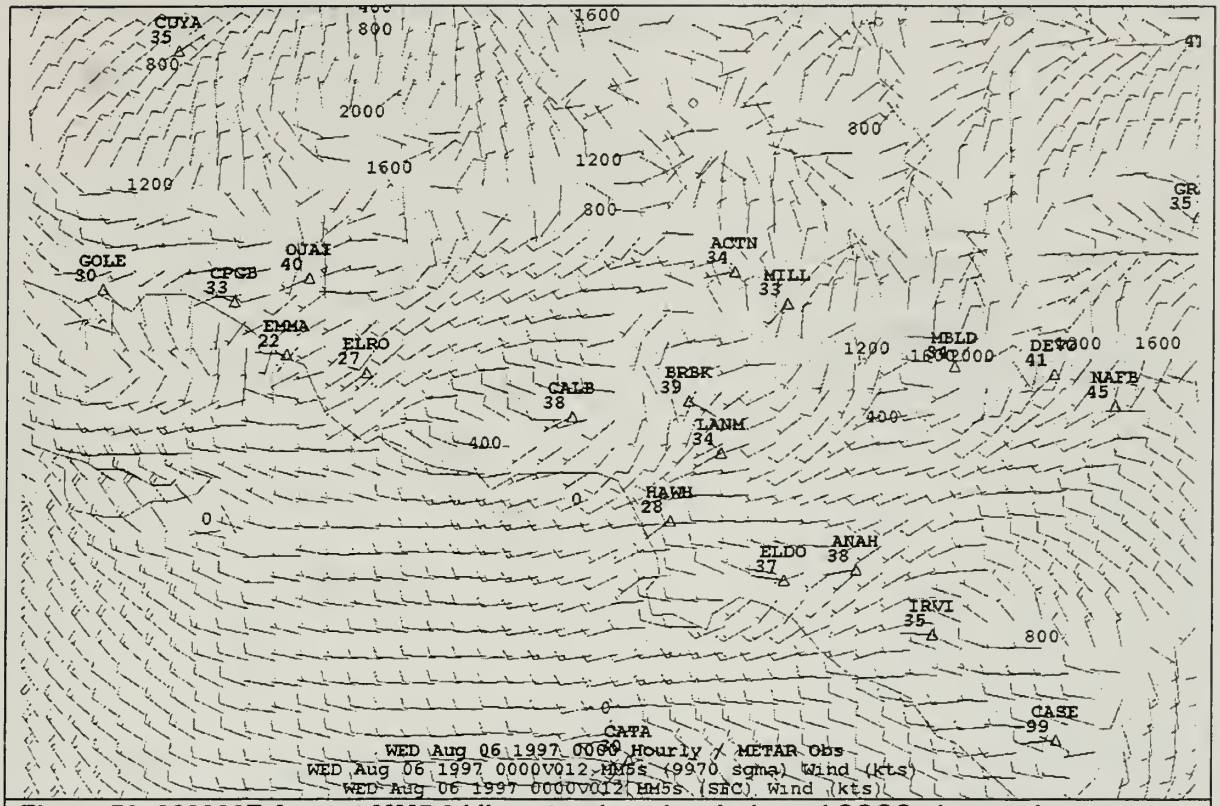

Figure 52 060000Z August MM5 3 kilometer domain winds and SCOS observations.

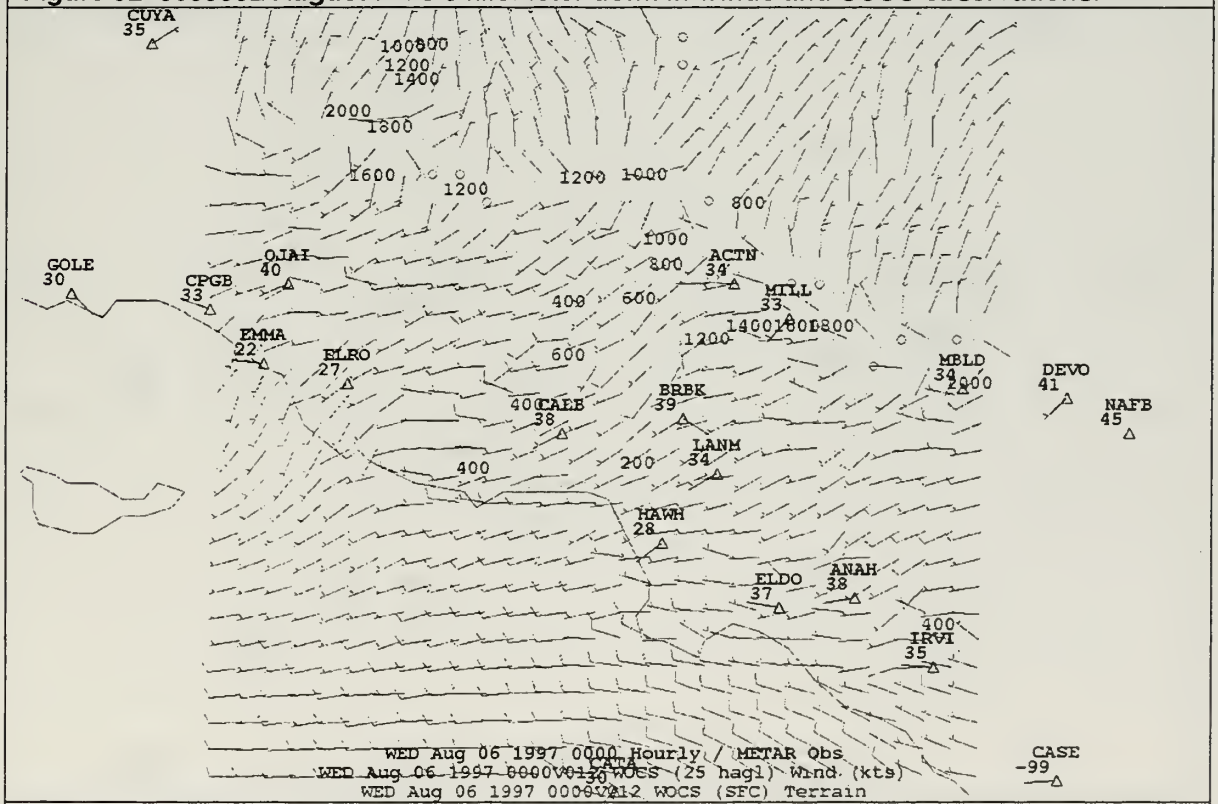

Figure 53 060000Z August WOCSS winds and SCOS observations.

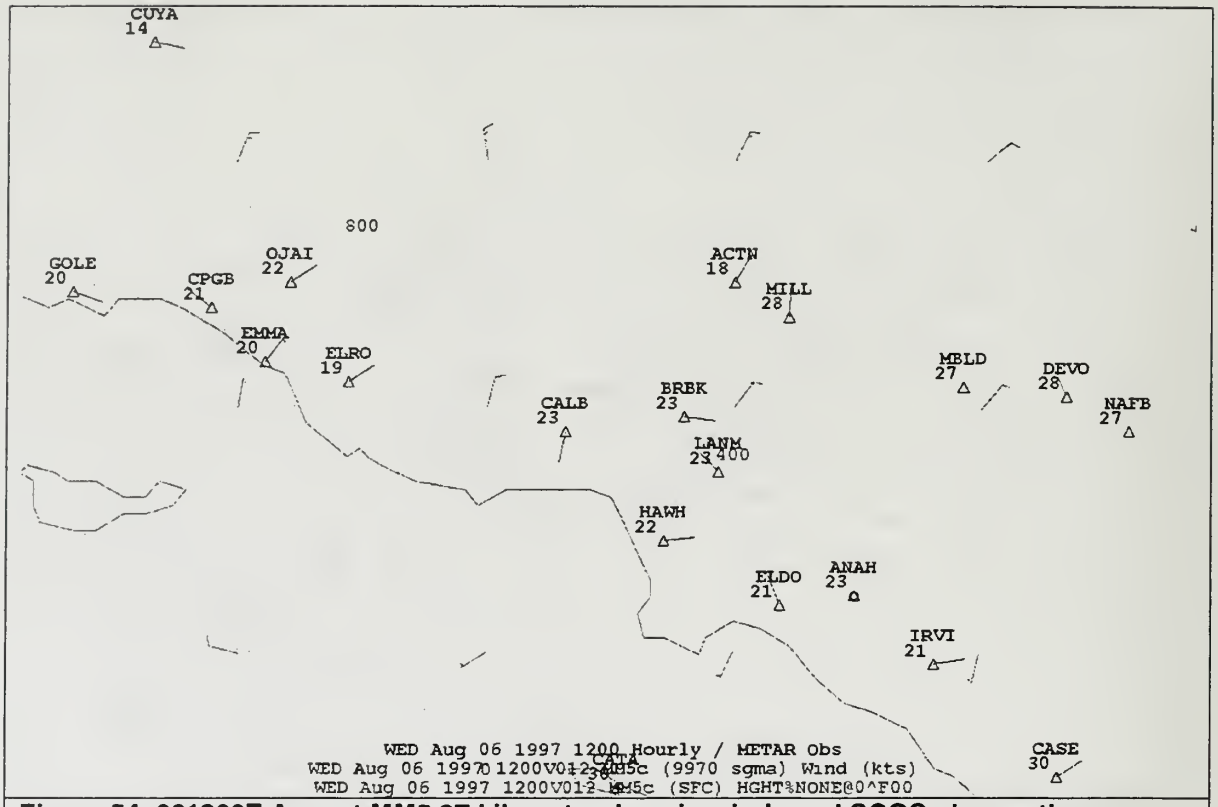

Figure 54 061200Z August MM5 27 kilometer domain winds and SCOS observations.

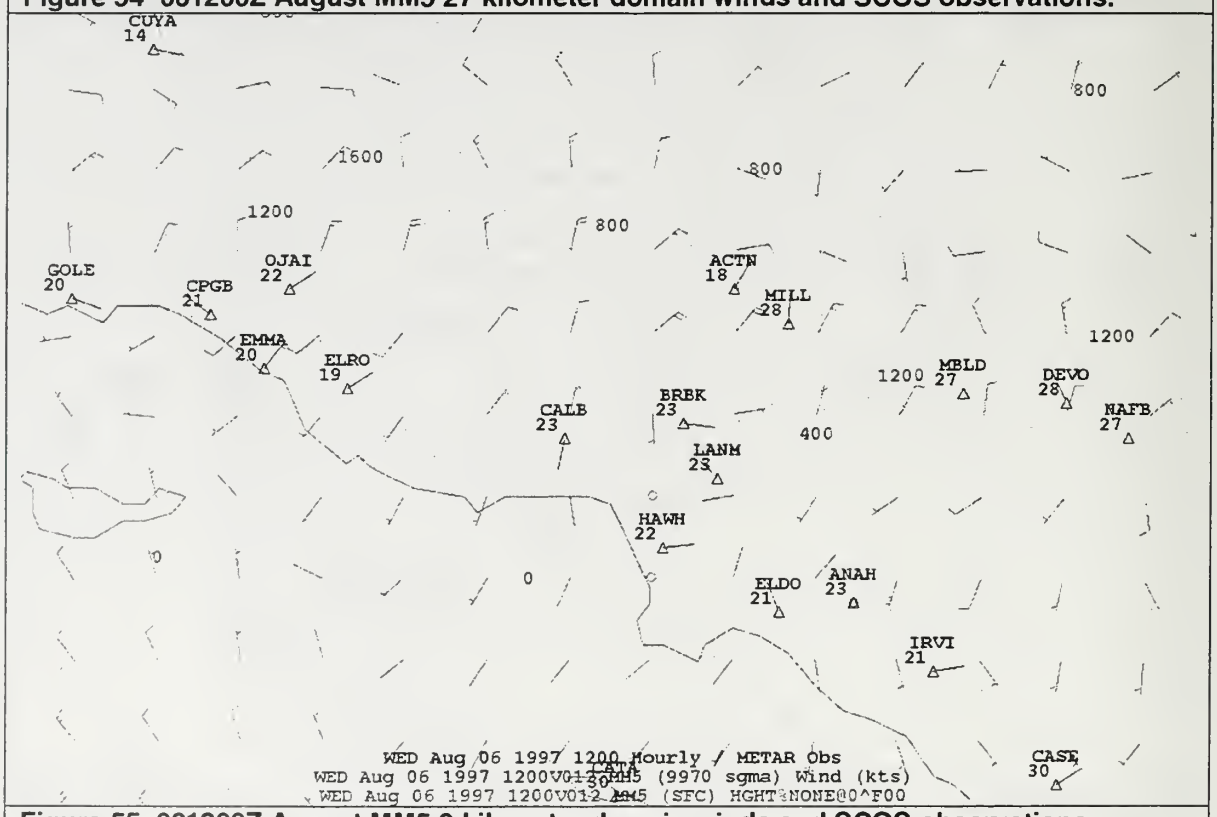

Figure 55 061200Z August MM5 9 kilometer domain winds and SCOS observations.

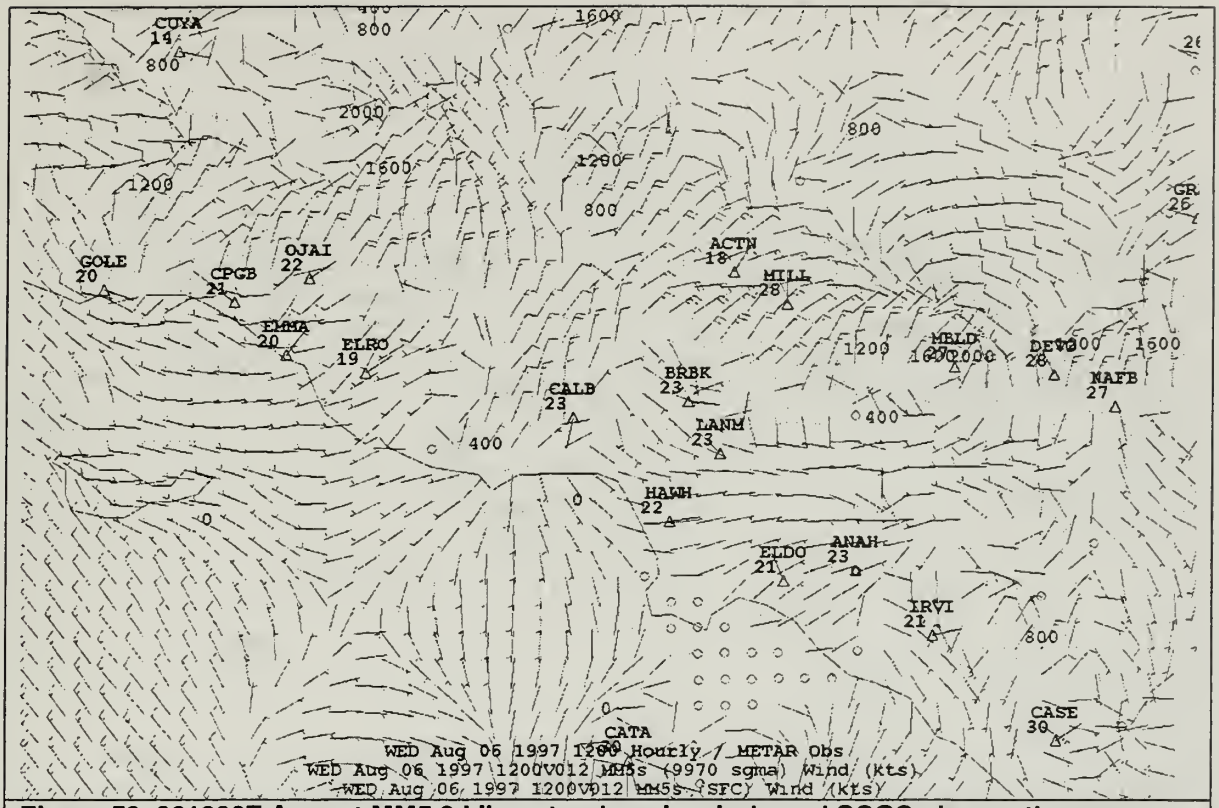

Figure 56 061200Z August MM5 3 kilometer domain winds and SCOS observations.

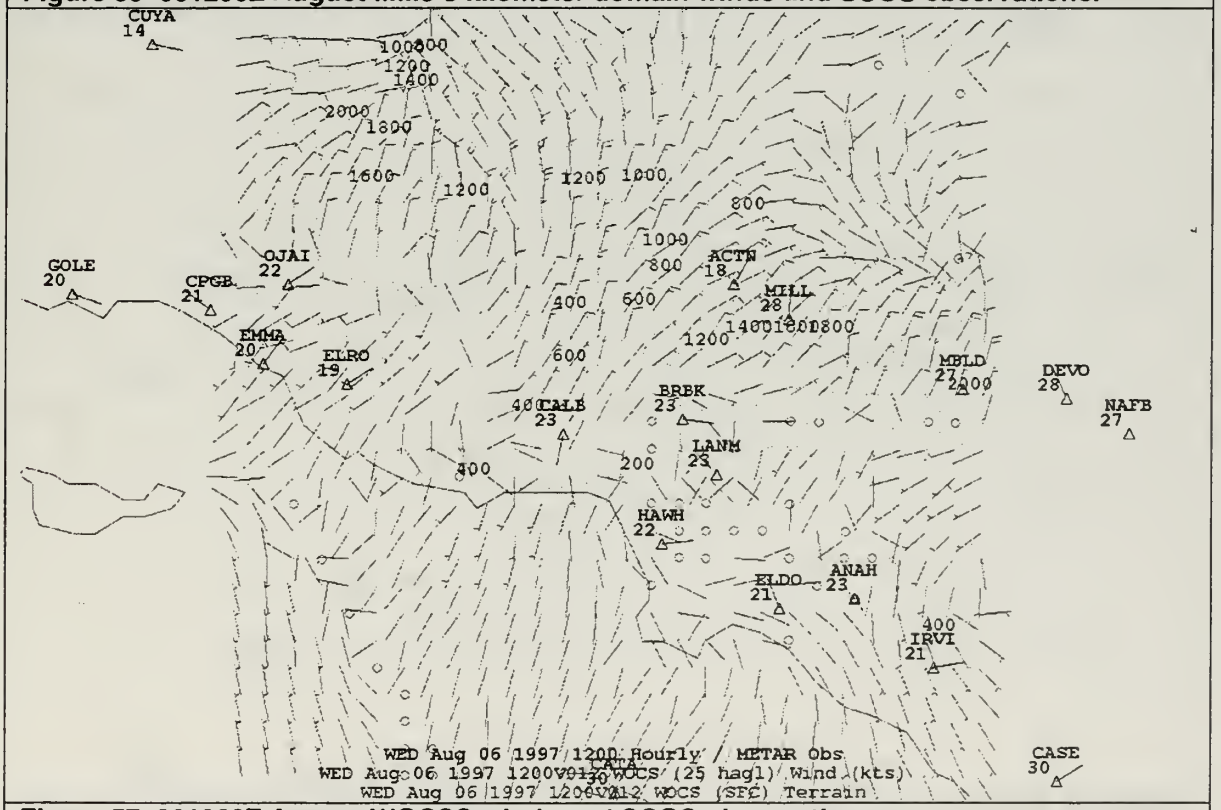

Figure 57 061200Z August WOCSS winds and SCOS observations.

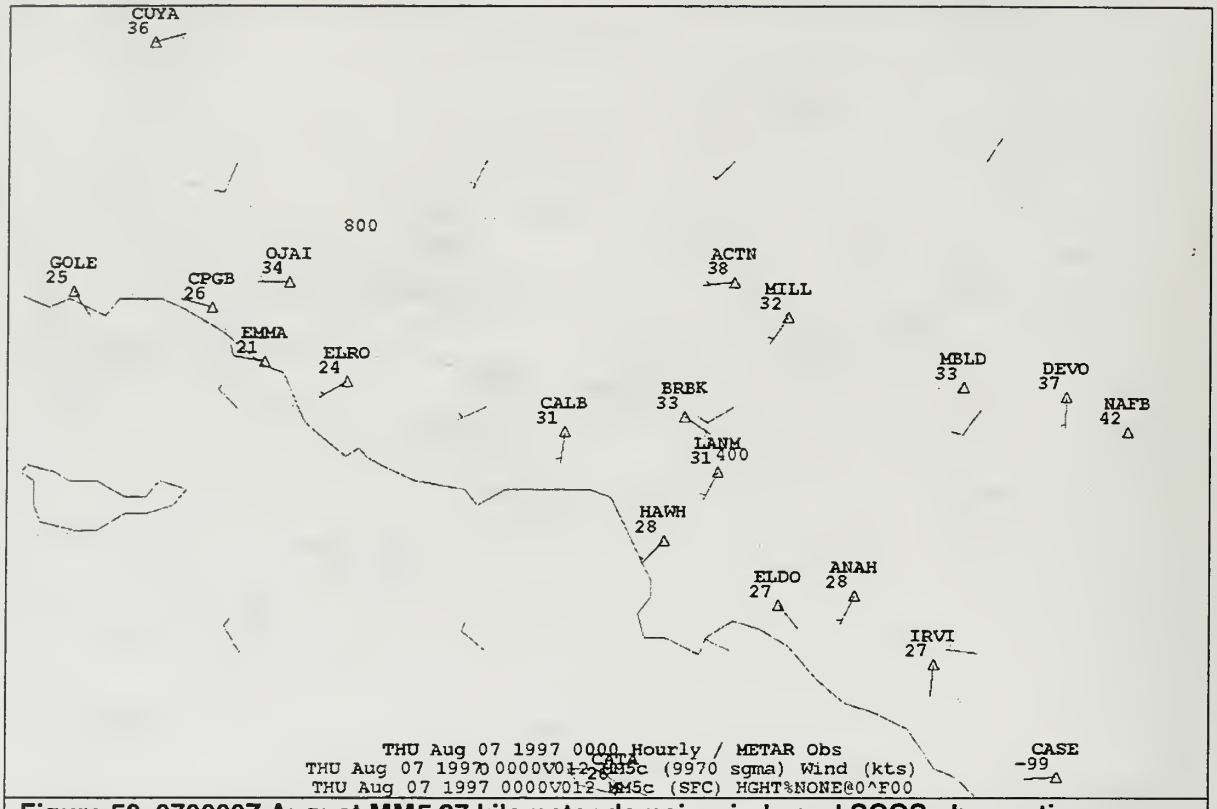

Figure 58 070000Z August MM5 27 kilometer domain winds and SCOS observations.

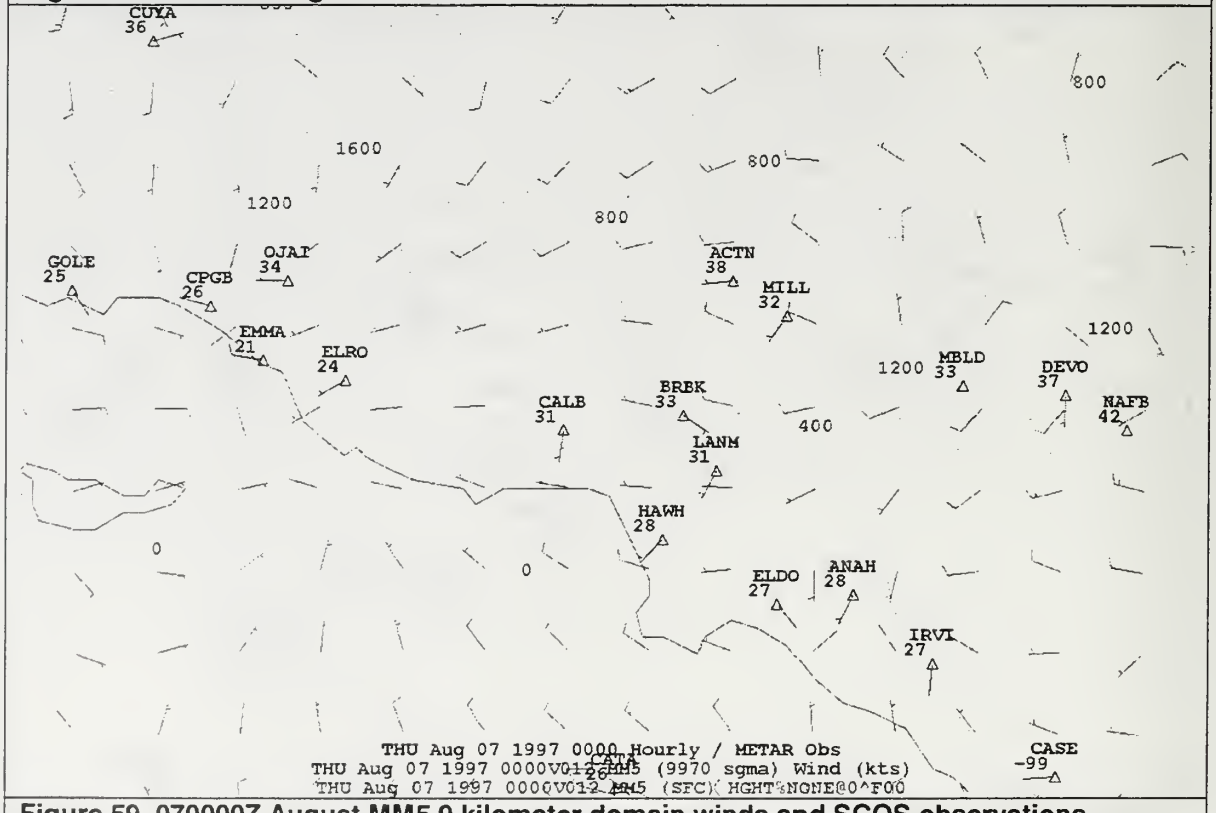

Figure 59 070000Z August MM5 9 kilometer domain winds and SCOS observations.

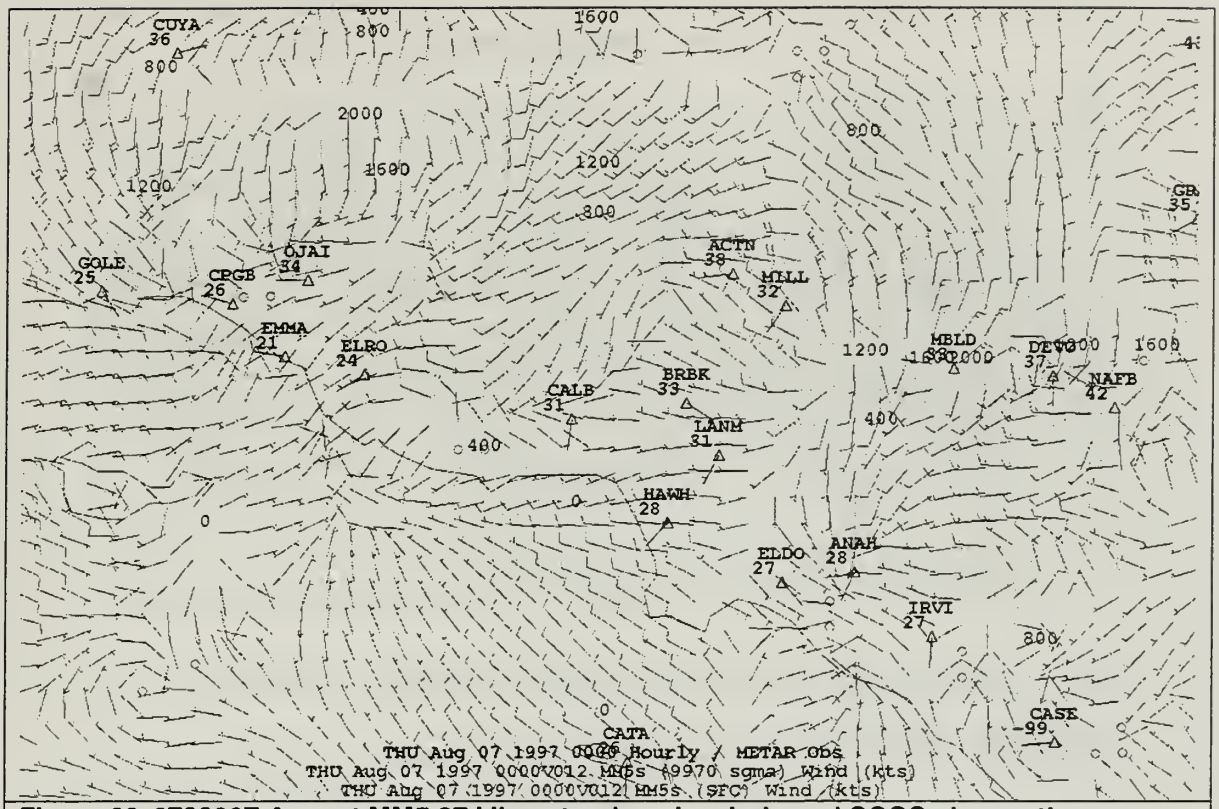

Figure 60 070000Z August MM5 27 kilometer domain winds and SCOS observations.

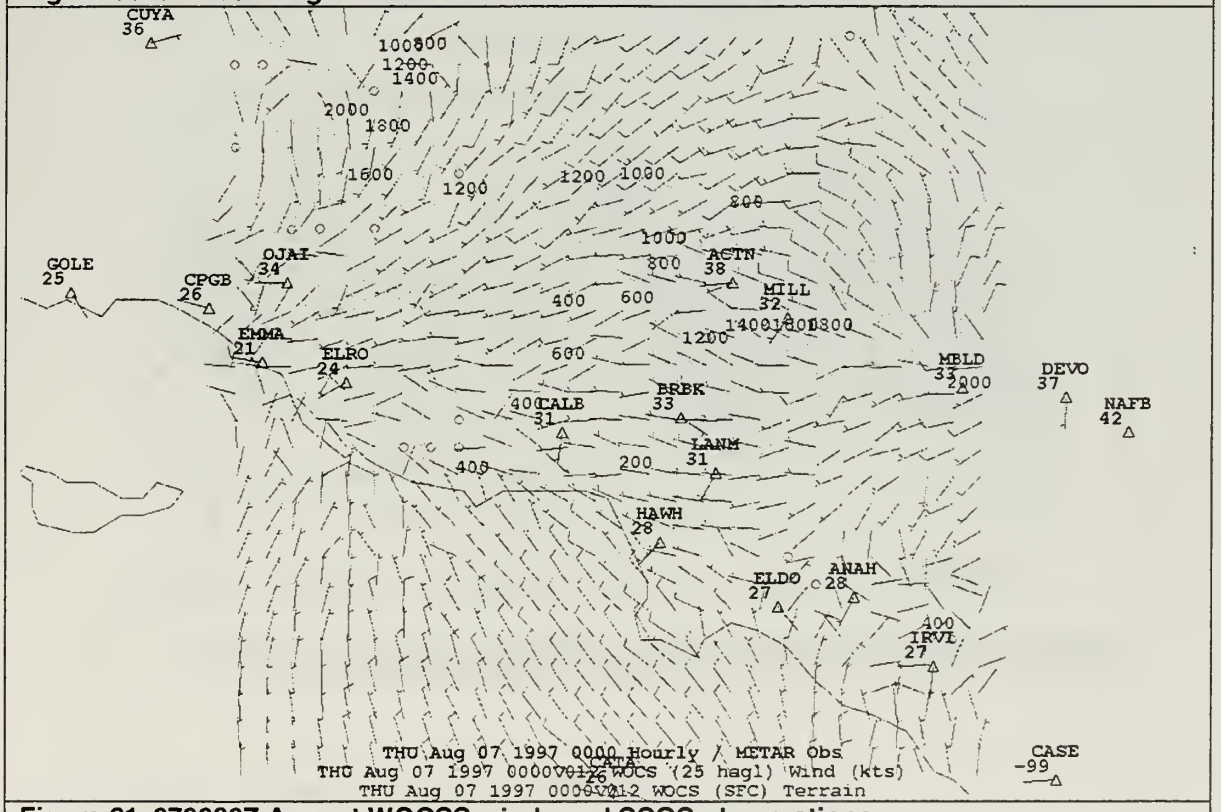

Figure 61 070000Z August WOCSS winds and SCOS observations.

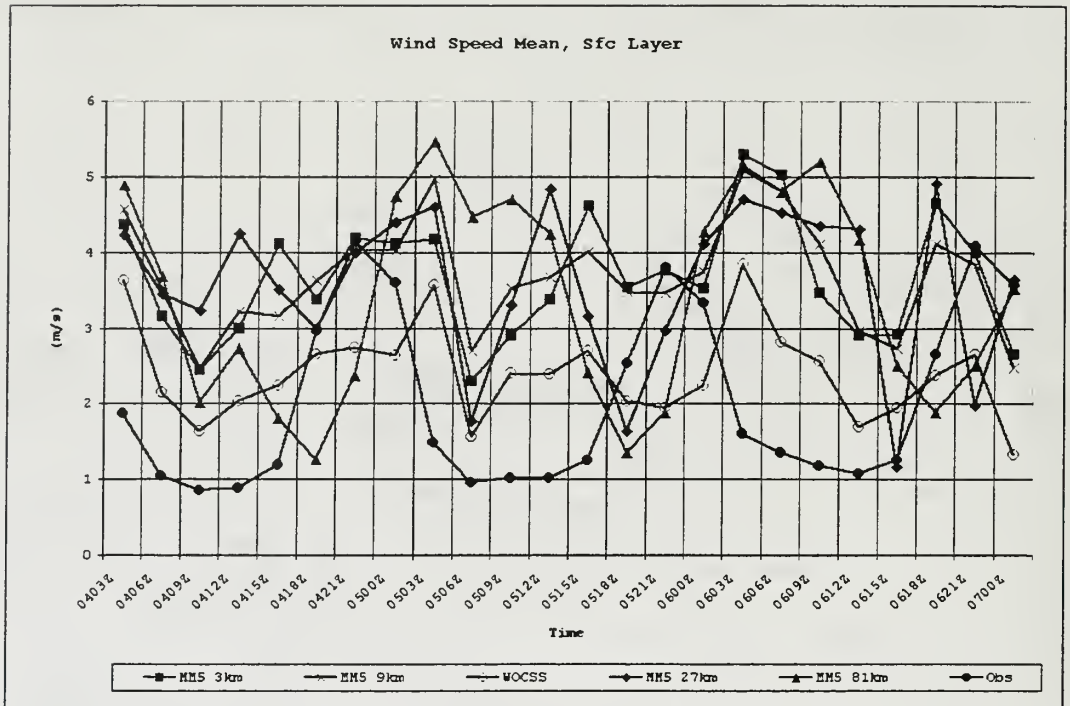

Figure 62. Surface layer wind speed mean time series.

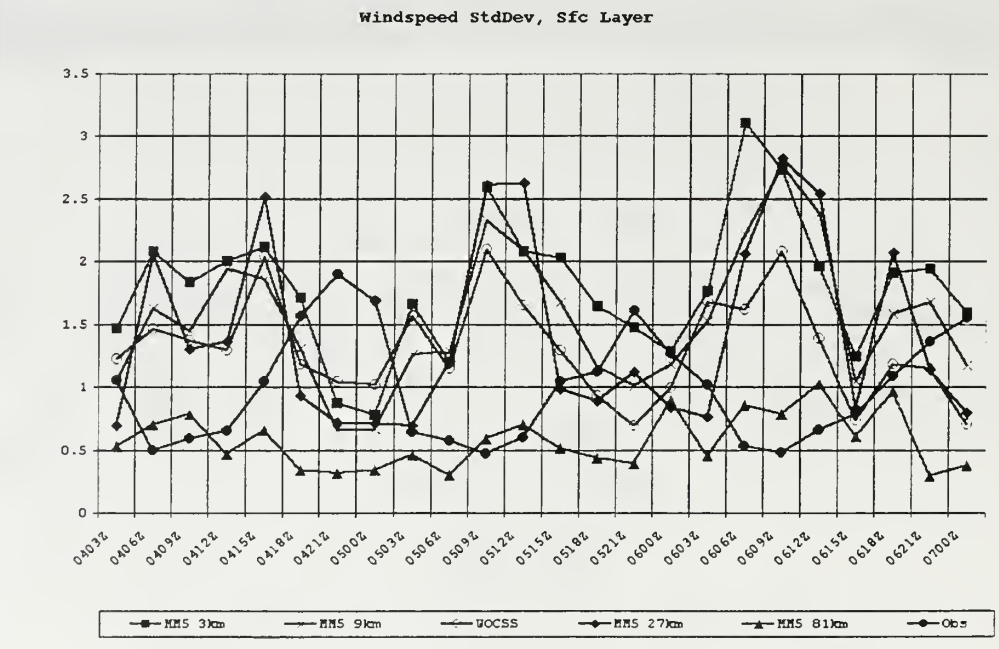

Figure 63. Surface layer wind speed standard deviation time series.

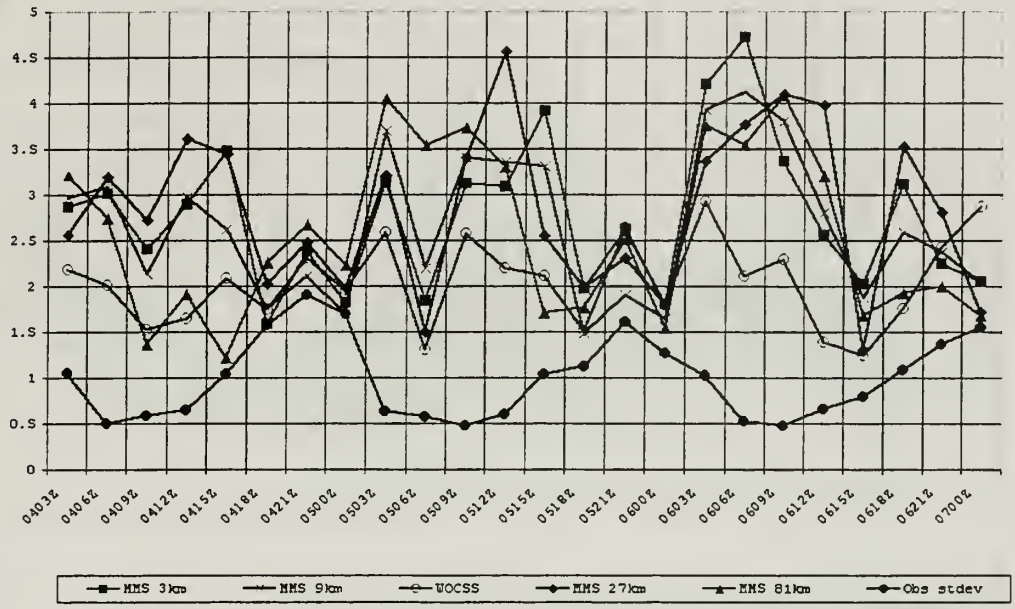

Figure 64. Surface layer wind speed RMSD time series.

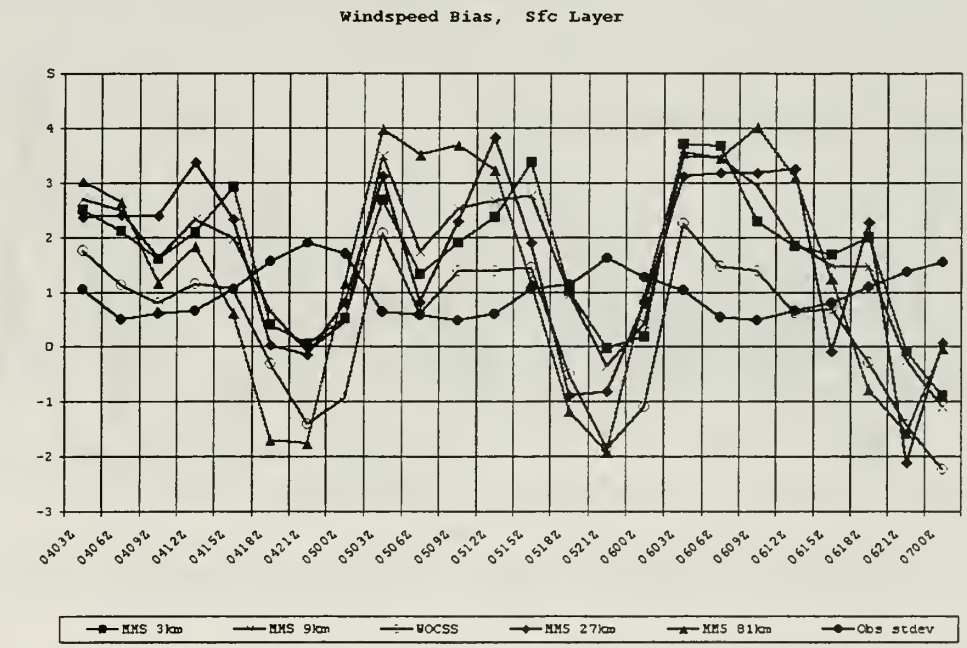

Figure 65. Surface layer wind speed bias time series.

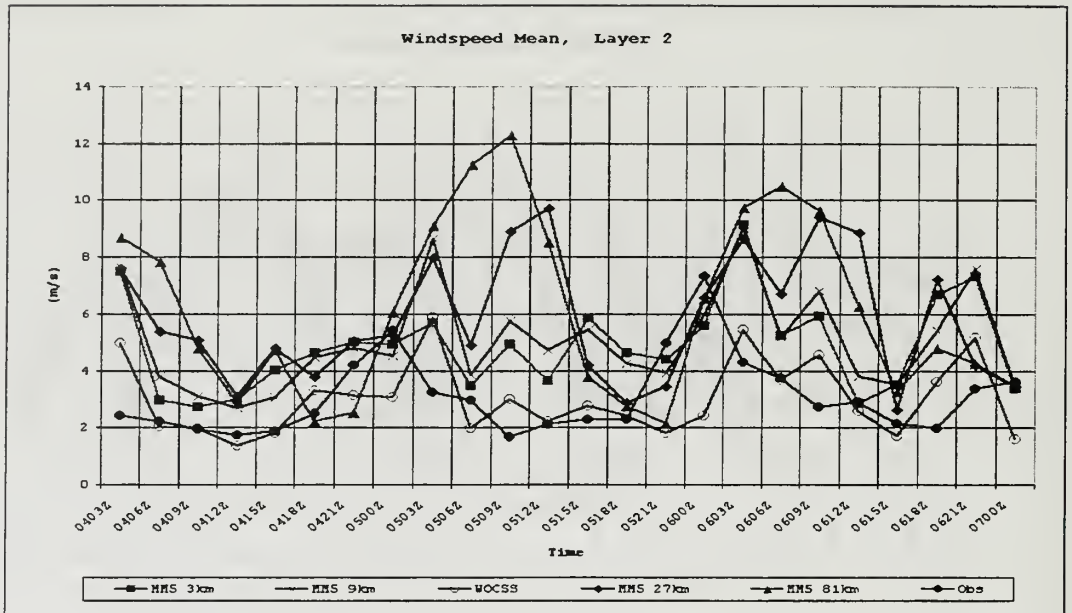

Figure 66. Layer 2 wind speed mean time series.

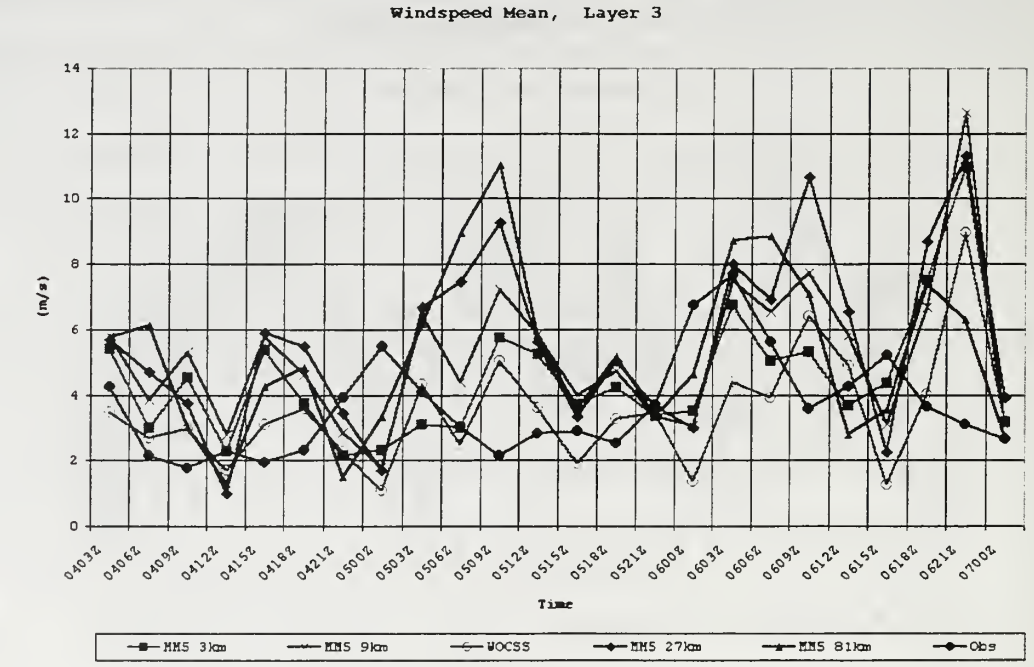

Figure 67. Layer 3 wind speed mean time series.

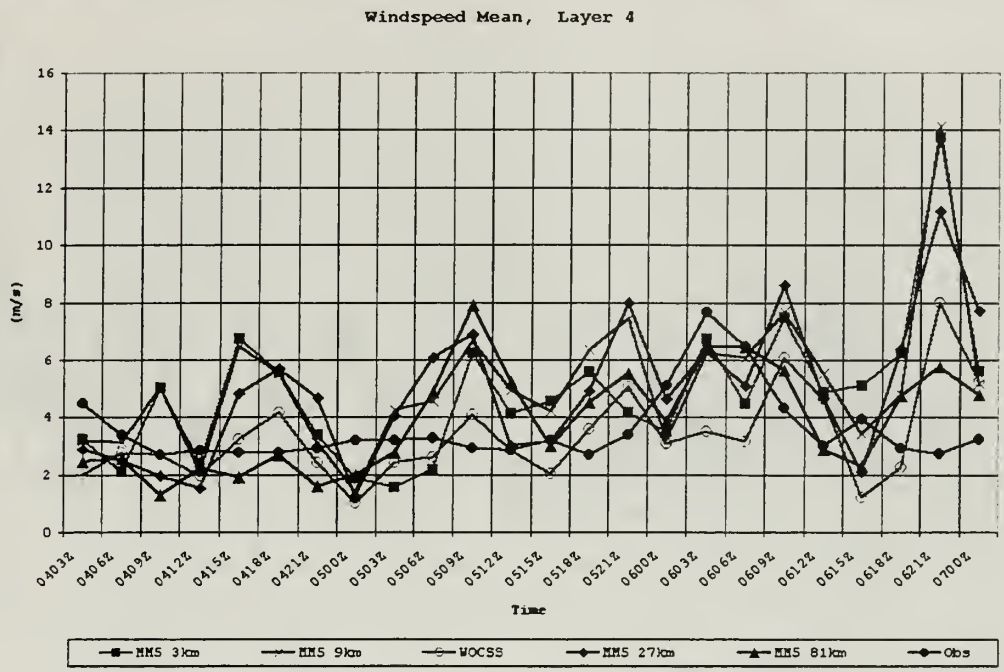

Figure 68. Layer 4 wind speed mean time series.

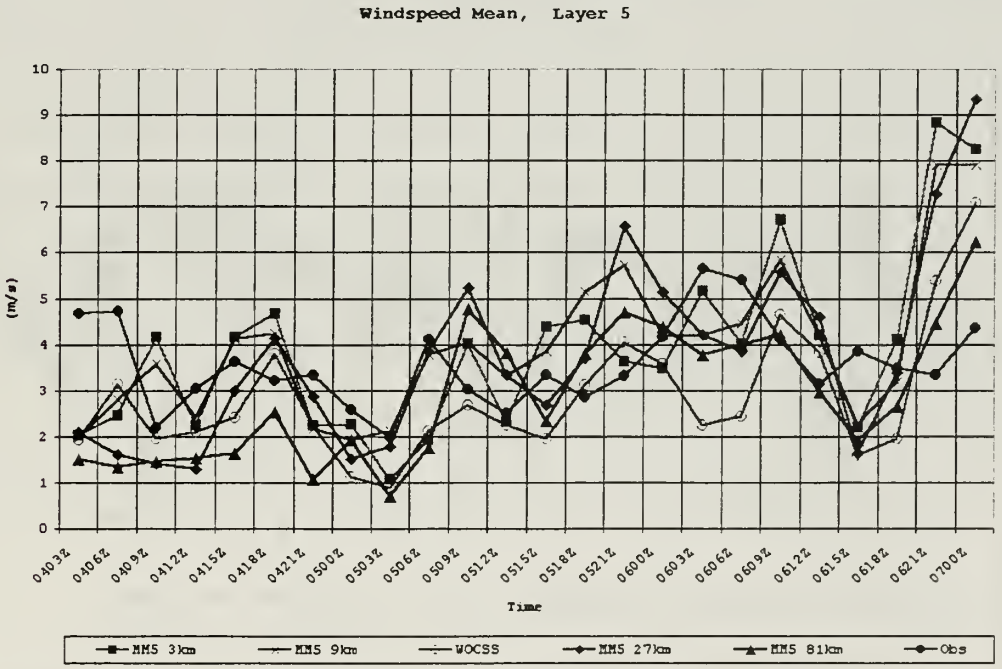

Figure 69. Layer 5 wind speed mean time series.

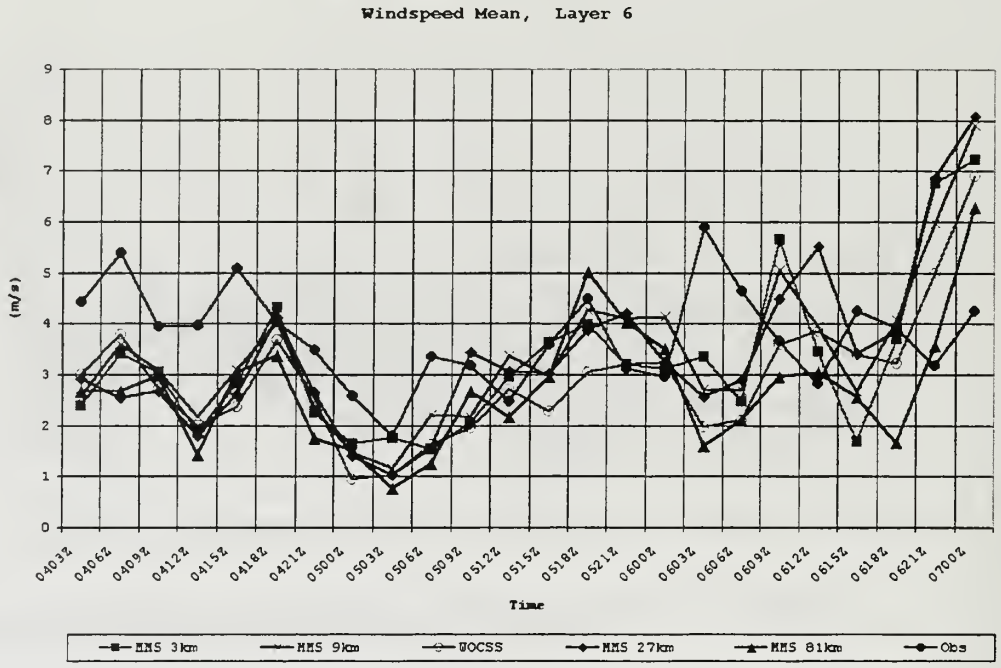

Figure 70. Layer 6 wind speed mean time series.

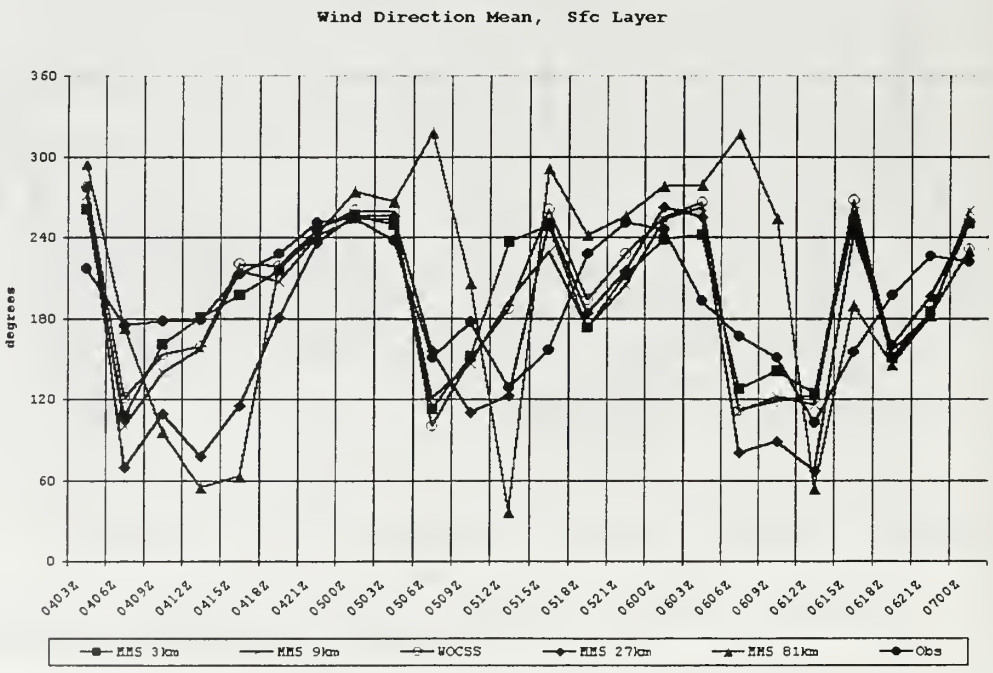

Figure 71. Surface layer wind direction mean time series.

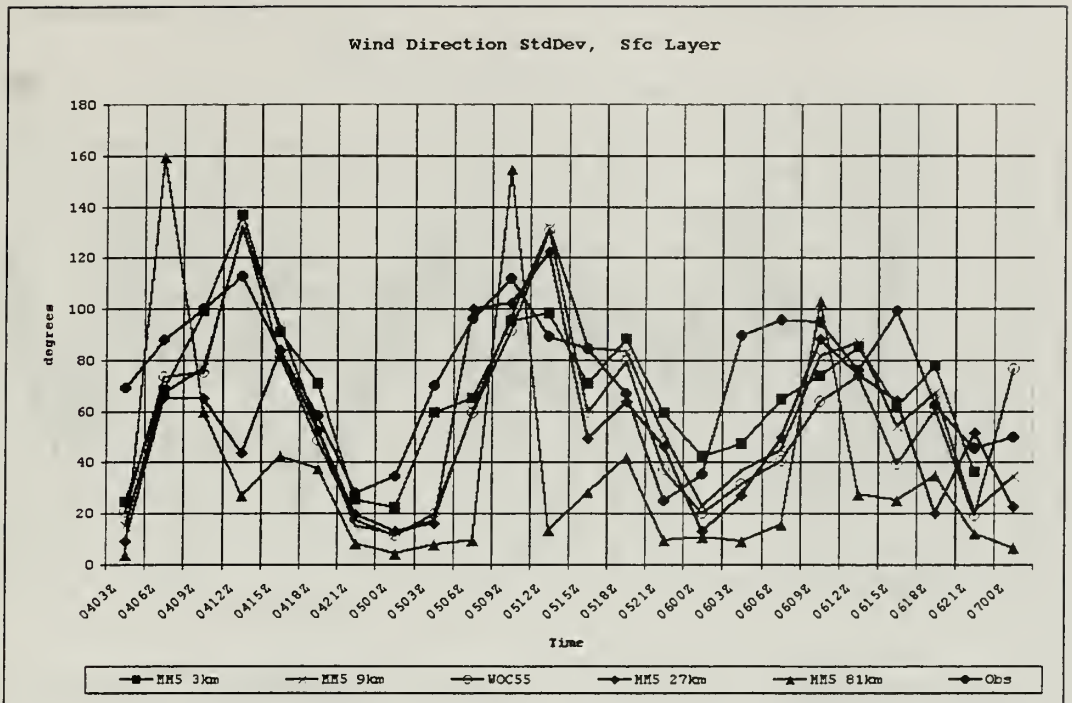

Figure 72. Surface layer wind direction standard deviation time series.

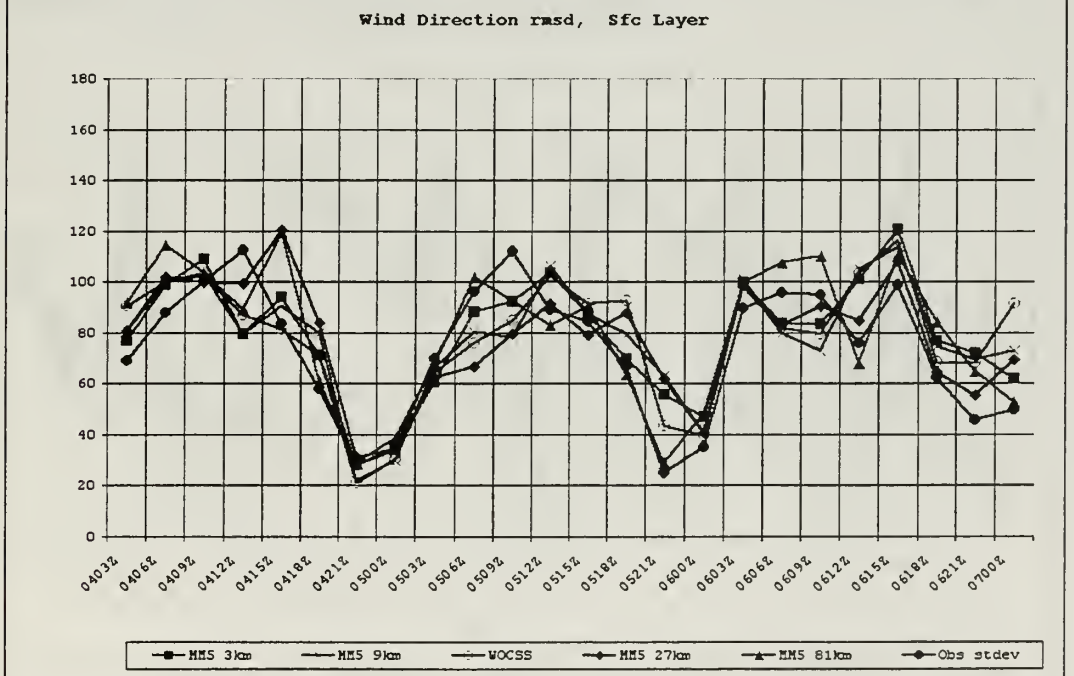

Figure 73. Surface layer wind direction RMSD time series.

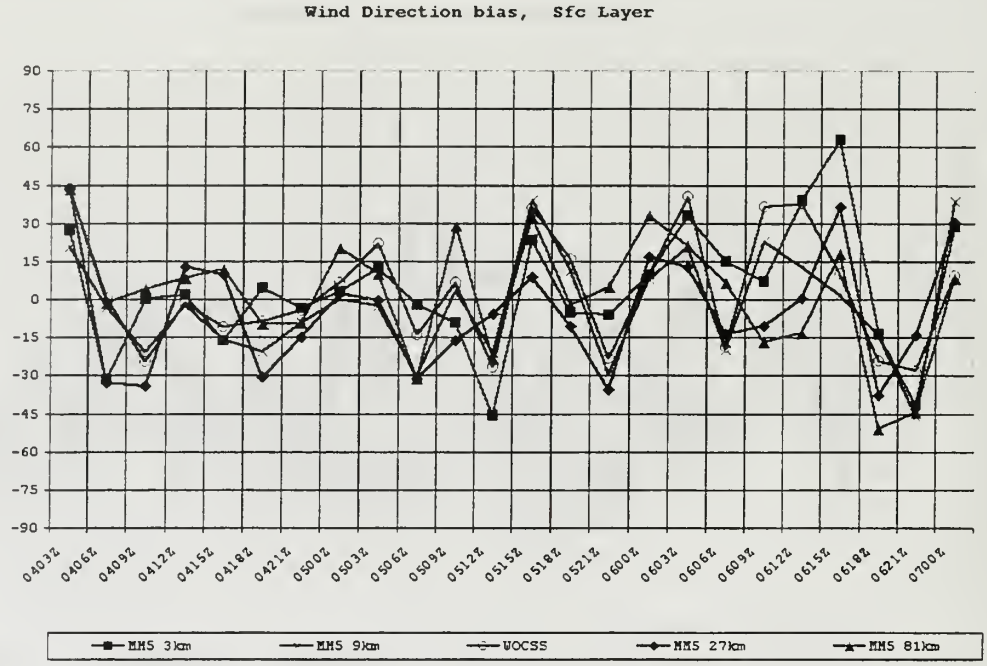

Figure 74. Surface layer wind direction bias time series.

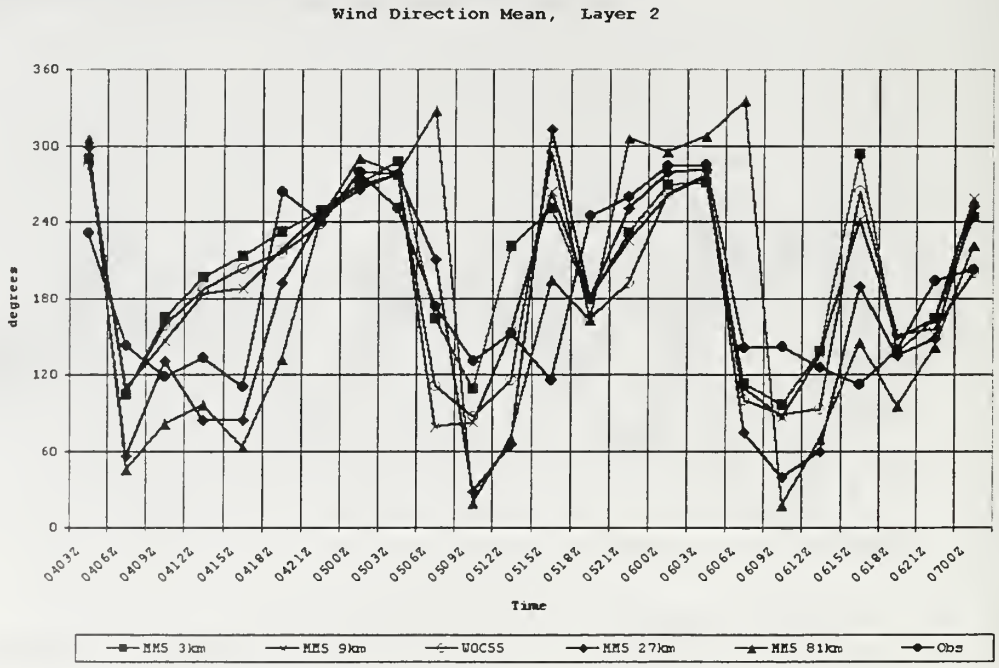

Figure 75. Layer 2 wind direction mean time series.

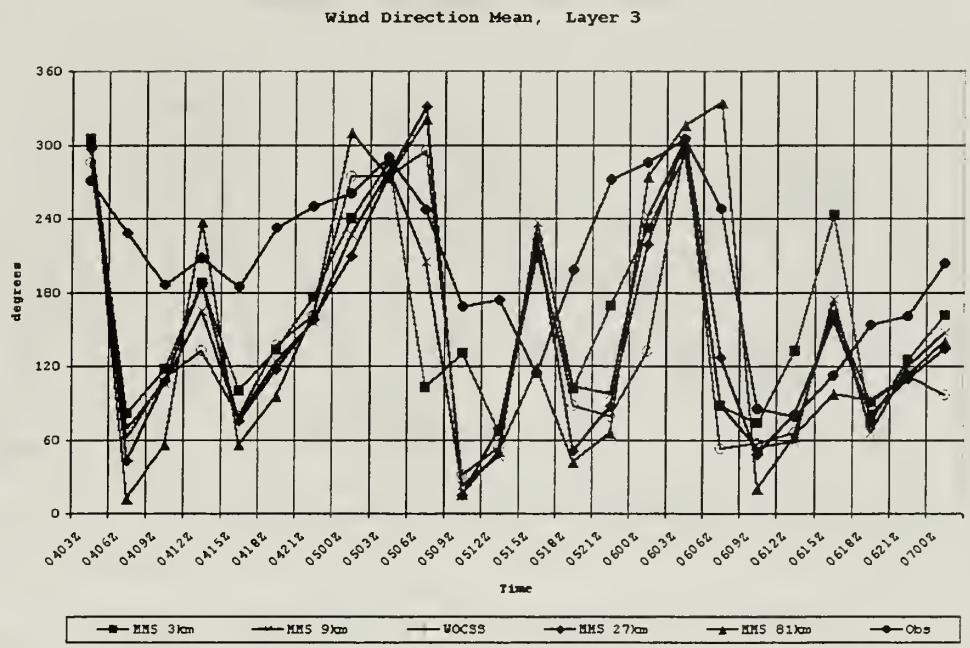

Figure 76. Layer 3 wind direction mean time series.

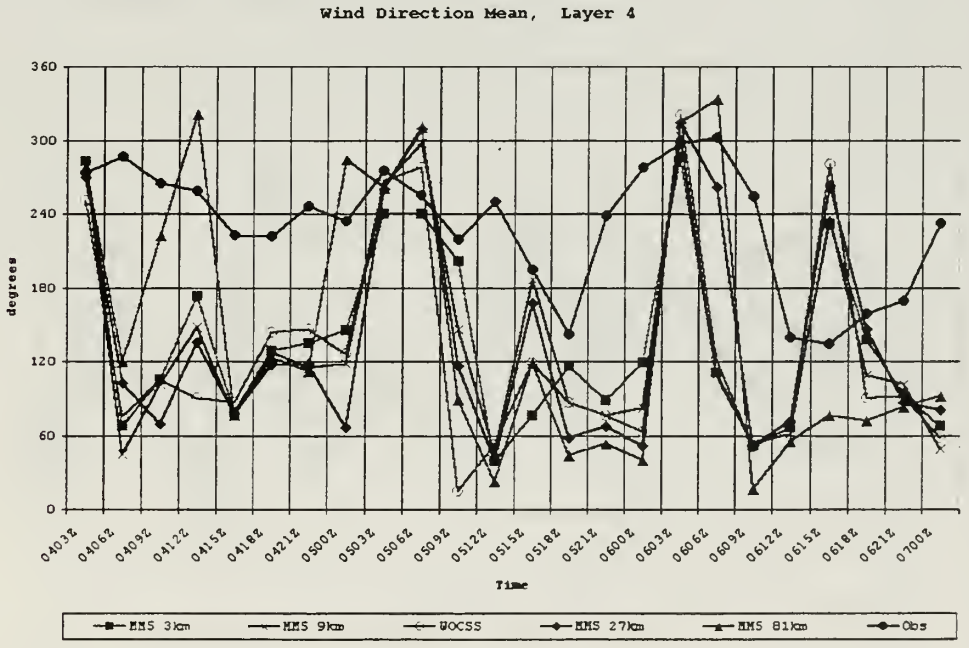

Figure 77. Layer 4 wind direction mean time series.

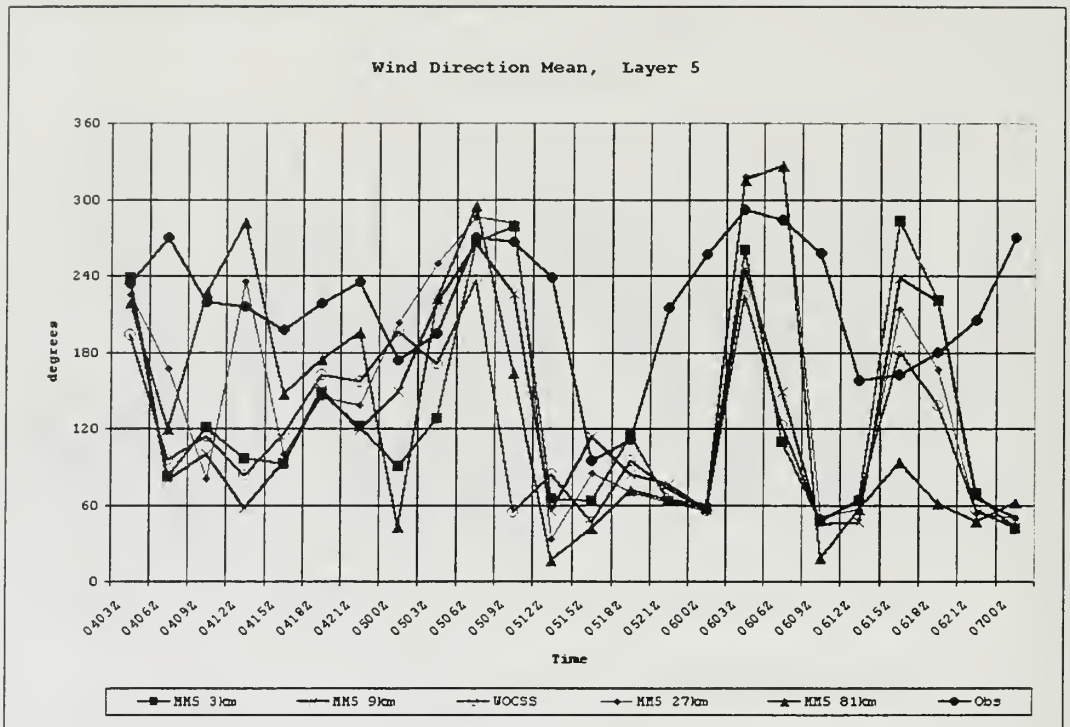

Figure 78. Layer 5 wind direction mean time series.

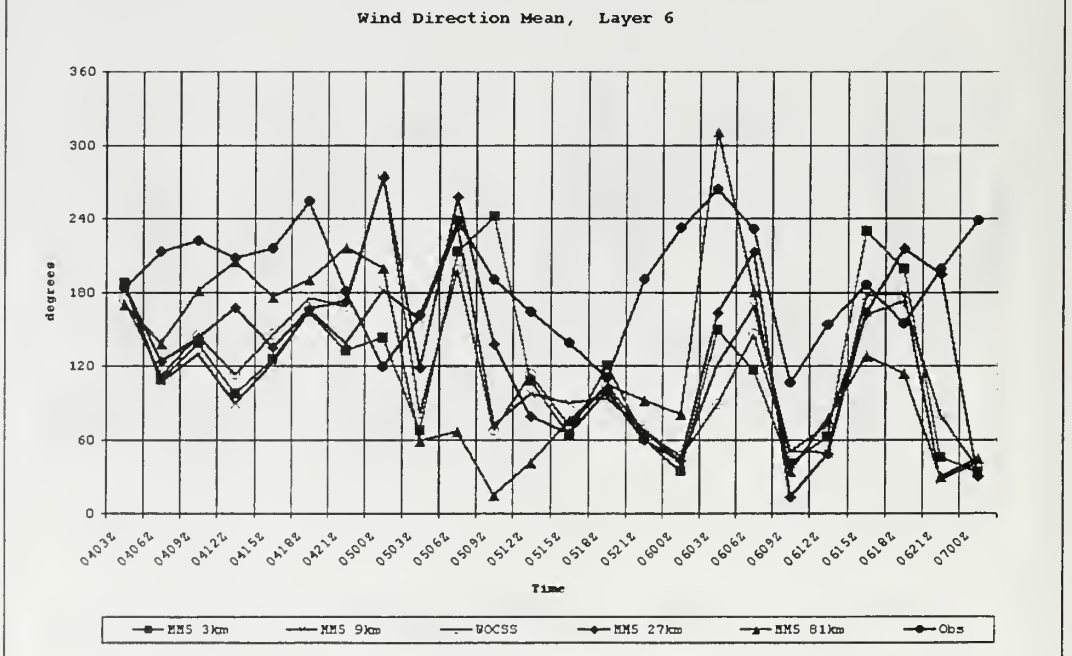

Figure 79. Layer 6 wind direction mean time series.

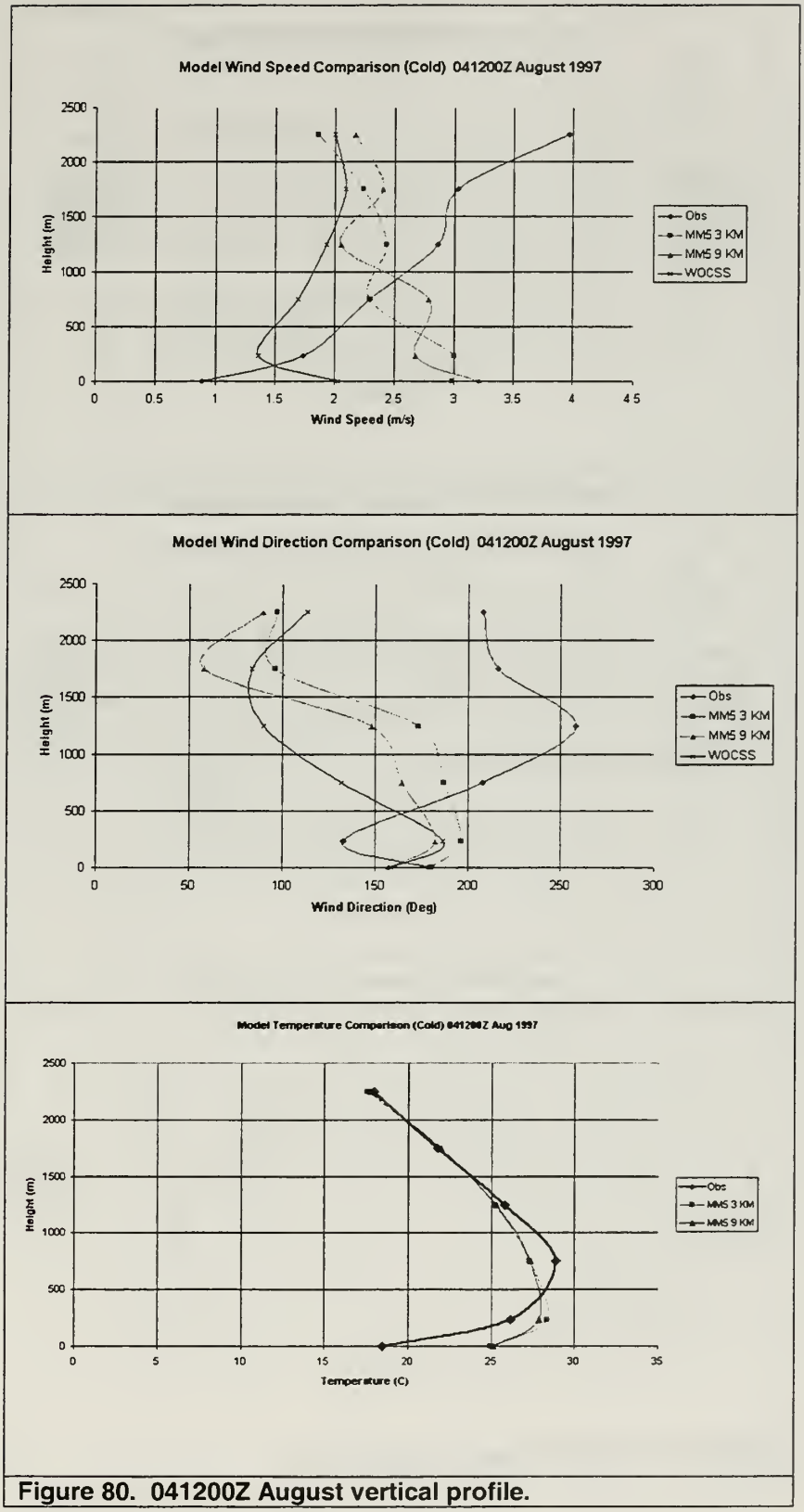

Figure 80. 041200Z August vertical profile.

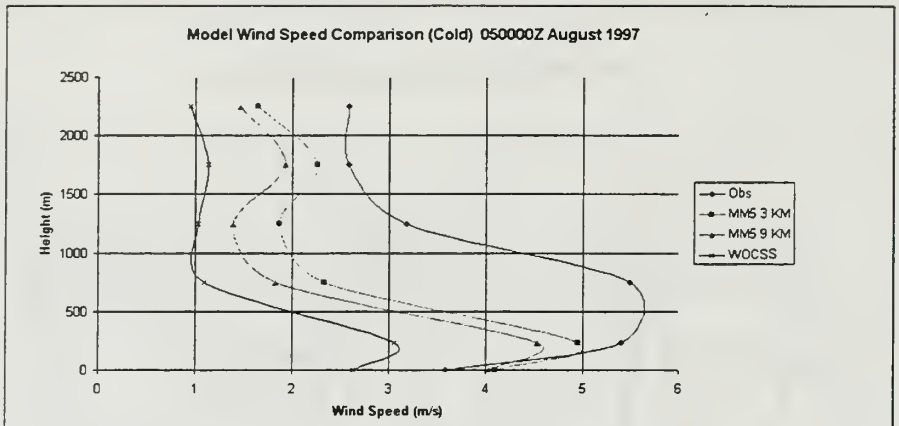

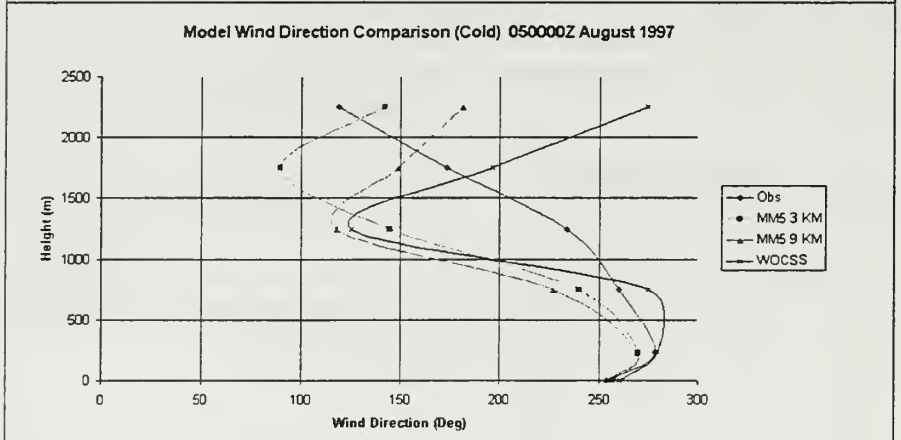

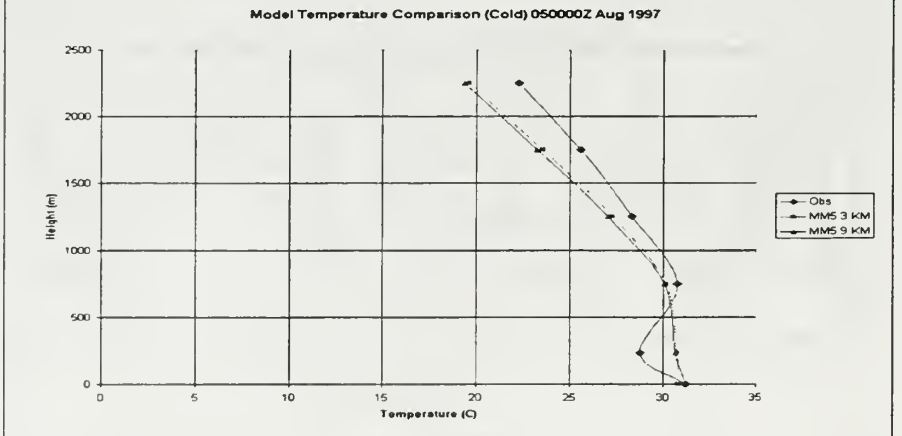

Figure 81. 050000Z August vertical profile.

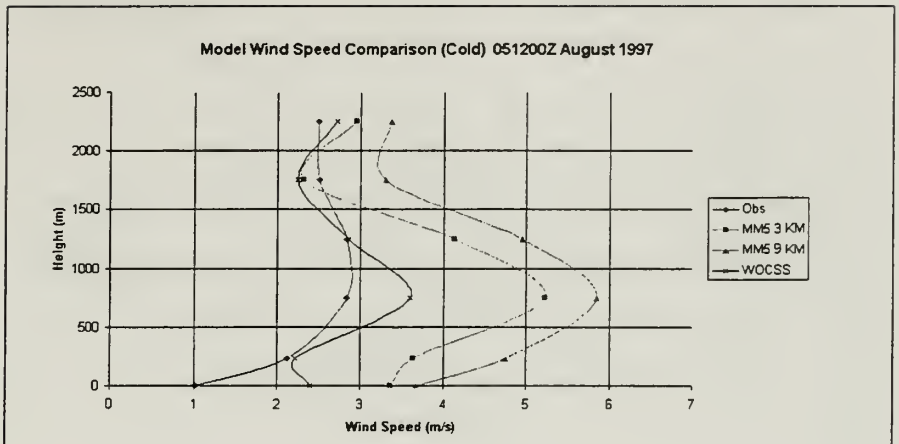

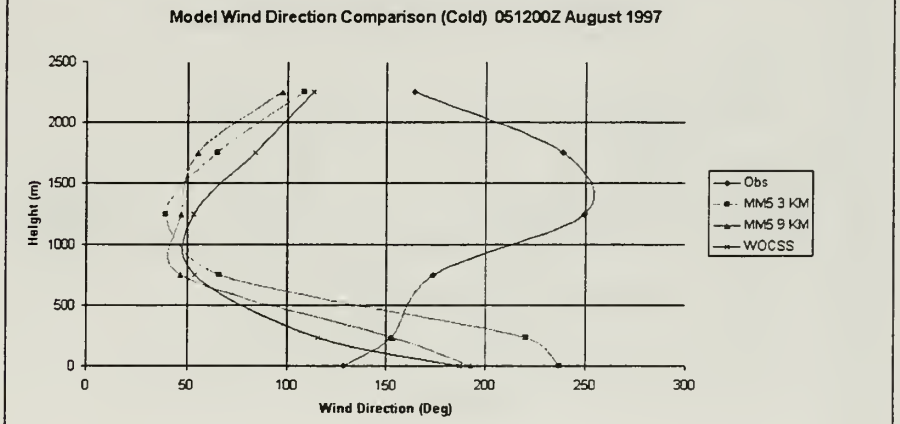

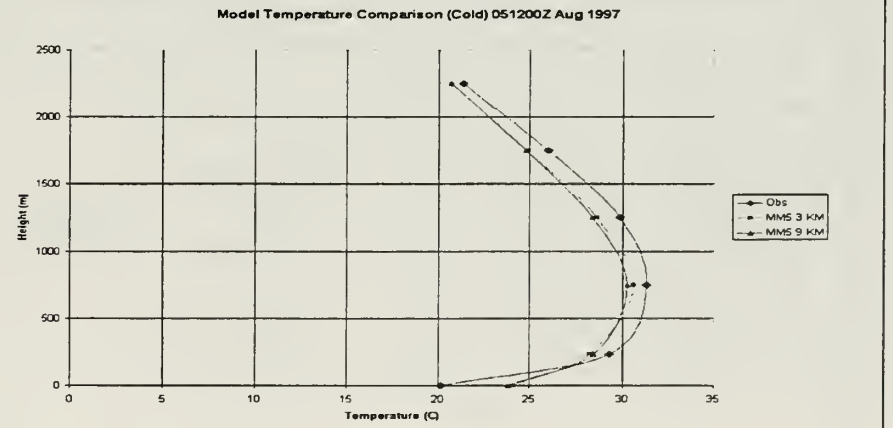

Figure 82. 051200Z August vertical profile.

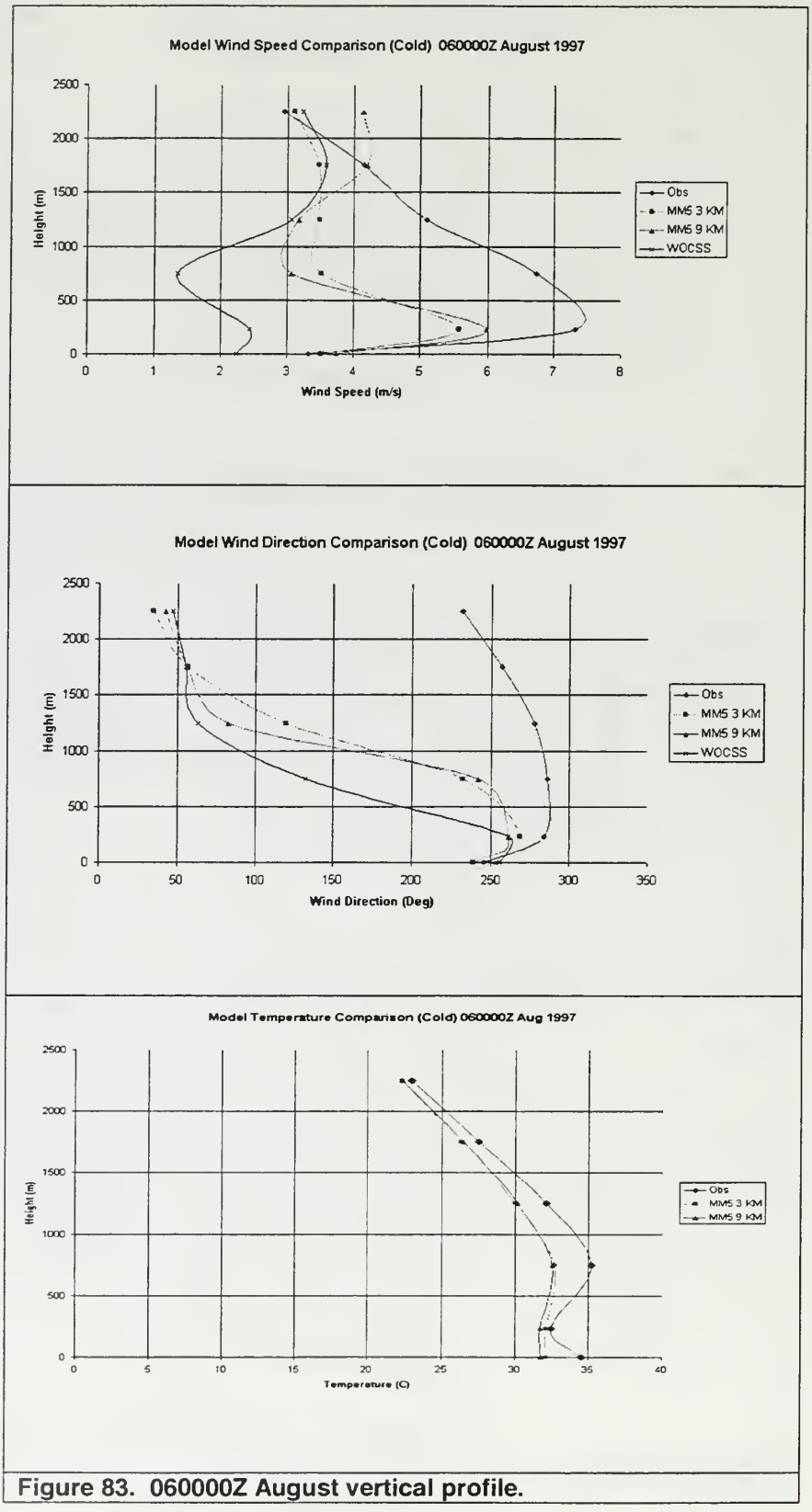

Figure 83. 060000Z August vertical profile.

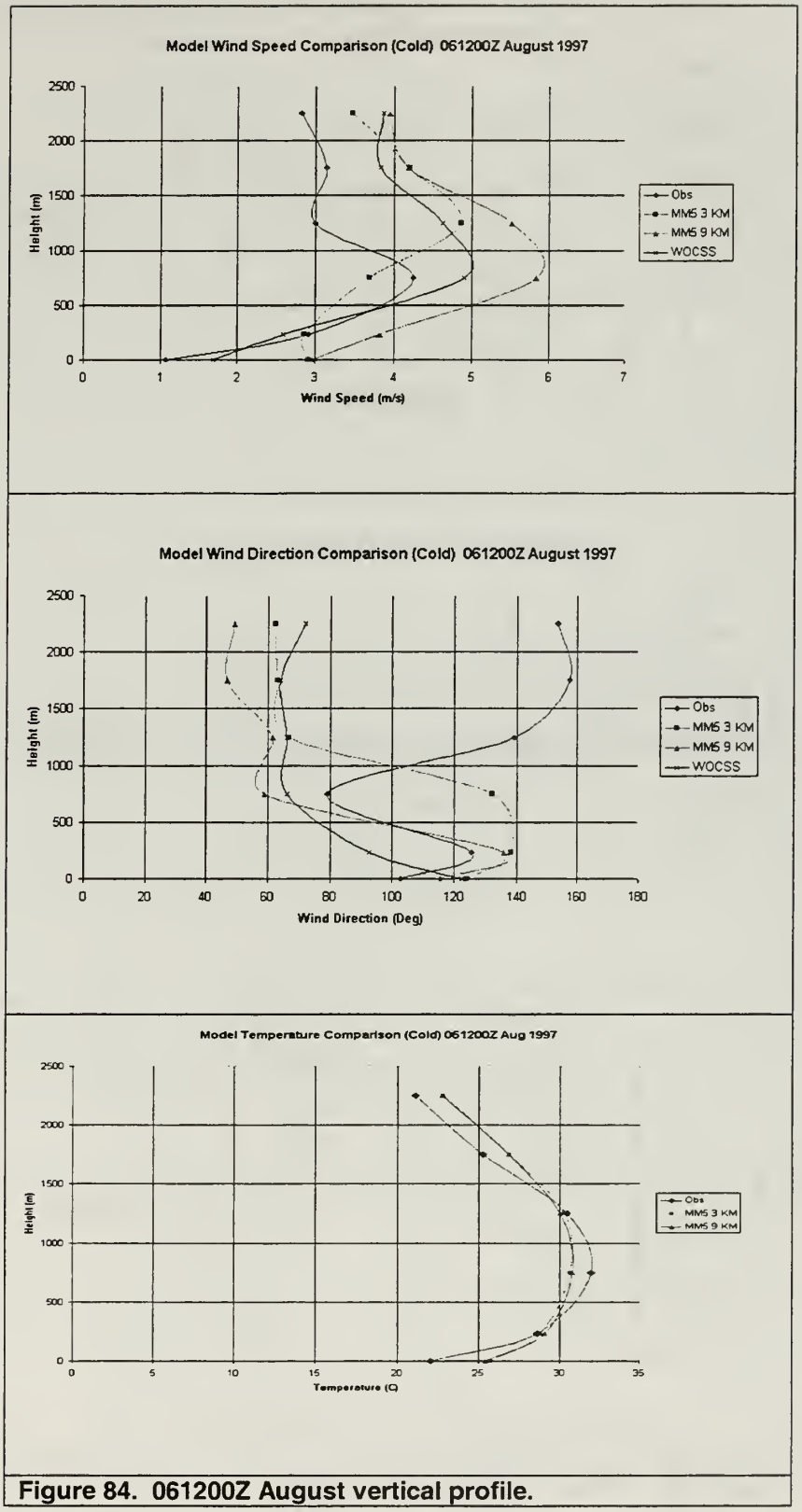

Figure 84. 061200Z August vertical profile.

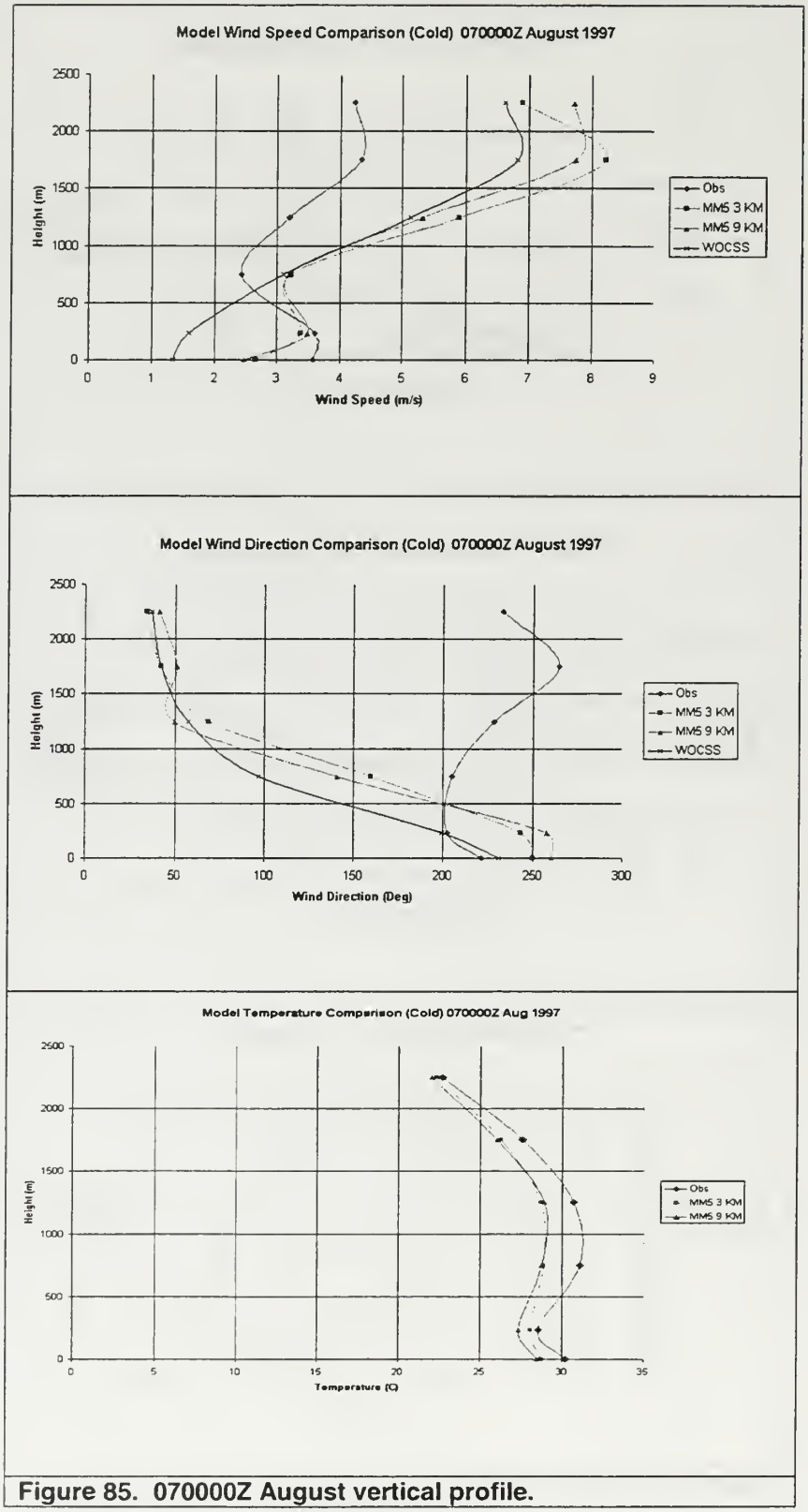

Figure 85. 070000Z August vertical profile.

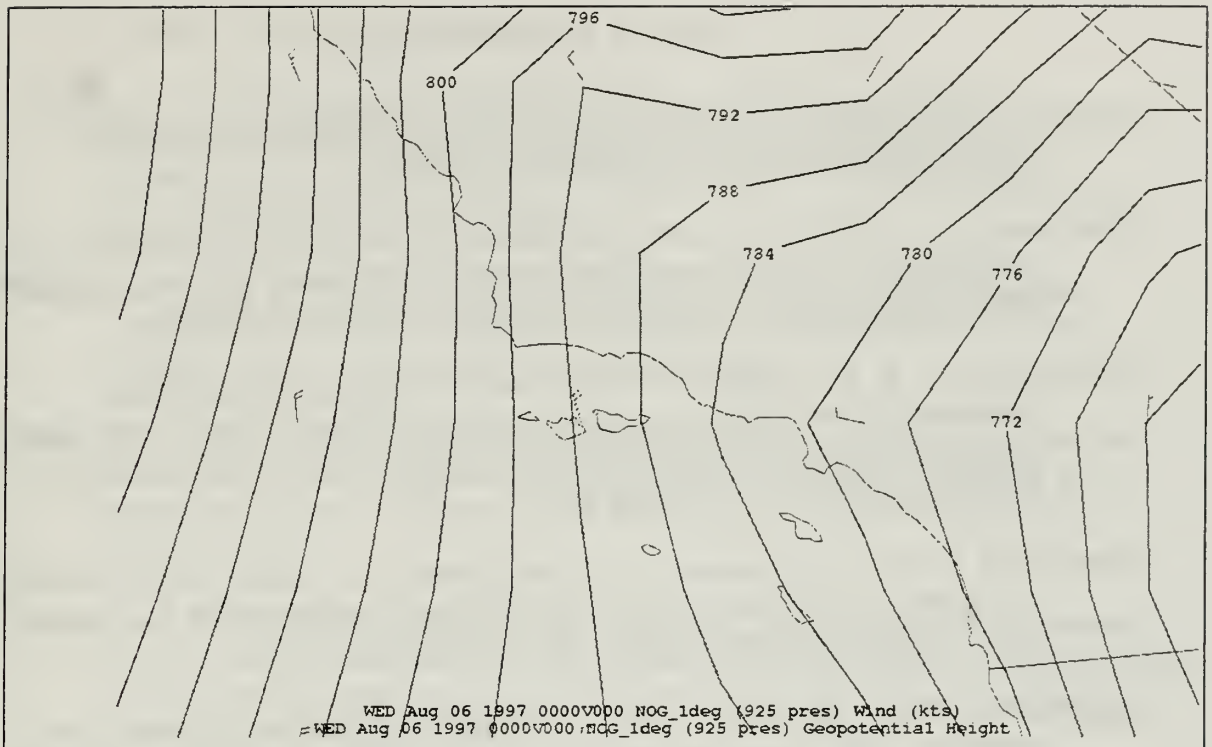

Figure 86. 06000Z August 97 925 mb geopotential heights and winds (NOGAPS 1°).

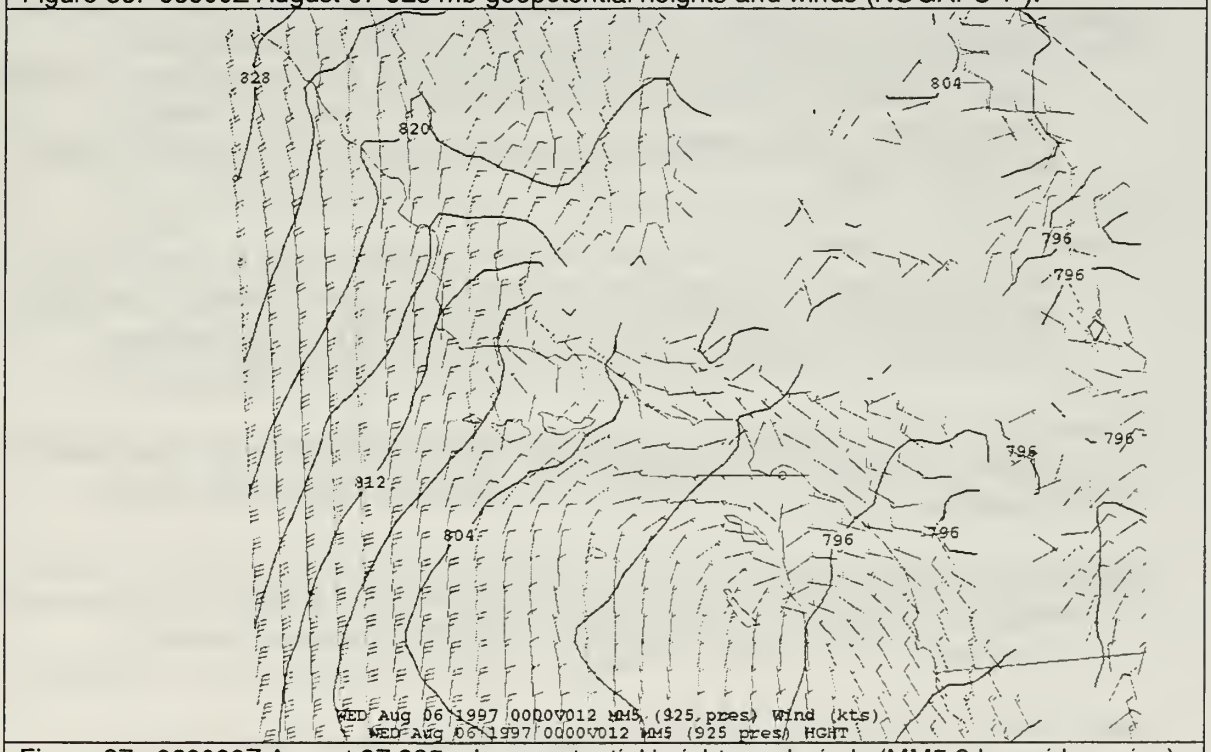

Figure 87. 060000Z August 97 925 mb geopotential heights and winds (MM5 9 km grid spacing).

LIST OF REFERENCES

Anthes, R.A., 1986: *The General Question of Predictability*. P.S. Ray(Ed), American Meteorological Society, pp. 636-655.

Blackadar, A.K., 1979: *High Resolution Models of the Planetary Boundary Layer*. Advances in Environmental Science and Engineering Volume 1, J. Pfafflin and E. Ziegler (Eds.), Gordon and Breach, STATE, pp 50-85.

Boucouvala, D., R. Bornstein, D.K. Miller, and J. Wilkinson,2000: "MM5 Simulation of the Meteorological Conditions During a South Coast Ozone Study (SCOS97) Episode," paper presented at NATO/ITM Conference, Boulder, Colorado, 15-19 May 2000.

Bhumralkar, C.M., R.L. Mancuso, F.L. Ludwig and D.S. Renne, 1980: A Practical And Economic Method For Estimating Wind Characteristics At Potential Wind Energy Conversion Sites, *Sol. Energy,* 25, 55-65.

California Air Resources Board,2000: "1997 Southern California Ozone Study – NARSTO." [http://www.arb.ca.gov/research/scos/scos.htm]. August 2000

Dudhia J., D. Gill, Y. Guo, and K. Manning, 2000: National Center for Atmospheric Research, *PSU/NCAR Mesoscale Modeling System Tutorial Class Notes and User's Guide: MM5 Modeling System Version 3.*, January 2000. [http://www.mmm.ucar.edu/mm5/mm5-home.html]. 12 November 1999.

Gayno, G.A., N.L. Seaman, A.M. Lario, and D.R. Stauffer, 1994: *Forecasting Visibility Using a 1.5-Order Closure Boundary Layer Scheme in a 12km Non-Hydrostatic Model.* Tenth American Meteorological Society Conference on Numerical Weather Prediction, July 18-22, pp. 18-20.

Kuypers, M.A., 2000: *Understanding Mesoscale Error Growth And Predictability*, Master's. Thesis, Naval Postgraduate School, Monterey, California, September 2000.

Leidner, S., D. Stauffer, and N. Seaman, 1999: Improving Short-Term Numerical Weather Prediction In The California Coastal Zone By Dynamic Initialization Of The Marine Boundary Layer, *Mon. Wea. Rev.*, submitted.

Lorenz, E.N., 1982: Atmospheric Predictability Experiments With A Large Numerical Model. *Tellus*, 36A, 505-513.

Lorenz, E.N., 1993: *The Essence of Chaos.* University of Washington Press,

Seattle, 227pp.

Ludwig, F.L., J.M. Livingston, and R.M. Endlich, 1991: "Use of Mass Conservation and Critical Dividing Streamline Concepts for Efficient Objective Analysis of Winds in Complex Terrain", *J. Appl. Meteor.,* v. 6., pp. 1490-1499, November 1991.

Ludwig, F.L. and D. Sinton, 2000: "Evaluating an Objective Wind Analysis Technique with a Long Record of Routinely Collected Data", *Amer. Meteor. Soc.,*v. 39., pp. 335-348, March 2000.

Miller, D.K., 1999: Considerations in building and using a real-time mesoscale numerical forecast system. Class notes for *Forecasting analysis and prediction course.* Department of Meteorology, Naval Postgraduate School, 15pp.

Monterrosa, O.E., 1999: *Comparison of TAMS/RT Surface Wind, Temperature, and Pressure Fields with Surface Observations and Model Analyses in the SOCAL Area*, Master's Thesis, Naval Postgraduate School, Monterey, California, December 1999

National Center for Atmospheric Research Technical Note TN-398 + STR, *A Description of the Fifth Generation Penn State/NCAR Mesoscale Model (MM5),* Grell, G.A., J. Dudhia and D.R. Stauffer, June 1995.

National Oceanic and Atmospheric Administration (NOAA) Technical Memorandum NWS WR-261, *Climate of Los Angeles, California , January 2000.*

Nuss, W.A. and D.W. Titley, 1994: "Use of Multiquadric Interpolation for Meterological Objective Analysis," *Mon. Wea. Rev.*, v. 122, pp. 1611-1631, July 1994.

Perkey, D.J., 1986: Formulation of mesoscale numerical models. In: Mesoscale meteorology and forecasting, P.S. Ray, Ed., Am Meteor. Soc., 573-596.

Sterbis, C.J., 2000: *An Analysis of Short Term Mesoscale Forecasts in the Los Angeles Basin Using SCOS97 Data,* Mater's Thesis, Naval Postgraduate School, Monterey, California, September 2000.

THIS PAGE INTENTIONALLY LEFT BLANK

INITIAL DISTRIBUTION LIST

No. Copies

1. Defense Technical Information Center.....2
   8725 John J. Kingman Road, STE 0944
   Ft. Belvoir, Virginia, 22060-6218

2. Dudley Knox Library.....2
   Naval Postgraduate School
   411 Dyer Road
   Monterey, CA 93943-5101

3. Chairman, Code MR/Wx.....1
   Department of Meteorology
   Naval Postgraduate School
   Monterey, CA 93943-5101

4. Chairman, Code OC/Ga.....1
   Department of Oceanography
   Naval Postgraduate School
   Monterey, CA 93943-5101

5. Professor Douglas K. Miller.....1
   Department of Meteorology
   Naval Postgraduate School
   Monterey, CA 93943-5101

6. Professor R. Terry Williams.....1
   Department of Meteorology
   Naval Postgraduate School
   Monterey, CA 93943-5101

7. Commander
   Naval Meteorology and Oceanography Command.....1
   1020 Bach Boulevard
   Stennis Space Center, MS 39529-5005

8. Dr. Francis L. Ludwig 1
   Dept. of Civil and Env. Engineering
   Stanford University
   Stanford, California 94305-4020

9. Dr. Francis M. Fujioka 1
PSW Forest Fire Laboratory
4955 Canyon Crest Drive
Riverside, CA 92507-6099

10. Dr. Duane E. Stevens.....1
Department of Meteorology
University of Hawaii at Manoa
2525 Correa Road, HIG 333
Honolulu, HI 96822-2291

11. Lieutenant Renwick M. Mohammed.....2
4030 B Wilder Ave
Bronx NY 10466